EFFECTS OF AN AQUACULTURE FISH FARM ON THE SEDIMENT GEOCHEMISTRY OF A NATURALLY ANOXIC BASIN

by

Stormy Vandeplas

Submitted in partial fulfillment of the requirements
for the degree of Master of Science
at
Dalhousie University
Halifax, Nova Scotia
June 2023

TABLE OF CONTENTS

LIST OF TABLES

LIST OF FIGURES

ABSTRACT

The Whycocomagh Basin, located in the Bras d'Or Lakes, Nova Scotia, is a naturally deep and anoxic basin that presently houses a Steelhead Trout (*Oncorhynchus mykiss*) aquaculture farm operated as an economic resource by the We'koqma'q First Nation. However, the accumulation of free sulfide resulting from anaerobic processes poses challenges for the sustainable management of the fish farm pens. The accumulation of high concentrations of total dissolved free sulfide ($TS^{2-} = H_2S + HS^- + S^{2-}$) can be detrimental to the benthic community and have adverse effects on the surrounding biogeochemical environment. It also poses a risk to the farmed fish in the floating pens at the water surface. This study aimed to investigate the levels of sulfide accumulation at the sediment-water interface by conducting horizontal transects, both moving from shallow, nearshore waters toward the middle of the Basin and extending away from the fish farm parallel to the shoreline at similar depths to the fish pen array. Various parameters were measured, including dissolved oxygen (DO), porewater chemistry, microsensor profiling, and CHN analysis of sediment and water properties. Vertical profiles of ammonium (NH_4^+), dissolved iron (Fe^{2+}), carbon-to-nitrogen (C:N) ratio, nitrate plus nitrite ($NO_3^- + NO_2^-$), pH, and TS^{2-} were analyzed. The results revealed a decrease in DO with water depth at all sites, and anoxia was observed to begin at a depth of approximately 15 meters. Significant impacts were identified in the bottom sediment, with increased TS^{2-} and NH_4^+ production localized beneath the fish pens, and within a radius of 50-100 meters. Although there was a high level of organic enrichment beneath the fish farm, the water quality remained similar to that of sample sites located away from the farm. The localized effect at the sediment-water interface was evident, as concentrations returned to background levels within 100 meters from the fish farm. A reactive-transport model specific to the Whycocomagh Basin was developed to assess sediment recovery under various stocking scenarios. Observations revealed that the concentrations of TS^{2-} became elevated in the water column near the oxycline when the number of fish pens was increased and when they were located in waters less than ~23 meters deep. In contrast, when the same increased number of fish pens were placed in deeper waters (~48 meters), elevated concentrations were observed near the sediment-water interface. This finding suggests that relocating the farm to the deeper portions of the Basin could be beneficial in avoiding the shoaling of the oxycline. Considering the increasing prevalence of anoxia in aquatic ecosystems, implementing site-specific management strategies to monitor remineralization dynamics would contribute to sustainable practices for future fish farm facilities. To enhance the applications of this study, additional research should focus on the long-term effects of sulfide accumulation, seasonal variations, and the role of microbial communities in mitigating sulfide levels. These insights can inform the development of effective approaches to aquaculture in proximity to anoxic environments.

LIST OF ABBREVIATIONS AND SYMBOLS USED

Abbreviations	Descriptions
AP Transect	Transect moving away from the F1 site
BdOL	Bras d'Or Lakes
BOD	Benthic Oxygen Demand
CTD	Conductivity-Temperature-Depth
DBL	Diffusive Boundary Layer
DEM	Digital Elevation Model
DFO	Fisheries and Oceans Canada
DIN	Dissolved Inorganic Nitrogen ($NO_3^- + NO_2^- + NH_4^+$)
DO	Dissolved Oxygen
DOM	Dissolved Organic Matter
D1	Deep Site (2019, 2020)
EMP	Environmental Monitoring Program
EPA	Environmental Protection Agency
Fe_2^+	Dissolved Iron
FeS	Iron Sulfide
FeS_2	Pyrite
F1	Fish Pen Site (2019, 2020)
H_2S	Hydrogen Sulfide
IC	Inorganic Carbon
Ka	Kilo-annum (one thousand years)
NaOH	Sodium Hydroxide
Na_2S	Sodium Sulfide
NE	Northeast
NH_4^+	Ammonium

Abbreviations	Descriptions
$NO_3^- + NO_2^-$	Nitrate + Nitrite
NW	Northwest
N_2	Nitrogen Gas
OC	Organic Carbon
OM	Organic Matter
O_2	Oxygen Gas
POM	Particulate Organic Matter
PSU	Practical Salinity Units
RPD	Redox Potential Discontinuity (Layer)
R1	Reference Site 2019
R2	Reference Site 2020
SC	Sediment Core
SD Transect	Transect from the shallow sites (S1, S2) towards the deep site (D1)
SO_4^{2-}	Sulfate
Spp.	Species (plural)
SRB	Sulfate-Reducing Bacteria
SWI	Sediment-water interface
S^0	Elemental Sulfur
S1	Shallow Site 2019
S2	Shallow Site 2020
TC	Total Carbon (OC and IC)
$TiCl_3$	Titanium Chloride
TIN	Total Inorganic Nitrogen
TS^{2-}	Total “dissolved” free sulfides ($H_2S + HS^- + S^{2-}$)
WC	Water Column

Symbol	Description	Units
C_{rem}	Carbon Remineralization	mmol $d^{-1}yr^{-1}$
db	Pressure	Decibars
Δ	Change	-
g	Gravitational Acceleration	m s^{-2}
k	Diffusion coefficient	m^2 s^{-1}
∂	Partial derivative	-
N_{rem}	Nitrogen Remineralization	mmol $d^{-1}yr^{-1}$
N^2	Buoyancy Frequency	s^2
ΔNH_4^+	Change in ammonium	mmol m^{-2} d^{-1}
φ	Porosity in sediment	%
ρw	Density	kg m^{-3}
$\Delta \rho w$	Change in Density	kg m^{-3}
S	Salinity	PSU
T	Temperature	°Celsius
ΔTS^{2-}	Change in sulfide	mmol m^{-2} d^{-1}
t	Time	days
V_p	Pore Volume	cm^3
V_t	Total Volume	cm^3
z	Depth	m or cm

ACKNOWLEDGMENTS

I would like to express my heartfelt gratitude to my supervisor Christopher Algar for giving me the invaluable opportunity to pursue my career and expand my knowledge in Oceanography. I will forever be grateful for his belief in my abilities, constant encouragement, and unwavering support. I am fortunate to have learned under his guidance, as he has been patient, positive, and accommodating throughout my time here.

I would also like to extend my sincere appreciation to my committee members for their support, constructive feedback, and valuable critiques. I am grateful to Craig Brown and Vicki Gozzola for their assistance and guidance in understanding the Whycocomagh Basin bathymetry and creating site maps for the study. Special thanks to Ramon Filguera for sharing his expertise in aquaculture and contributing to the formation of the reactive-transport model, which significantly expanded my knowledge in aquaculture chemistry and influences. I am also indebted to Bruce Hatcher for his enthusiasm and profound understanding of the Bras d'Or Lakes ecosystem. His guidance, expertise, and thoroughness have been invaluable throughout this process.

My sincere gratitude goes to the Algar-Buchwald lab for their kindness and inclusiveness. I am particularly grateful to Maria Armstrong, whose patience and guidance helped me grasp complex chemical analysis concepts, and Katie Frame, whose unparalleled enthusiasm in all aspects of oceanography has been inspiring.

I would like to acknowledge and thank several individuals and organizations who contributed to the successful completion of this study. First and foremost, I would like to thank

the Cape Breton Divers and Marine Services (CBDMS) and the W.V. Gumby crew for their invaluable operational assistance during the collection of sediment cores. I would also like to extend my appreciation to the Cape Breton University R.V. Exocet crew, who provided assistance with CTD casts, Niskin bottle sampling, sediment grab sample collection, and porewater extraction. Additionally, I am grateful to Peter Cranford and his team from the Department of Fisheries and Oceans (DFO) for their assistance in collecting samples during my absence.

To my boyfriend Benjamin Penton, thank you for joining me on this incredible adventure. Your unwavering support has meant the world to me and Noodle, and I appreciate your presence throughout this journey.

Lastly, I extend my deepest gratitude to the We'koqma'q First Nation for entrusting us with this project and for their continued support. Your collaboration and partnership have been instrumental in the success of this research.

CHAPTER 1

INTRODUCTION

Coastal waters, such as estuaries and inland seas, provide four main classifications of ecosystem services (cultural, provisioning, regulating, and supporting) from which society derives benefit (Lakshmi, 2021) and are significant from a global biogeochemical perspective; they make up only ~7-10% of the global ocean yet comprise ~10-30% of the global primary production (Bauer *et al.*, 2013). These ecosystems are important hydrologic, biogeochemical, and trophic transition zones between fresh and marine waters, and changes to these regional systems, both temporally and spatially, can alter their stability and disrupt natural processes at regional scales (Petrie & Bugden, 2002; Paerl *et al.*, 2006).

Long-term trends of oxygen decline are observed to be greatest within 30 km of coastal waters and are occurring at faster rates than in the open ocean (Gilbert *et al.*, 2010; Ni *et al*., 2019). In water, the solubility of oxygen gas (O_2) is relatively low and exhibits a decline with rising temperature and salinity. It diffuses through water more slowly than air. Thus, small shifts in concentration can have serious consequences on the structure of an ecosystem (Diaz*,* 2010; Ni *et al.,* 2019). Over the last century, oxygen-deficient coastal waters have expanded due to rising global temperatures and increased coastal eutrophication, which can have natural (e.g., chemical weathering, rainfall) and human-induced (anthropogenic) causes (Holmer & Kristensen, 1992; Diaz, 2010; Carstensen *et al.,* 2014; Ni *et al.*, 2019). Recent estimates suggest coastal eutrophication now covers an area of 240,000 km^2 of the seafloor (Carstensen *et al,* 2014). Eutrophication arises when high concentrations of inorganic nutrients increase the rate of

primary production and nutrient enrichment in excess of normal ecosystem processes (Diaz *et al.,* 2012). According to Paerl *et al.* (2006), increased nutrient loading, "...has been the primary causative factor for increased algal blooms, decreases in water clarity, and expanded hypoxia". Pollutant discharges have increased concurrently with various anthropogenic sources including inadequate sewage treatment discharge from coastal watersheds, excess fertilizer run-off from agriculture, and other commercial activities such as deforestation, papermills and aquaculture (Gray *et al.,* 2002; Strain & Yeats, 2002; Schendel *et al.,* 2004).

Both natural and anthropogenic effluents lead to an increase of readily decomposable organic matter (OM) in both particulate forms (POM), typically larger than 0.2 microns (isolated by the filtration of seawater), and dissolved forms (DOM) below 0.2 microns (Monroy *et al.,* 2017). Regardless of the source of OM, its decomposition by aerobic organisms increases the biological oxygen demand (BOD) of the system (Wildish *et al.,* 2001; Gray *et al.,* 2002; Brooks *et al.*, 2003; Cranford *et al.,* 2017). As time progresses, aerobic organisms in the water column degrade this OM, leading to an increase in oxygen consumption through respiration. Many particles (including feces and detritus) sink through the water column to the seafloor, where they may be further consumed; initially by aerobic biota in most environments, but then only by anaerobic microbes once all the oxygen is consumed through aerobic respiration. The by-products of this anaerobic respiration are reduced compounds that can then be re-oxidized when oxygen becomes available (Cranford *et al.,* 2017, 2020). The accumulation of these compounds creates an "oxygen debt" that must be repaid before a system can return to oxic conditions. This means that hypoxic and anoxic conditions are challenging to reverse once they occur (Gray *et al.,* 2002; Shaw, 2006). In stratified coastal waters, reduced water circulation can develop naturally into hypoxia, or even anoxia, whenever the BOD exceeds supply. The BOD is typically

concentrated at the seabed which results in anoxic conditions in extreme cases (Gray *et al.,* 2002; Diaz, 2010; Cranford *et al.,* 2017; Kelley *et al.,* 2019). While some species can tolerate or adapt to low oxygen conditions, most benthic epifaunal and infaunal species cannot survive in completely anoxic conditions (*i.e.,* devoid of dissolved oxygen), particularly if high concentrations of sulfide are present (Holmer *et al.*, 2005).

1.1 Carbon and Sulfur Cycling in Sediments

Benthic sediments are important regulators of the overlying water chemistry, and therefore play a key role in the development of hypoxia and anoxia in bottom water. Benthic fluxes can act as sources or sinks of nutrients and redox-sensitive solutes. As OM accumulates on the sea floor it is oxidized by benthic fauna and microorganisms through respiration. The by-products of respiration can either accumulate in the porewaters between sediment particles or be transported back to the overlying water through a combination of diffusion, involving the passive movement of dissolved compounds between the sediment and water, and various biologically mediated exchange processes, such as bioturbation (exchange processes occurring from the burrowing or feeding activities of organisms) and bio-irrigation (flushing and circulation processes throughout burrows facilitated by organisms in the sediment) (Gray *et al.,* 2002; Brooks *et al.*, 2003; Belley & Snelgrove, 2016; Cranford *et al.,* 2017). Under high accumulation conditions, reduced compounds, and excess OM increase the BOD, shoaling the oxygen penetration into the sediments and decreasing benthic faunal diversity and activity (Middelburg & Levin, 2009; Setaji *et al.,* 2017).

As oxygen is depleted in the upper layer of the sediment, oxygen supply is exceeded by metabolic demand and microorganisms begin to use alternative, less thermodynamically

favorable chemical species. These dissolved chemical species are distributed following a sequence of terminal, electron acceptors following the pattern recognized by Froelich *et al.* (1979), starting with available dissolved oxygen and then nitrate/nitrite, metal oxides, sulfate, and finally carbon (methane reduction) (Fig. 1.1; Hammond, 2001; Vaquer-Sunyer, 2010; Ramírez-Pérez *et al.,* 2015).

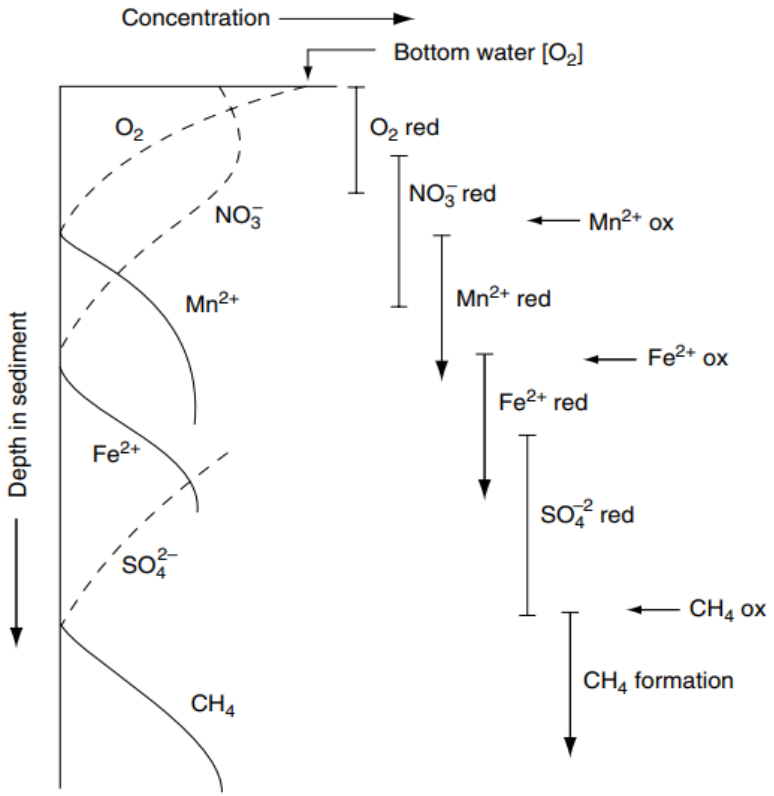

Figure 1.1: *A schematic diagram explaining the succession of chemical trends in pore water profiles as organic matter degrades and utilizes available and thermodynamically favorable electron acceptors. Emerson & Hedges (2008).*

Sulfate reduction is quantitatively the most important terminal process for OM decomposition in coastal sediments due to its abundance and availability in seawater compared to other electron acceptors (Jorgensen, 1977). This process is carried out by sulfate-reducing bacteria (SRB), which oxidize OM by reducing sulfate (SO_4^{2-}) into unstable, reduced sulfur species ($H_2S + HS^- + S^{2-}$). These reduced products from sulfate reduction are collectively referred to as total dissolved 'free' sulfides (TS^{2-}).

In the presence of dissolved oxygen (DO), TS^{2-} in sediments can be removed through re-oxidation back to SO_4^{2-} or precipitation into elemental sulfur (S^0) (Böttcher & Thamdrup, 2001). This removal process can occur either abiotically or biotically, involving microbial activity from species such as *Beggiatoa spp.* or newly discovered cable bacteria (Bjerg *et al.,* 2016). These microorganisms facilitate the conversion of sulfides to either sulfate or elemental sulfur, thereby reducing the concentration of TS^{2-} in sediments (Böttcher & Thamdrup, 2001). TS^{2-} can also bind to dissolved iron (Fe^{2+}) to form unstable iron sulfide (FeS) minerals. If burrowing infauna are present beneath the sediment-water interface (SWI), they can mix oxidized iron hydroxide ($FeOH_2$) minerals down into the anoxic sediments through the process of bioturbation. These iron hydroxides are then microbially reduced, liberating Fe^{2+}, which can then bind to TS^{2-} and over time convert to more stable pyrite (FeS_2) or iron monosulfide (FeS), which are considered permanent sinks and the main burial processes for TS^{2-} in many coastal environments (Boesen & Postma, 1988). The processes for FeS mineralization drive the sulfide zone deeper into the sediments creating a suboxic zone devoid of both oxygen and TS^{2-}. If bioturbation activity declines, such as due to the development of hypoxia, the suboxic zone narrows and TS^{2-} rises toward the SWI, potentially fluxing into the bottom water (Berner, 1985).

The onset of TS^{2-} accumulation in the sediments and/or water column can be detected by the depth of the redoxcline, or more specifically the redox potential discontinuity (RPD) layer, which represents the sharp transition zone between oxidizing (oxic) and reducing (anoxic) environments (Rosenberg *et al.*, 2001). The upward diffusion of TS^{2-} at the RPD layer can also create a unique environment for sulfur-oxidizing bacteria species, such as *Beggiatoa spp.*, visible in the formation of bacterial mats on the sediment surface or suspended in the water column (Rosenberg & Díaz, 1993; Hammond, 2001). The depth of the RPD layer depends upon the balance between DO diffusion versus DO consumption (Vistisen & Vismann, 1997; Barton *et. al.,* 2014). Increased input of effluents may increase remineralization rates of OM and render the sediments more susceptible to increased TS^{2-} (Njiru *et al.,* 2012), causing the RPD to shoal and widening the present anoxic zone, eventually reaching into the overlying water column.

Pearson (1978) conducted a study from 1970 to 1973 and developed an energy flow model for the input and output of organic matter of an oxygen-deficient estuary in a semi-enclosed fjord (due to a narrow 12 m long sill) along the coast of Sweden. The fjord has a max depth of 50 m and a salinity of ~22-30 with a naturally occurring anoxic zone beginning below the oxycline at 15-20 m. They found that if the influx of OM exceeds the outflux, DO concentrations will continue to be reduced and the RPD layer will continue to rise toward the surface waters (Pearson, 1978).

1.2 Aquaculture as a Contributor to Coastal Hypoxia and Anoxia

Preventing the development of anoxic conditions is a key goal for the sustainable development of aquaculture and is often the basis for regulatory frameworks in many jurisdictions globally (Biermann *et al.,* 2017). Aquaculture systems account for 45% of total global aquatic food production (Subasinghe *et al.,* 2009) and can enrich adjacent sediments with organic matter, contributing to eutrophication, hypoxia, and anoxia. Deposition of OM, primarily from fish feed and fecal waste, alters the sediment geochemistry of the SWI and impacts the response time of an ecosystem to trophic change (Pearson, 1978; Strain & Yeats, 2002; Hargrave, 2010; Cranford *et al.,* 2017). While salmonids, such as steelhead trout, are more acclimated to varying aquatic habitats, hypoxic conditions for salmonids typically begin when DO levels decrease to 2.5-3.0 mg/L (~78.0-94.0 μM); most salmonids exhibit mortality when DO levels reach between 1.0-2.0 mg/L (~31.0-63.0 μM) (Gray *et al.,* 2002; Carter, 2005). DO concentrations should remain above 3.9 mg/L (121.9 μM) to prevent juvenile mortality, although growth and metabolism begin to be affected by ~6.0 mg/L (187.5 μM) (Gray *et al.*, 2002; Carter, 2005). Overall, reduced oxygen levels, particularly in aquatic environments, can lead to decreased survival and emigration of aerobic organisms, causing reductions in the local abundance of wild fish populations and a loss of benthic biodiversity (Schendel *et al.,* 2004; Anttila *et al.,* 2015).

High levels of TS^{2-} are highly toxic to various aerobic organisms affecting their metabolism in ways to which most species cannot readily acclimate (Gray *et al.,* 2002; Hargrave *et al.,* 2008; Karstensen *et al.,* 2015; Cranford *et al.,* 2017). Micromolar (μM) concentrations of

TS^{2-} can begin to inhibit the respiratory chain between 2 to 38 μM, and higher concentrations can impede the delivery of oxygen to the mitochondria and important enzymes, as well as bind to blood proteins, such as hemoglobin, further restricting respiratory processes and forcing a higher oxygen utilization (Vaquer-Sunyer, 2010). Mass mortalities of benthic organisms may become a consequence of environmental stressors as TS^{2-} concentrations rise to toxic levels in benthic sediments and water columns (Gray *et al.,* 2002; Vaquer-Sunyer, 2010).

For these reasons TS^{2-} concentrations are widely used as an indicator of anoxic conditions as the toxic effects on benthic fauna have an inverse relationship to the oxic state of sediments (Holmer & Kristensen, 1992; Hargrave, 2010). In several countries, including Canada, aquaculture Environmental Monitoring Programs (EMPs) use a benthic mean standard concentration measurement of TS^{2-} in the top few centimeters of the sediment column to assess the gradient of organic enrichment that could affect benthic species (DFO, 2015; Cranford *et al.,* 2017). Under the Canadian Fisheries and Coastal Resources Act (Government of Canada, 2021), Nova Scotian aquaculture operations are required to comply with the provincial EMPs as per the stipulation of leases and licenses issued. For Nova Scotia, a lease site classified as having failed to comply with EMP standards has mean sediment TS^{2-} concentrations of > 3,000 μM (hypoxic) and ≥ 6,000 μM (anoxic) (Province of Nova Scotia, 2021). By locating aquaculture leases in well-oxygenated waters with rapid circulation, or in deep water, the implications of OM accumulation and high BOD on benthic assemblages are more readily avoided, as these environments tend to have a higher capacity to dilute and disperse fish farm waste products (Giles, 2008; Keeley *et al.,* 2019).

Monitoring standards for benthic enrichment are mainly reflective of oxygenated systems with benthos present (both macro- and micro-organisms). However, the environmental impacts

of naturally occurring anoxia on benthic communities and how the effects of anthropogenic enrichment should be monitored in them is less well studied. The benthic communities in naturally occurring anoxic zones are already microbially dominated, lacking the benthic macrofauna that current regulations have been developed to protect. There are some examples of aquaculture farms above natural anoxic, semi-enclosed marine systems, mainly in the Black and Mediterranean Seas (Poulos, 2020), the Black Sea being the largest anoxic basin in the world (Wijsman *et al,* 2001; Tugrul *et al.,* 2014;). These farms are typically situated over strongly stratified water columns exceeding 500 m depths, effectively mitigating waste deposition and resuspension directly beneath farmed areas (Kapranov *et al.,* 2021).

The motivation for this thesis is to examine the influence of an aquaculture farm on a naturally occurring anoxic zone located in a shallow, estuarine environment. The We'koqma'q First Nation's Steelhead Trout (*Oncorhynchus mykiss*) Aquaculture Farm is situated above the permanently anoxic Whycocomagh Basin, located in the western portion of the Whycocomagh Bay. The Whycocomagh Bay is part of the Bras d'Or Lakes, recognized as a UNESCO Biosphere Reserve, and is a coastal, inland-estuary system on Cape Breton Island, Nova Scotia, Canada. The Whycocomagh Basin, characterized by its roughly circular shape and steep sides, reaches a depth of 48 meters. Due to its location approximately 70 kilometers away from open-ocean boundaries and its encirclement by the shoreline and shallow sills, the Basin experiences limited influence from tidal currents and mixing, which contribute to restricted water circulation. Restricted water circulation and low water currents within the Basin have likely resulted in a greater deposition of less dense particles on the seafloor. This, along with the presence of BOD, contributes to a further reduction in the potential for oxygen renewal (Pearson, 1978; Strain & Yeats, 2002). Freshwater-flow into the Whycocomagh Bay stems from numerous small brooks

and rivers, as well as rainfall (Gurbutt & Petrie, 1995). The farm was started in 2016, and currently operates approximately 70 open mesh fish pens producing roughly a million fish per year and utilizing approximately 2500 metric tons of feed (Melissa Rommens, farm consultant; personal communication). The Whycocomagh Basin remains vertically stratified throughout the year with a strong redoxcline that separates an upper oxygenated layer from the anoxic bottom water (Fig. 1.2) (Gurbutt & Petrie, 1995; Petrie & Budgen, 2002). There are associated hazards from the potential upwelling of anoxic water, which has killed open-pen fish in the basin before (Robin Stuart, former farm manager; personal communication), making sustainable management of the fish farm challenging.

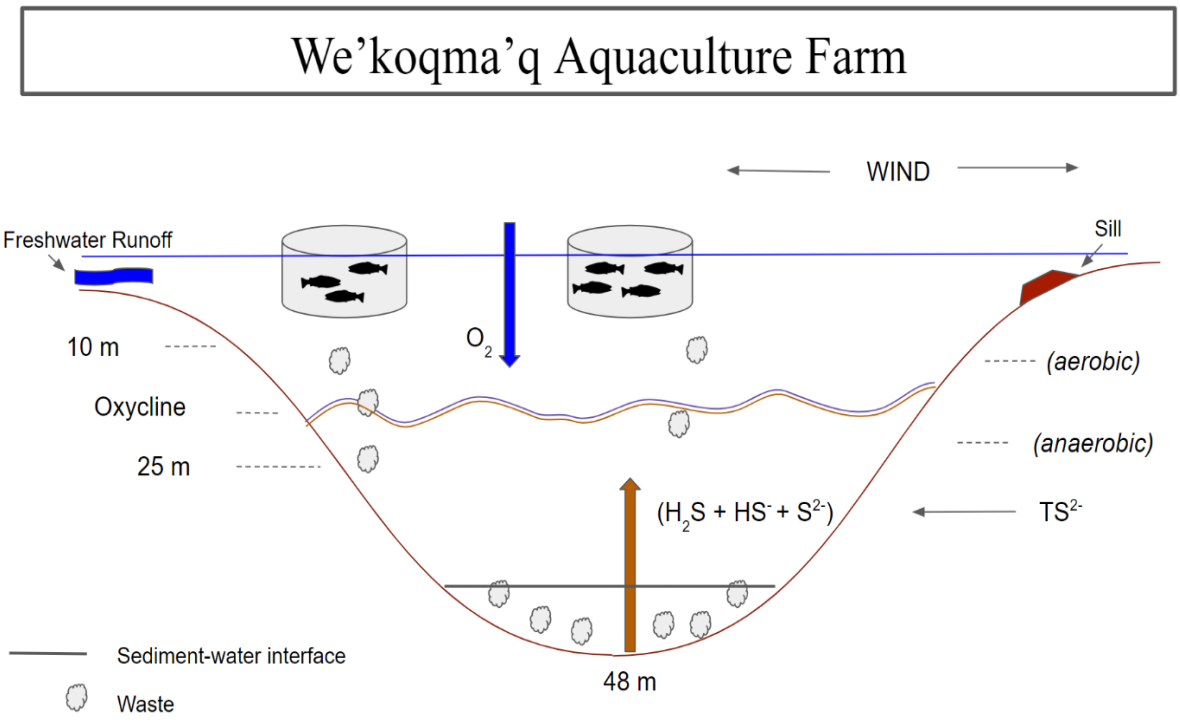

Figure 1.2: *Schematic diagram of the We'koqma'q Aquaculture Farm in the semi-enclosed Whycocomagh Basin exhibiting the oxic and anoxic layering system and total sulfide biogeochemical cycling. In the surface oxic layer, influence from air-sea gas exchange (deemed as wind), and freshwater inputs from the surrounding watershed help to circulate dissolved oxygen. Fish pens extend to ~8 m depth, just above the oxycline, which fluctuates between ~15 – 20 m throughout the year and divides the upper aerobic and lower anaerobic layers. Organic matter (fish waste, excess food, etc.) accumulates on the bottom beneath the pen arrays as waste. The waste material is then utilized by SRB in the anoxic layer, producing hydrogen sulfide and other ionization byproducts.*

The bottom 30 m of the Whycocomagh Basin have been measured as anoxic for half a century and TS^{2-} levels are naturally high, resulting in the absence of epibenthic macrofauna (Krauel, 1975; Strain & Yeats, 2002; Punshon *et al.,* 2022). These features make the Basin an ideal location to study the effect of aquaculture on benthic ecosystems already adapted to anoxic, high sulfide conditions. Furthermore, background (naturally occurring or baseline) sulfide levels in the Basin sediments are above the limits prescribed in the Nova Scotia Provincial Aquaculture

EMP Standards (Fisheries and Coastal Resources Act, 1996), suggesting current regulations are insufficient for monitoring the environmental effects of the farm. This raises the question of whether current standards are suitable for quantifying the impacts of aquaculture on such naturally occurring anoxic zones. To address this, my thesis will investigate the following two questions: 1) *How does accumulated farm waste alter sediment carbon and sulfur cycling in the sediments beneath the fish pens in the Whycocomagh Basin?* and 2) *How do the altered sediment dynamics and sediment sulfide production due to fish farm waste affect the concentration of sulfide in the water column of the anoxic zone?*

1.3 Outline

To answer these questions, the thesis is divided into four chapters, organized in the style of a publication:

- **Chapter 2** outlines the Bras d'Or Lakes and historical background information about Whycocomagh Bay and Whycocomagh Basin. Details of the sample site and methods used in this study are also presented.
- **Chapter 3** presents the results of the methods detailed in Chapter 2 and focuses on determining what effect the accumulation of farm waste has on the organic carbon and sulfur cycling in the sediments. To do this, sediment organic carbon and porewater geochemistry were measured over a two-year field study (2019-2020). Sediments were sampled at a fish pen site and a reference site, both during a period of active farming (2019) and after 1 year of fallowing (2020). By examining the geochemical profiles of the sediments (e.g., sulfide, ammonium, iron, nitrate/nitrite, organic carbon, and inorganic nitrogen) at the farmed and

reference sites, the influence of the aquaculture farm on sediment geochemistry was determined.

- **Chapter 4** presents a summary of the main results in Chapter 3 compared to the literature, along with sediment sulfide fluxes, both from reference sediment and beneath the fish pens (estimated from the data presented in Chapter 3). These fluxes were then used as boundary conditions for a simple reactive-transport model representing sulfur cycling in the anoxic zone of the Whycocomagh Basin to predict how continued farming might impact sulfide concentrations in the bottom water.
- **Chapter 5** provides a summary of the study's final conclusions and limitations, along with a discussion of future research directions.

The First Nations apply the Mi'kmaq principle of Netukulimk to aquaculture which highlights that if practices harm Mother Earth, they will be discontinued (Prosper, 2011). This approach can benefit from a two-eyed seeing approach (both an Indigenous and Western lens). The hope is that the work presented in this thesis can foster Netukulimk by helping farm managers understand the relationship between the fish farm and ecosystem that supports it.

CHAPTER 2

BACKGROUND AND METHODS

In estuaries and coastal basins, the relatively shallow water depth ensures a large portion of sinking organic matter accumulates on the sediments, and sediment remineralization plays an important role in the development of coastal hypoxia and anoxia. In this thesis, the Whycocomagh Basin is used to study how perturbations from OM loading alter the sediment biogeochemistry in coastal waters that have already transitioned to anoxia. The Whycocomagh Basin is an ideal location for such a study since it has a persistent, naturally occurring anoxic zone with sulfidic bottom water, historical observations of the hydro-chemical and chemical water column properties (as discussed later), and a fin-fish aquaculture operation. The aquaculture farm provides point-source inputs of labile OM in the form of fish waste and excess feed accumulating on the sediments beneath the fish pens. Examining the sediments both near and away from a fish pen array and after one year of fallowing (periodic cessation of fish production) provides an opportunistic perturbation experiment of how OM enrichment from the fish pens alters sediment geochemistry in a permanently anoxic environment. In addition, the examination of how the enrichment of OM from the fish pens affects the sediment geochemistry of the Basin yields valuable knowledge that can aid the We'koqma'q First Nation in their efforts to sustainably manage the aquaculture farm in alignment with the principles of Netukulimk.

2.1 Hydrography of the Bras d'Or Lakes

The Bras d'Or Lakes (BdOL) constitute several inter-connected basins and channels with variable depths (average 30 m; maximum 280 m) covering a total area of 1080 km^2 (Fig. 2.1). Glaciation and deglaciation periods over ca. ~15 ka have been inferred from sea level curves, bathymetry, and sediment core profiles, exhibiting the fluctuation of ice cover and melt that led to the formation of the BdOL. The recent period of rising sea level (~10–4 ka) created the present marine conditions in the estuary, with an average salinity range of ~20-26 PSU (Lambert, 2002; Shaw *et al.,* 2002; Yang *et al.,* 2007).

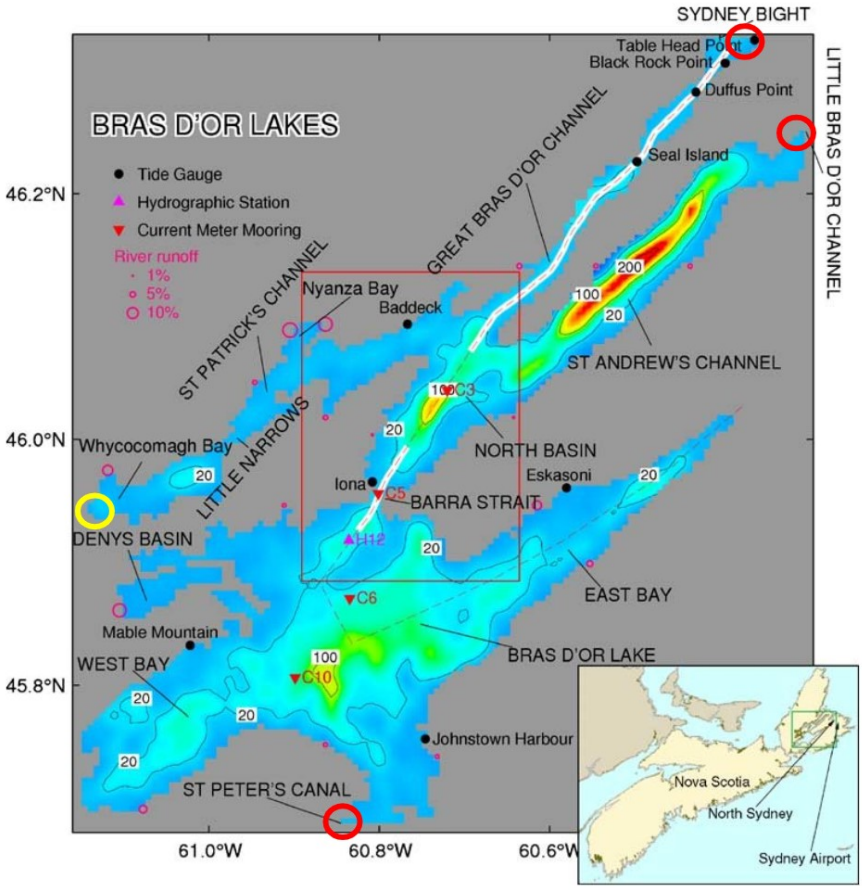

Figure 2.1: *Map of the Bras d'Or Lakes of Cape Breton Island, Nova Scotia, Canada. Bathymetric features are exhibited by the colored shading and the depths in meters. The yellow circle is referred to as the Whycocomagh Basin, where the We'koqma'q Aquaculture Farm is located. Open red circles represent the three Atlantic Ocean outlets that exchange with the lake system. The red rectangle, labeled channels, tidal gauges, hydrographic stations, meter moorings, and depth contours can be reviewed in-depth in Petrie & Budgen (2002) and Yang et al. (2007).*

The BdOL has three outlet exchanges with the Atlantic Ocean, with the Great Bras d'Or Channel being the most significant. That Channel and the Little Bras d'Or Channel constitute the primary oceanographic transition zone between the waters of the NW Atlantic (Sydney Bight) and those of the BdOL (Yang *et al.*, 2007). Restricted seawater inflow from the eastern channels, and to a lesser extent, the St. Peter's Canal, result in spatially variable thermoclines and

haloclines among the secondary channels and bays in the estuary. The geographic and oceanographic complexity creates a great diversity of habitats in the BdOL for both warm and cold-water organisms – with resident species representing more than 30 degrees of latitude along the Atlantic Coast (Lambert, 2002). Yang *et al.* (2007) created an ocean-circulation model to examine the BdOL estuary's response to local hydrodynamic forcing and connected circulation systems. They demonstrated reduced hydrodynamic connectivity in the western portions of the BdOL system, partially offset by land-based freshwater inputs. These western areas typically have low-slope shorelines with marshes that are natural accumulation zones for the buildup of organic and inorganic materials (Shaw, 2006). Some of these areas, such as the Whycocomagh Bay, experience natural algal blooms and, or enrichment of nutrient and mineral loads.

2.1.1 The Whycocomagh Bay

The Whycocomagh Bay is an enclosed estuarine embayment located far inland (~60-70 km) from its ocean-connecting channel, and is isolated from the rest of the BdOL system by the Little Narrows sill (~0.2 km wide, ~0.5 km long, and ~15 m deep). The primary sediment in the Whycocomagh Bay is lacustrine, which refers to sediments associated with lakes, and marine mud, which is bioturbated, brown silty mud found in marine or oceanic environments, often containing portions of silt and sand (Shaw *et al.*, 2002); some small areas consist of ice-contact deposits which derived from glacial till forming moraine ridges and drumlins in the bay (Petrie & Bugden, 2002). Semi-diurnal tidal mixing of water in the BdOL is considerably more vigorous towards the Sydney Bight and decreases toward zero in the Whycocomagh Bay due to restricted water exchange from the Little Narrows, limiting the intertidal range to < 5 cm on average (Petrie & Bugden, 2002), with a net water circulation of < 100 $m^3 s^{-1}$ near-surface (0-10 m) and

~100-200 m^3 s^{-1} sub-surface (≥10+ m) (Gurbutt & Petrie, 1995; Petrie & Budgen, 2002). Ice cover in the Whycocomagh Bay varies between years, but on average accumulates from January to April, with ≥ 70% ice coverage peaking in March (Petrie & Budgen, 2002; Manning *et al.,* 2019). Variable ice cover in the winter prevents vertical mixing with the deep water (Krauel, 1975; Manning *et al.,* 2019). Fresher, surface waters from watershed inflow are stratified above denser, saline sub-surface waters derived from ocean inflow (Petrie & Budgen, 2002).

Whycocomagh Bay is comprised of two basins (eastern and western) that are separated by a shallow (~7 m deep), Mid Bay sill (Fig. 2.2). The eastern basin is much larger and slopes gradually from a wide margin toward a maximum depth of ~38 m. The western basin, referred to as the Whycocomagh Basin, is smaller and contains a deep (~48 m), steep-sided basin that is largely surrounded by land and permanently anoxic below ~20 m depth (Krauel, 1975; Punshon *et al.,* 2022). Previous analysis of nutrient and oxygen data has revealed distinct regenerative processes for DO and OM degradation in both basins. The estimated flushing times for the Whycocomagh Basin indicate that surface waters undergo flushing approximately every 0.7 years, while deep waters experience flushing approximately every 2.0 years (Krauel, 1975; Petrie & Budgen*,* 2002; Strain & Yeats, 2002; Manning *et al.,* 2019).

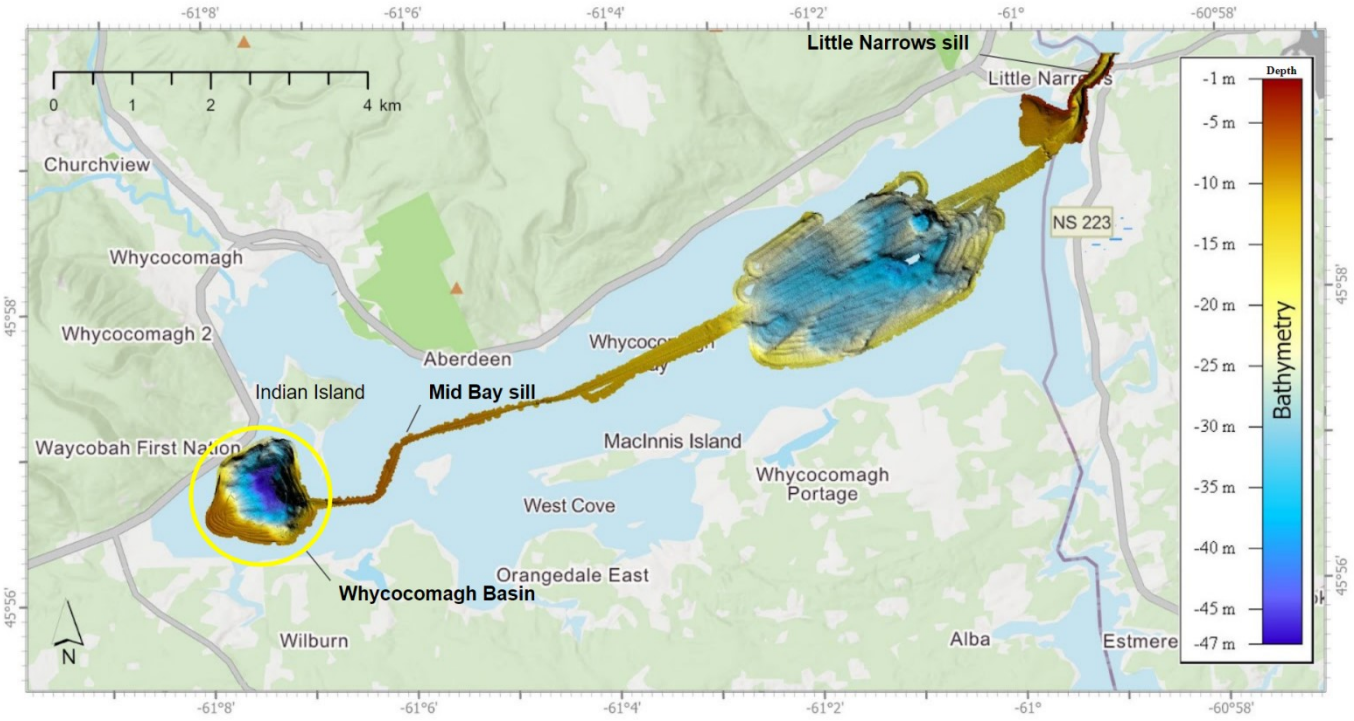

Figure 2.2: *A digital elevation model (DEM) of the Whycocomagh Bay seafloor was created using multibeam bathymetric data sourced from the Canadian Hydrographic Service Non-Navigational (NONNA) Bathymetric Data (Canadian Hydrographic Service, 2022). The DEM was created with the assistance of Dr. Craig Brown's Lab at Dalhousie University. The Little Narrows sill acts as a barrier, separating the Bay from the rest of the BdOL. The Whycocomagh Basin is indicated by a yellow circle, while the approximate location of the Mid Bay sill is identified (Shaw et al., 2006). The color ramp on the right-hand side corresponds to the depth (in meters) of the seafloor, accompanied by geographic coordinates.*

The BdOL is home to five major First Nation communities, including the We'koqma'q First Nation, who reside along Whycocomagh Bay and have experienced a steady increase in population (Parker *et al.,* 2007). In the past, quarrying and industrial shipping/transport of gypsum and limestone took place along Whycocomagh Bay, facilitated by a loading facility located at the Little Narrows. The NE and NW regions of Cape Breton Island saw a boom in industrial forest development and urbanization for the pulp and paper industry and exports from 1899 to the 1960s, known as the Big Lease, which included transport along the Bay toward the eastern channels and covered over 620,000 acres (Sandberg, 1991). Since road and railway

systems were not yet developed in the area, the main route for logging exports was via waterways and shipping piers. The extractive nature of forestry likely resulted in increased organic nutrient effluent (primarily cellulose) into the watersheds and significant levels of bark deposits along the shores of the greater BdOL. The cumulative anthropogenic effects from land-based inputs (such as agriculture, deforestation, and sewage treatment discharge), recreational boating, and fin-fish aquaculture have already been ranked as high in the Whycocomagh Bay watersheds, rendering the Bay more susceptible to these adverse effects if they were to grow (Pease, 1974; Strain & Yeats, 2002; Parker *et al.,* 2007; Sterling *et al.,* 2014).

Previous biological surveys of the BdOL found that Whycocomagh Bay is one of two areas with low species diversity and has limited commercial fisheries leases, with wild oysters being the most significant, until overfishing and parasites reduced their numbers to small pockets (Lambert, 2002; Parker *et al.* 2007). In the 1970s, Rainbow Trout aquaculture operations were introduced to the area, and due to past and recent escapee events, a feral, reproducing population now exists, contributing to an increased popularity of the fishery in the region (Alexander *et al.* 1986; Parker *et al.,* 2007; Madden *et al.,* 2010).

2.1.2 The Whycocomagh Basin

As of 2004, no commercial Rainbow Trout aquaculture operations in the BdOL were sustained, despite several attempts. In the 1980s, over a million Rainbow Trout escaped and formed feral, reproductively successful populations. These populations are particularly abundant in the Skye River that flows into the Whycocomagh Bay (Parker *et al.,* 2007). The current fish farm sites operated by the We'koqma'q First Nation have been in operation since 2011-2012. Prior to the establishment of the fish farm, however, there was little evidence that the

development of the anoxic zone in the Basin could be attributed to anthropogenic eutrophication, as is the case for most marine eutrophic coastal zones (Kirchman, 2021).

Based on EMP data from 2012 to 2019, the average sediment sulfide concentrations at the existing We'koqma'q Aquaculture Farm fall within the Hypoxic B and Anoxic categories according to Hargrave *et al.'s* (2008) quantitative ecological quality status (EQS) application for sediment benthic enrichment measurements (DFO Maritimes Region, 2018). However, Cranford *et al.* (2017) discovered that the standard protocols for measuring TS^{2-} concentrations for EQS assessments, such as those used by Hargrave *et al.* (2008), underestimate impact thresholds due to the loss of TS^{2-} by the original S2-ISE method. Concentrations were much higher when measured using the S2-UV method, which should lead to reclassification as Anoxic. The authors also suggested that employing multiple indicators in regularly oxygenated systems would yield a more comprehensive understanding of benthic conditions. Conversely, in naturally deoxygenated sediments like those found in the Whycocomagh Basin, where oxygen levels are consistently low, the authors suggest that a single-indicator approach is sufficient.

The Whycocomagh Basin experiences limited surface and sub-surface tidal mixing, resulting in poor water circulation and increased nutrient retention. This has led to a high demand for oxygen and the expansion of the anoxic zone with a 10-12 m thick oxic surface layer and an anoxic layer at depths below 15-20 meters (Manning *et al*., 2019), Historical measurements of bottom water chemistry at depths of ~44 meters showed no detectable concentrations of DO and $NO_3^- + NO_2^-$ (0.0 µM), but detected 30-62 µM of TS^{2-} and 66-136 µM of NH_4^+ (Krauel *et al.,* 1975; Strain & Yeats, 2002). Recent measurements by Punshon *et al.* (2022) revealed a tenfold increase in TS^{2-} concentrations to 734 µM in June and 1,047 µM in December, along with a threefold increase in NH_4^+ concentrations to 315.5 µM in June and a slight decrease to 291.0 µM

in December, indicating an increase in eutrophication. Bottom water temperatures in the Whycocomagh Basin range between 1.8 - 3.2 °C (Krauel, 1975; Strain & Yeats, 2002), with a more recent measurement showing a slight decrease to 2.9 °C (Punshon *et al.,* 2022). Studies have also observed decreasing deep water salinity values over time, with measurements of 22.7 - 24.9 PSU in 1973-75 (Krauel*,* 1975), 23.05 - 23.07 PSU in 1995-97 (Strain & Yeats, 2002), and more recently, 22.9 PSU in 2017 (Punshon *et al.,* 2022).

The Whycocomagh Basin experiences annual cycling of OM input, which is balanced by a net loss during the winter months through physical (i.e., diffusion across the oxycline) and biological processes (i.e., sulfate-reducing bacteria or sulfur-oxidizing bacteria, *Beggiatoa spp*.) (Manning *et al.,* 2019). However, currently, there seems to be no steady-state in the Basin. Recent studies indicate that there is an increase in OM input from anthropogenic sources, such as nearby sewage effluent and aquaculture operations, leading to increases in bottom water values (Punshon *et al.,* 2022). This suggests that the Whycocomagh Basin is experiencing increased organic enrichment loading to the benthic environment, which could lead to the accumulation of pollutants on the seabed. This, in turn, could impact sediment biogeochemistry and the aquaculture facility (Karakassis *et al.,* 2000; Punshon *et al.,* 2022).

2.2 Methods

2.2.1 Study Site and Sample Descriptions

Sediment and water sampling was conducted at the We'koqma'q Aquaculture Farm located in the Whycocomagh Basin (45.946°N, 61.125°W) during November 2019 and September 2020 (Fig. 2.3). Samples were collected toward the end of the farming season to measure the greatest impact of solid fish farm effluent on the biogeochemistry of the Basin, and on days with little wind so the boat was stable during sampling. In 2019, the farm housed approximately 70 fish pens making up 7 pen arrays in the Basin. However, it is important to note that fish pen arrays were not always stocked and were not static between years and were moved to various locations within the Basin, with approximately to allow for the fallowing/restocking of pens during each season.

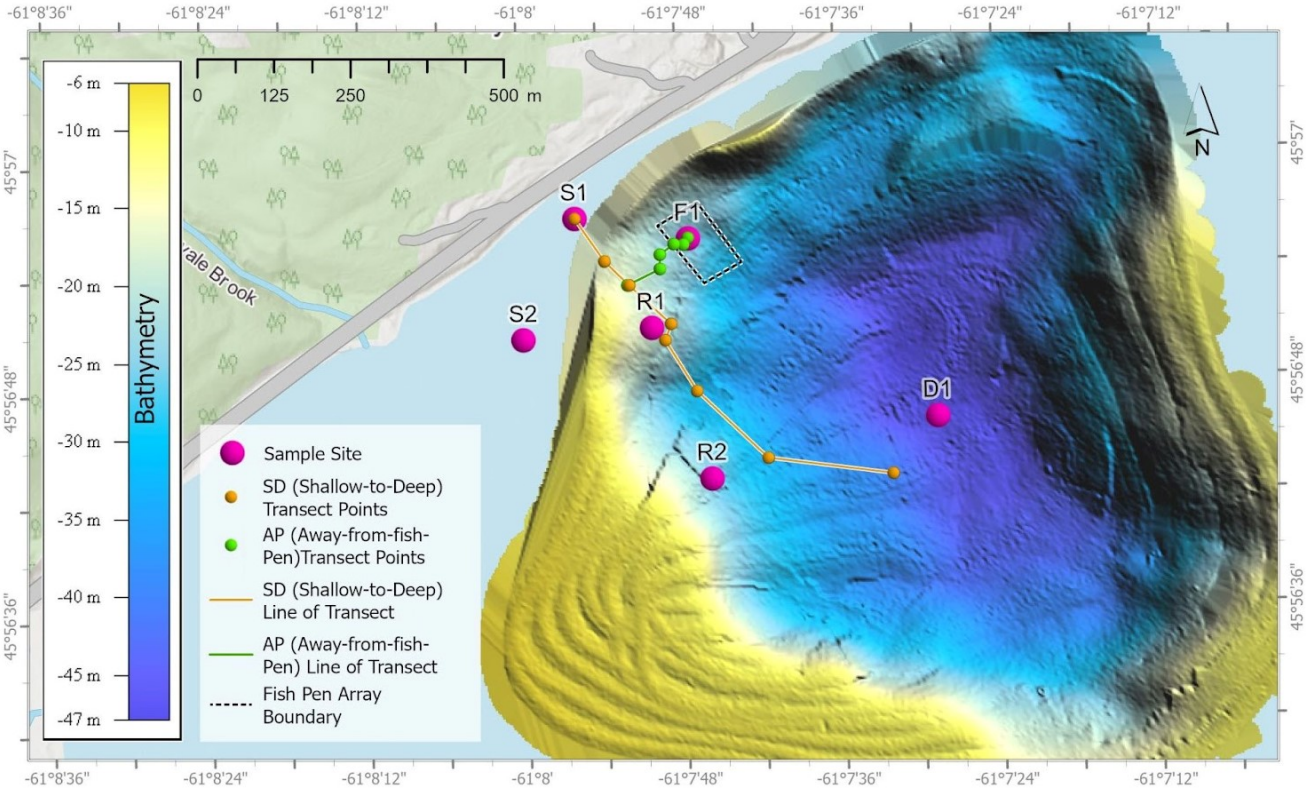

Figure 2.3: *The location of the water column and sediment core sample sites (S1, S2, R1, R2, F1, D1) positioned above digital elevation model (DEM) bathymetry contours of the Whycocomagh Basin. Bathymetric DEM imaging was provided by Dr. Craig Brown's Lab at Dalhousie University, utilizing the Canadian Hydrographic Service Non-Navigational (NONNA) Bathymetric Data (Canadian Hydrographic Service, 2022). The sediment grab transect lines and associated transect points are depicted. The SD Transect is represented by the orange line, which extends from shallow to deep waters, while the AP Transect is indicated by a green line, moving away from the boundary of the fish pen array (shown as dashed-lined rectangle) at similar depths.*

In 2019, water samples and two sediment cores were collected at a shallow site (S1), a fish pen site (F1) located near the center of an active fish pen array, and a reference site (R1). In 2020, water samples and three sediment cores were collected at a shallow site (S2), the fish pen site (F1) during a fallowing period, and a reference site (R2). Locations and types of samples collected at each site are summarized for 2019 (Table 2.1) and 2020 (Table 2.2). In 2019, the F1 site was stocked with adult Steelhead Trout but was fallow when sampled again in 2020. In

2020, the shallow and reference sites were sampled at different locations as a result of the relocation of fish pens and, or equipment above the initial sample sites. However, these sites were selected to ensure they represented similar, undisturbed locations at comparable depths. In both years, only water column samples were collected at the deep site (D1), which is located at the deepest point in the Whycocomagh Basin (48 m) and is also an Atlantic Zone Monitoring Program site (*Atlantic Zone Monitoring Program (AZMP)*, 2022).

Table 2.1: *November 2019 sample site characteristics. Samples taken refer to water column (WC) and, or sediment core (SC). The sample analysis performed is indicated with a (Y). Details on sample analysis and methods can be found in Table 2.3.*

Site Description	Site #	Lat/ Long	Status	Sample Taken	Core #	Water Depth (m)	Sample Analysis			
							Porewater	CHN	Microsensor	Porosity
Shallow (2019)	S1	45.94903, -61.13245	NA	WC, SC	C1	11	**Y**	**Y**	-	-
Shallow (2019)	S1	45.94903, -61.13245	NA	WC, SC	C8	11	-	-	**Y**	**Y**
Reference (2019)	R1	45.9475, -61.1306	NA	WC, SC	C5	23	**Y**	**Y**	-	-
Reference (2019)	R1	45.9475, -61.1306	NA	WC, SC	C12	23	-	-	**Y**	**Y**
Fish Pen (2019)	F1	45.94876, -61.1298	Stocked	WC, SC	C2	25	**Y**	**Y**	-	-
Fish Pen (2019)	F1	45.94876, -61.1298	Stocked	WC, SC	C10	25	-	-	**Y**	**Y**
Deep (2019)	D1	45.9461, -61.1246	NA	WC	NA	48	-	-	-	-

*Status: Stocked (fish present in fish pen), Fallow (no fish present in fish pen), NA (no fish or fish pen present)

Table 2.2: *September 2020 sample site characteristics. Samples taken refer to water column (WC) and, or sediment core (SC). The sample analysis performed is indicated with a (Y). Details on sample analysis and methods can be found in Table 2.3.*

Site Description	Site #	Lat / Long	Status	Sample Taken	Core #	Water Depth (m)	Sample Analysis			
							Porewater	CHN	Microsensor	Porosity
Shallow (2020)	S2	45.94736, -61.13331	NA	WC, SC	C1	10	**Y**	**Y**	-	-
Shallow (2020)	S2	45.94736, -61.13331	NA	WC, SC	C2	10	**Y**	**Y**	-	-
Shallow (2020)	S2	45.94736, -61.13331	NA	SC	-	10	-	-	**Y**	**Y**
Reference (2020)	R2	45.94660, -61.1297	NA	SC	-	31	-	-	**Y**	**Y**
Reference (2020)	R2	45.94660, -61.1297	NA	WC, SC	C5	31	**Y**	**Y**	-	-
Reference (2020)	R2	45.94660, -61.1297	NA	WC, SC	C10	31	**Y**	**Y**	-	-
Fish Pen (2020)	F1	45.9488, -61.1298	Fallow	SC	-	25	-	-	**Y**	**Y**
Fish Pen (2020)	F1	45.9488, -61.1298	Fallow	WC, SC	C11	25	**Y**	**Y**	-	-
Fish Pen (2020)	F1	45.9488, -61.1298	Fallow	WC, SC	C12	25	**Y**	**Y**	-	-
Deep (2020)	D1	45.94625, -61.12661	NA	WC	NA	48	-	-	-	-

*Status: Stocked (fish present in fish pen), Fallow (no fish present in fish pen), NA (no fish or fish pen present)

Finally, sediment surface grab samples were collected at points along two transect lines shown in Figure 2.3: 1) the SD Transect going from shallow to deep waters (orange line), and 2) the AP Transect moving away from the fish pen array at similar depths (green line). In 2019, eight transect points were collected along the SD Transect and six were collected along the AP Transect. In 2020, only four of the eight SD Transect points were collected and only one of the six AP Transect points was collected.

For each sample type (water column, sediment core, and sediment grab) a subset of measurements for TS^{2-} ($H_2S + HS^- + S^{2-}$), dissolved inorganic nitrogen ($NO_3^- + NO_2^-$, NH_4^+), Fe^{2+}, DO and total carbon (TC), both organic and inorganic, and total inorganic nitrogen (TIN) were analyzed following the methods outlined in Table 2.3. One sediment core from each site was used for sediment micro-profiling at high-resolution (~100 μm) of DO (at the shallow sites only), pH, and H_2S across the SWI.

Table 2.3: *Dissolved nutrient analysis methods. Full citations of methods in bibliography.*

Nutrient	Sample Type	Instrument	Method	Detection Limit (μM)	Citation
Ammonium (NH_4+)	Porewater, Filtered Seawater	Thermo Scientific Evolution 260 Bio UV-Visible Spectrophotometer	Indophenol Blue	1	Solorzano, (1969).
Dissolved Iron (Fe^{2+})	Porewater	Thermo Scientific Evolution 260 Bio UV-Visible Spectrophotometer	Ferrozine	2	Stookey, (1970).
Nitrate +Nitrite ($NO_3^- + NO_2^-$)	Porewater, Filtered Seawater	Analytical Sciences NOx 5100 Thermalox Detector	Vanadium Reduction & Chemo-luminescence Detection	0.4	Braman & Hendrix, (1989).
Total Free Sulfide (TS^{2-})	Porewater, Filtered Seawater	(2019) Thermo Scientific Orion™ Aquamate 8000 UV Spectrophotometer	Methylene Blue	3	Cline, (1969).
		(2020) Thermo Scientific Evolution 260 Bio UV-Visible Spectrophotometer	Direct UV Spectrophotometric Detection	0.5	Guenther et al., (2001).
Total Carbon (TC) and Total Inorganic Nitrogen (TIN)	Dry Sediment	Elemental Vario MicroCube Analyzer	Dry Combustion and Gas Detection	NA	NA

*Method detection limit (EPA, 2016).

2.2.2 Water Sampling

Water sampling and CTD casts were done from a rigid-hull inflatable boat (R.V. Exocet) fitted with an electric winch. At the D1 site, discreet water samples were collected in 2019 (at 0, 1, 5, 10, 12.5, 15, 17.5, 20, 30, 40, and 45 m) and in 2020 (at 0, 1, 5, 10, 12.5, 15, 17.5, 20, 25, 35, and 47 m) using a mix of 2L and 5L Niskin Bottles. Water samples were subsampled and analyzed for TS^{2-} and dissolved nutrients ($NO_3^- + NO_2^-$, NH_4^+, Fe^{2+}) and filtered on the boat using a 0.45-micron PES syringe filter. Analytical determinations were made according to the methods outlined in Table 2.3. A 25 cm Secchi disk was deployed at the D1 site for both years to gauge turbidity.

Conductivity-Temperature-Depth (CTD) casts for hydrographic properties of temperature (T), salinity (S), density (ρ) were measured at the F1 and D1 sites using a Seabird Electronics SBE-25 CTD equipped with an SBE-43 dissolved oxygen sensor, thermometer, pressure gauge, conductivity probe, and fluorometer. Depth was measured by pressure in decibars (db), where 1 db corresponds to an increment of ~1 m depth. T was measured in degrees Celsius (°C) and the units for S were reported in Practical Salinity Units (PSU).

For measurements of stratification, the density of seawater (ρ_w) and buoyancy frequency (N^2) were calculated using the *OCE R Package* by Kelley *et al.* (2022). Density was computed using the following equation of state for seawater written approximately as:

$$\Delta\rho_w = \rho(T, S, db) \quad \text{(Eq. 1)}$$

where ($\Delta\rho_w$) is the change in density over time with in-situ temperature (T), salinity (S), and pressure (db). Calculations result in a number on the order of 1000 $kg^1\ m^{-3}$. Buoyancy frequency (N^2) was calculated according to the following equation:

$$N^2 = \left(\left(-\frac{g}{\rho_{w(0)}}\right)\left(\frac{\delta\rho_w(z)}{\delta z}\right)\right) \quad \text{(Eq. 2)}$$

where (N^2) is the buoyancy frequency, (g) is the gravitational acceleration, and ($\rho_{w(0)}$) is the average density at a specific depth (z).

2.2.3 Sediment Grab Samples

Sediment grab samples were collected along the two transect lines (SD and AP) in 2019 and 2020 (Fig. 2.3). The SD Transect was approximately 350 m long and provided an estimate of background sediment TS^{2-} concentrations in the basin at different depths going from shallow waters (~10 m depth) toward deeper waters (~40 m depth). The sediment grab wire could not reach the deep site (D1 site) in the basin, so the deepest grab sample collected for the SD Transect was ~31 m. The AP Transect was approximately 200 m long and provided an estimate of sediment TS^{2-} concentrations at similar depths (20-25 m) moving away from the fish pen array (F1 site) parallel to the shoreline.

In 2019, sediment grab transect samples were collected in collaboration with Dr. Peter Cranford (St. Andrews Biological Station, DFO) and again in 2020 at approximately similar locations. A total of 14 sediment grab samples were collected in 2019 using an Ekman Grab (box size: 152 x 152 mm; volume of box: 3.5 L). In 2020, only four sediment grab locations in 2019 were sampled beginning ~50 m from the start of each transect using a Peterson Grab (box size: 180 x 220 mm; volume of box: 9.9 L).

For both years, Niskin bottles were also used to collect bottom water samples (~1 m above the sediment) at each transect point. Bottom water was filtered on the boat using a 0.45-micron PES syringe filter and was subsampled for the analysis of TS^{2-} and dissolved nutrients. Samples were preserved using the same methods for sediment porewater (details in section 2.3.5). The Rhizon method (Seeberg-Elverfeldt *et al.,* 2005) was used to extract porewater from the top layer of each grab sample on the vessel (Fig. 2.4). The extracted porewater was subjected to chemistry analysis (TS^{2-}, NH_4^+, Fe^{2+}) as per Table 2.3, and the results represented the average sediment chemistry in the top ~2-5 cm.

Figure 2.4: *Sediment grab sample using rhizon samplers to extract pore water nutrients.*

2.2.4 Sediment Core Samples

Undisturbed, settled sediment cores were collected just below the SWI using coring devices (Fig. 2.5). In 2019, a KC Denmark multi-corer used 60 cm x 10 cm polycarbonate core lines and collected two sediment cores from the S1, R1, and F1 sites. In 2020, a hypoxic corer, built following the outline in Gardner et al, (2009), used a 30 cm x 10 cm acrylic core line to collect three sediment cores from the S2, R2, and F1 sites. Cores were collected aboard the vessel *RV Gumby*. Once the samples were back on the vessel, a tight-fitting cap and electrical tape were used to securely store, retain, and seal the contents of the cores.

Figure 2.5: *Left, a multi-corer being placed on the RV Gumby for use in 2019. Right, the hypoxic corer constructed in 2020 following the design of Gardner et. al, (2009).*

For both years, the sediment cores were stored vertically in a cooler and maintained at in-situ temperatures using ice. In 2020, each core was placed within a slightly larger outer tube filled with an anoxic solution of sodium ascorbate to prevent interaction with the atmosphere and

preserve anoxic conditions. All cores were transported back to Dalhousie University and stored in a cold room for analysis within 48 hours. Sediment cores were then analyzed for sediment chemistry (TS^{2-} and dissolved nutrients) at 2 cm depth intervals (details in section 2.3.6). For each year, a single core was used for microsensor profiling (H_2S, pH, and DO; details in section 2.3.7).

2.2.5 Sediment Grab Porewater Extraction

Porewater from the sediment grabs was extracted using Rhizon samplers (5 cm long samplers with a pore size of 0.15-microns) connected to a 10 mL syringe under a vacuum seal that allows sediment porewater to be drawn through the Rhizon sampler into the syringe (Seeberg-Elverfeldt et al., 2005). Rhizon samplers were placed in the center of the sediment grab sample (Fig. 2.4), with approximately 2-5 cm penetration into the surface of the sediment.

TS^{2-} is readily oxidized in the presence of oxygen, so the extracted porewater from the sample was either analyzed immediately (in 2019) or fixed with a zinc acetate solution to prevent oxidation to sulfate (in 2020). In 2019, porewater grab samples were analyzed for TS^{2-} directly on board the boat using a portable spectrophotometer and the Direct UV method for sulfide determination (Cranford et al., 2017). In 2020, samples were pipetted into a 5 mL tube containing 0.5 mL of 5% zinc acetate solution and stored in a fridge until analysis. Porewater grab samples for nutrients (Fe^{2+}, NH_4^+ and $NO_3^- + NO_2^-$) were placed into 15 mL centrifuge tubes, transported in a cooler, and then stored in a freezer until analysis (Stookey, 1970).

2.2.6 Sediment Core Sectioning and Porewater Extraction

Sediment cores were sectioned using a core extruder to push the sediment out of the core liner and sliced at ~2 cm increments to a depth of ~30 cm, then transferred to 50 mL centrifuge tubes. Some sections did not slice properly or contained more sediment, so section increments varied per individual core. Sectioning was performed quickly to minimize exposure to air which could affect sulfide concentrations. All samples were collected using the same method, so data was assumed to be comparable (Brodecka-Goluch et al., 2019). Porewaters were separated from the solid fraction by centrifuging at 5000 rpm for 15 mins. The samples were then transferred into an anaerobic chamber where the porewater was drawn up using a syringe and filtered with a 0.45-micron PES syringe filter, where they were then divided into separate sample vials for analysis of TS^{2-} and dissolved nutrients.

For TS^{2-}, 2 mL of porewater was pipetted into a vial containing 0.5 mL of 5% zinc acetate solution. For Fe^{2+}, 0.2 mL of porewater was pipetted into a vial with 0.2 mL of Ferrozine reagent and 1.6 mL of Milli-Q water. The remaining porewater sample (~3-4 mL) was collected in a 5 mL centrifuge tube for NH_4^+ and $NO_3^- + NO_2^-$ analysis. All sample vials were capped in the anaerobic chamber and then stored until analysis. TS^{2-} and Fe^{2+} samples were stored in the fridge (4 °C). Dissolve nitrogen samples were stored in the freezer (-20 °C) upright in racks.

The concentrations of TS^{2-}, NH_4^+, and Fe^{2+} for sediment porewater were analyzed using the Thermo Scientific Evolution 260 UV-Visible Spectrophotometer (Table 2.3). Concentrations were determined using calibration lines using known concentrations of standard solutions. TS^{2-} concentrations were measured using the Methylene Blue Method (Cline, 1969), NH_4^+ concentrations were measured using the Ammonium Spectrophotometric Indophenol Blue

Method (Solorzano, 1969), and Fe^{2+} concentrations were measured using the Ferrozine Method (Stookey, 1970). $NO_3^- + NO_2^-$ was analyzed using an Analytical Sciences NOx 5100 Thermalox detector and analyzer with a vanadium chloride reactant to measure nitric oxide (NO) gas produced (Braman & Hendrix, 1989).

All sediment porewater samples were analyzed in duplicates, except $NO_3^- + NO_2^-$ due to sample volume limitations. Sample preparation included making calibration standards and following the methodologies for each analyte (Table 2.3). For the spectrophotometric methods, standards were made with Milli-Q water and all porewater samples were diluted in Milli-Q water before analysis (1:5 to 1:200 dilutions) to ensure concentrations were within the linear range and to avoid the influence of sample matrix effects on sample accuracy and precision. Detection limits for each method were determined in-lab by repeated analysis of low standards or blanks, using the US Environmental Protection Agency (EPA) method detection limit procedure (EPA, 2016; Table 2.3).

A small quantity of sediment from each section interval was dried, ground to a fine powder using a mortar and pestle, and analyzed for TC and TIN using a CHN Elemental MicroCube analyzer (Table 2.3) at the Dalhousie CERC Lab. The majority of TC analyzed in the sediment samples was organic carbon (OC). Before analysis, a representative subset of samples was tested for inorganic carbon (IC) content by analyzing the sediment before and after acid fumigation (Harris et al., 2001). The results showed that the sediment samples had negligible IC content, and therefore all other samples were analyzed without the acid fumigation step, and TC was considered equal to the OC content.

The supply of particulate organic matter often leads to porous sediments in fish farms (Holmer & Kristensen, 1992). To determine porosity, the volumetric proportion of porewater to bulk sediment was calculated for each core section using the equation:

$$Porosity\ (P_t) = Pore\ Volume\ (Vp)\ /Total\ Volume(Vt) \quad \text{(Eq. 3)}$$

where (V_p) represents the volume of porewater (in cm^3), and V_t represents the total volume of wet sediment (in cm^3). Porosity was determined by considering the water content and solid phase density of the sediments. Water content was determined from the difference between wet weight and dry weight after drying sediments in an oven at 60°C. Dry sediments were quantitatively transferred to a 25 mL graduated cylinder, and the solid phase density was calculated by measuring the volume displacement after adding a fixed volume of water (Seitaj *et al.,* 2017).

2.2.7 Micro-profiling

The top few centimeters of a sediment core from each site were micro-profiled for DO (shallow sites only), H_2S, and pH using a Unisense field microsensor system (Fig. 2.6). Micro-profiling was conducted in a cold room (~4°C) at Dalhousie University. For the shallow cores with oxygenated overlying water (C8 in 2019 and C3 in 2020), the overlying water was stirred by bubbling with air. In contrast, for cores with overlying anoxic water (C12, C10 in 2019; C4, C10 in 2020), a stream of N_2 gas was circulated across the sediment surface to prevent the introduction of DO. A Unisense Clark Type microelectrode, with a 100 μm type diameter (OX-100) was used for DO micro-profiling. DO micro-profiles were conducted from a few mm above the SWI (by eye) to approximately 8 mm depth at 0.1 mm increments. Using a Unisense pH-100 microsensor and SULF-100 microsensor (linear range of 10,000 μM), pH and H_2S

concentrations were measured from a few mm above the SWI down to 2 cm depth at 0.5 mm increments.

Figure 2.6: *A Unisense microsensor processing a core sample in a cold storage room.*

Using the equations of Jeroschewski *et al.* (1996) and Millero *et al.* (1988), as outlined in the *Hydrogen Sulfide Sensor Manual* (Unisense A/S, 2020), TS^{2-} concentrations were calculated using the H_2S partial pressure in the sediment porewater and considering the pH of the solution. The pH microsensor was calibrated using 4, 7, and 10 pH buffers in a three-point calibration. For the H_2S microsensor, an anaerobic stock solution of ~10,000 µM S^{2-} was prepared using a sodium sulfide solution (Na_2S x 9 H_2O), and the exact concentrations were determined using the Methylene Blue Method (Cline, 1969). A 1 mL stock solution was added to 40 mL of a pH 3 buffer containing Titanium (III) chloride ($TiCl_3$) to yield a final concentration of ~245 µM. A two-point calibration was then performed using this solution and the $TiCl_3$ pH 3 buffer solution free of TS^{2-}. The DO microsensor was calibrated using a two-point calibration curve using

oxygen-saturated seawater at in situ temperature and salinity, and an anoxic solution of 0.1 M sodium ascorbate and 0.1 M NaOH.

CHAPTER 3

RESULTS

In this chapter, various metrics of sediment organics were measured at sites near and far from the We'koqma'q Aquaculture Farm to quantify the sediment biogeochemistry in the Whycocomagh Basin. Specifically, the rates of carbon remineralization and sulfur cycling. Water column chemistry profiles were plotted against water depth (m). Sediment porewater chemistry and organic carbon and nitrogen content were plotted against sediment depth (cm) at the sediment-water interface. The approximate zones of DO concentration are indicated by light blue and light red shading for the aerobic and fully anoxic zones, respectively. Sampling was conducted during fish rearing in 2019 and after a year of fallowing in 2020 to evaluate temporal change over approximately 1 year of fallowing.

3.1 Hydrographic Properties

In 2019 and 2020, hydrographic properties (T, S, ρ_w) plotted against pressure, assuming a conversion of 1 decibar to 1 meter, in the Whycocomagh Basin were characteristic of highly stratified coastal waters (Fig. 3.1). In November 2019, water temperatures were 6.5 °C at the surface and increased to a maximum of 8.8 °C at 15 m (~15 db) before decreasing back down to 3 °C at 20 m (~20 db), with temperatures remaining constant through the rest of the water column (Fig. 3.1; A). Salinity was lowest at the surface at 18 PSU and increased linearly toward 20 m (~20 db) depth, where it remained constant at 22.7 PSU through the remainder of the water column. In September 2020, the surface waters were warmer and saltier compared to the

previous year (Fig. 3.1; C). The temperature of the water column decreased from 15.8 °C to 3 °C within the top 15 m (~15 db), with a thermocline present between 11-15 m, below which the temperature remained constant. Salinity in the surface waters was around 22 PSU and increased to 22.7 PSU at a depth of 18 m (~18 db), where it then remained constant. The lower salinity of surface waters in both years suggests the presence of freshwater input, likely originating from the Skye River or runoff from land in the watershed of the Basin. We also observed a higher surface temperature in 2020 compared to 2019, which is most likely attributable to the difference in sampling time (November 2019 *vs.* September 2020).

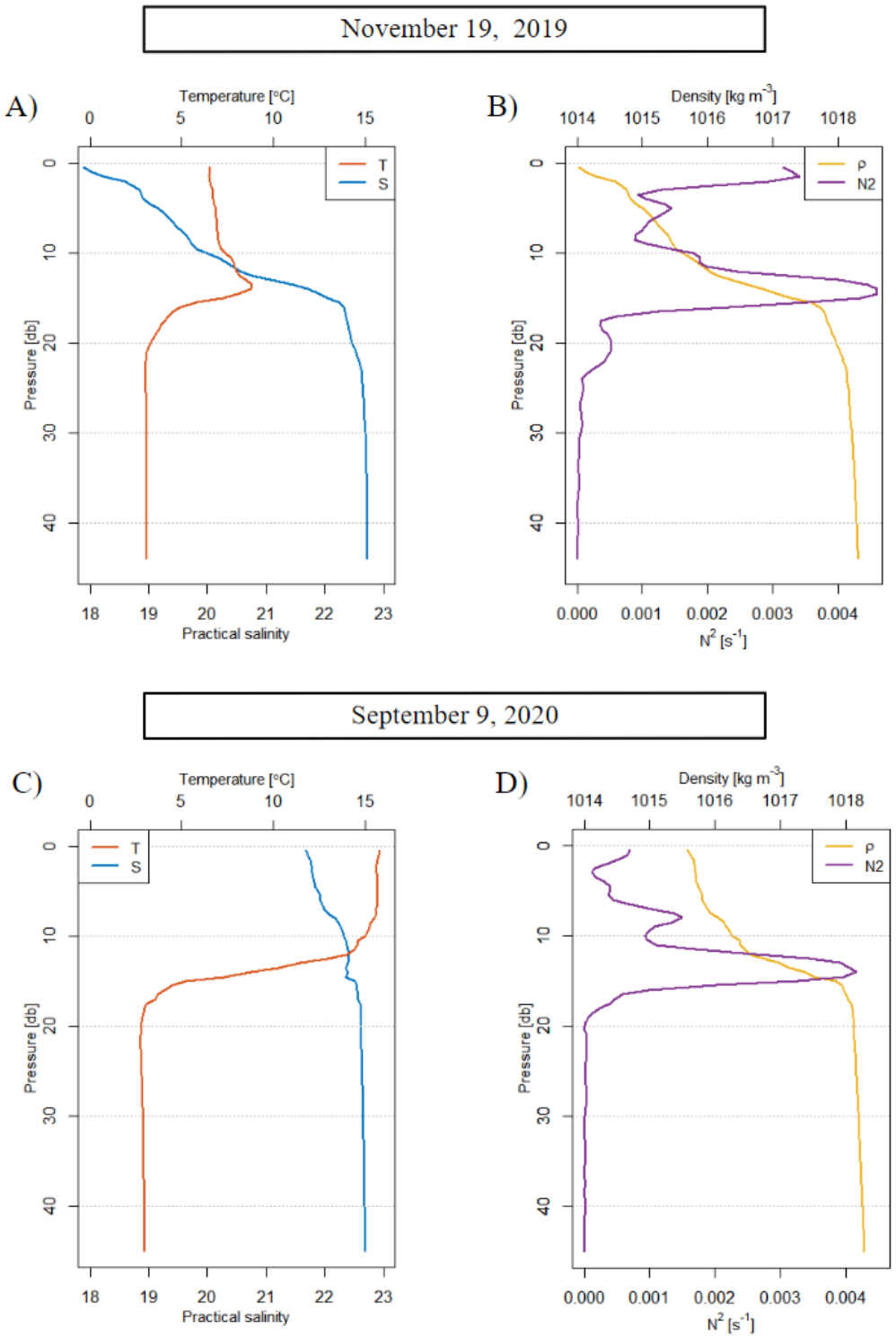

Figure 3.1: *Hydrographic properties at the D1 site measured in situ by CTD cast during 2019 (upper graphs) and 2020 (lower graphs). Profiles of temperature and salinity (A and C) and density and buoyancy frequency (B and D) are plotted against pressure (db).*

In both years, the temperature (T) and salinity (S) profiles created a strong pycnocline between 10-20 db which isolated the surface and subsurface waters at ~15 to 16 m depth (Fig. 3.1; A, C). In 2019, density (ρ_w) was ~1014 kg m^{-3} at the surface and increased to ~1018 kg m^{-3} at 14 m (~14 db) depth, remaining constant through the rest of the water column, and the buoyancy frequency (N^2), a measure of stratification, peaked at > 0.004 s^{-1} at the pycnocline (Fig. 3.1; B). In 2020, density was ~1015.5 kg m^{-3} at the surface and again increased to ~1018 kg m^{-3} by 15 m (~15 db), below which it remained constant and buoyancy frequency again peaked at > 0.004 s^{-1} at 14 m (~14 db) (Fig. 3.1; D). The interannual similarity of deep-water (> 20 m) T, S, and density properties (Table 3.1) suggests the water column remained stratified, with a much longer residence time of the water in the sub-pycnocline than in the surface layer for the duration of the 10 month study period.

Table 3.1: *Average deep water (>20 m) properties at the D1 site in 2019 and 2020.*

Year	Water Depth (m)	Temperature (°C)	Salinity (PSU)	Density (kg m^{-3})	Buoyancy Frequency (s^{-1})
November 2019	20-48	4.62 ± 1.98	21.65 ± 1.52	1017.22 ± 1.38	$8.32 \times 10^{-5} \pm 1.3 \times 10^{-5}$
September 2020	20-48	6.69 ± 5.54	22.46 ± 0.31	1017.52 ± 1.00	$1.65 \times 10^{-5} \pm 1.04 \times 10^{-5}$

3.2 Water Chemistry

3.2.1 Deep Site

Water column TS^{2-} depth profiles through the water column taken are shown alongside DO profiles at the deepest point in the basin (D1 site) for 2019 and 2020 (Fig. 3.2). The profile metrics illustrate the transition from oxic surface waters to anoxic bottom waters between 15-20 m depth. In 2019, DO concentrations were high at the surface (~300 μM; ~90% saturation), decreased gradually in the first 10 m, and then dropped rapidly between 15-20 m to below detection (0 μM) by 20 m (Fig. 3.2; A). In 2020, DO concentrations were similar (~240 μM; ~75% saturation) with lower concentrations in the surface, reflecting lower oxygen saturation at higher temperatures (Fig. 3.2; B). In both years, the oxycline closely aligned with the pycnocline at approximately 15 m depth. However, there was stronger stratification in September 2020 compared to a higher buoyancy frequency observed in November 2019. These differences could be attributed to the variations in sampling months and weather conditions, including factors such as wind speed, but could also be due to variations in TS^{2-} concentrations, which increased at 20 m in 2020 compared to at 15 m in 2019, and may contribute to the observed differences.

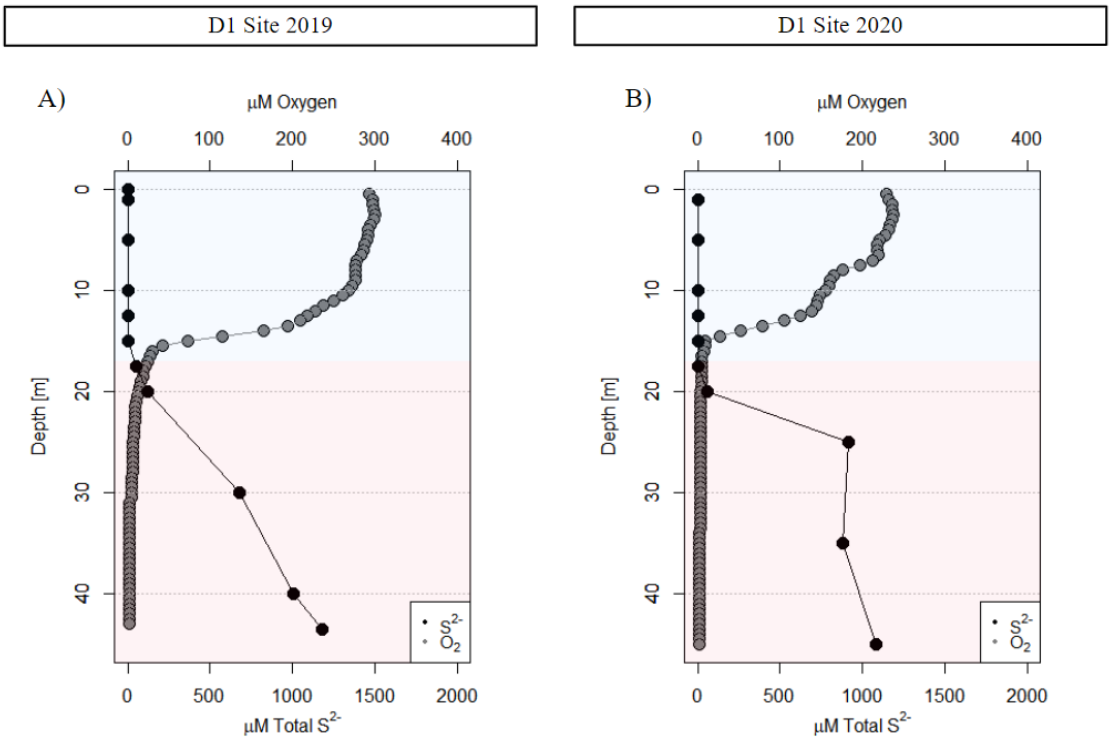

Figure 3.2: *Relationships between DO and TS^{2-} concentrations at the D1 site in the water column in 2019 (A) and 2020 (B). Light blue shading (aerobic) and light red shading (anaerobic) represent the approximate zones of DO concentration.*

TS^{2-} profiles exhibited an inverse relationship to the DO profiles, with total sulfide absent in the surface waters and increasing rapidly below the oxycline (Fig. 3.2; A, B). In both 2019 and 2020, the TS^{2-} concentration was 0 µM throughout the first 10 m and steadily increased to ~1000 µM by 40 m depth, with a more distinct crossover in 2019 (19 m) compared to a more pronounced gradient in 2020 (15-20 m). Although TS^{2-} concentrations appeared to increase more rapidly in 2019 than in 2020, both crossovers are indicative of the onset of anoxic conditions at approximately 15 m depth. At this depth, DO concentrations begin to decrease in concentration eventually to 0 µM.

At the D1 site, TS^{2-} and dissolved inorganic nitrogen ($NO_3^- + NO_2^- + NH_4^+$) concentrations below 20 m depth exhibited sharp transitions at the oxycline (Fig. 3.3). Sulfide

and ammonium concentrations increased significantly in the anoxic waters, with both below detection in the top 15 m. Sulfide concentrations at the bottom were ~1100 μM in 2019 and ~1000 μM in 2020 (Fig. 3.3; A). Ammonium concentrations increased up to 50 μM in 2019 and ~250 μM in 2020 at 35 m and 40 m, respectively (Fig. 3.3; B). In both years, the deepest ammonium sampling points decreased in concentration below 40 m depth, which is unexpected and unusual and cannot be explained with the available data (as discussed later). Iron concentrations were below the detection limit throughout the entire water column (Fig. 3.3; C). Nitrate/nitrite was low in the surface water, with a slight peak at 3.9 μM in 2019 near the base of the pycnocline at ~10 m, and values then decreased to 0 μM by 20 m depth (Fig. 3.3; D).

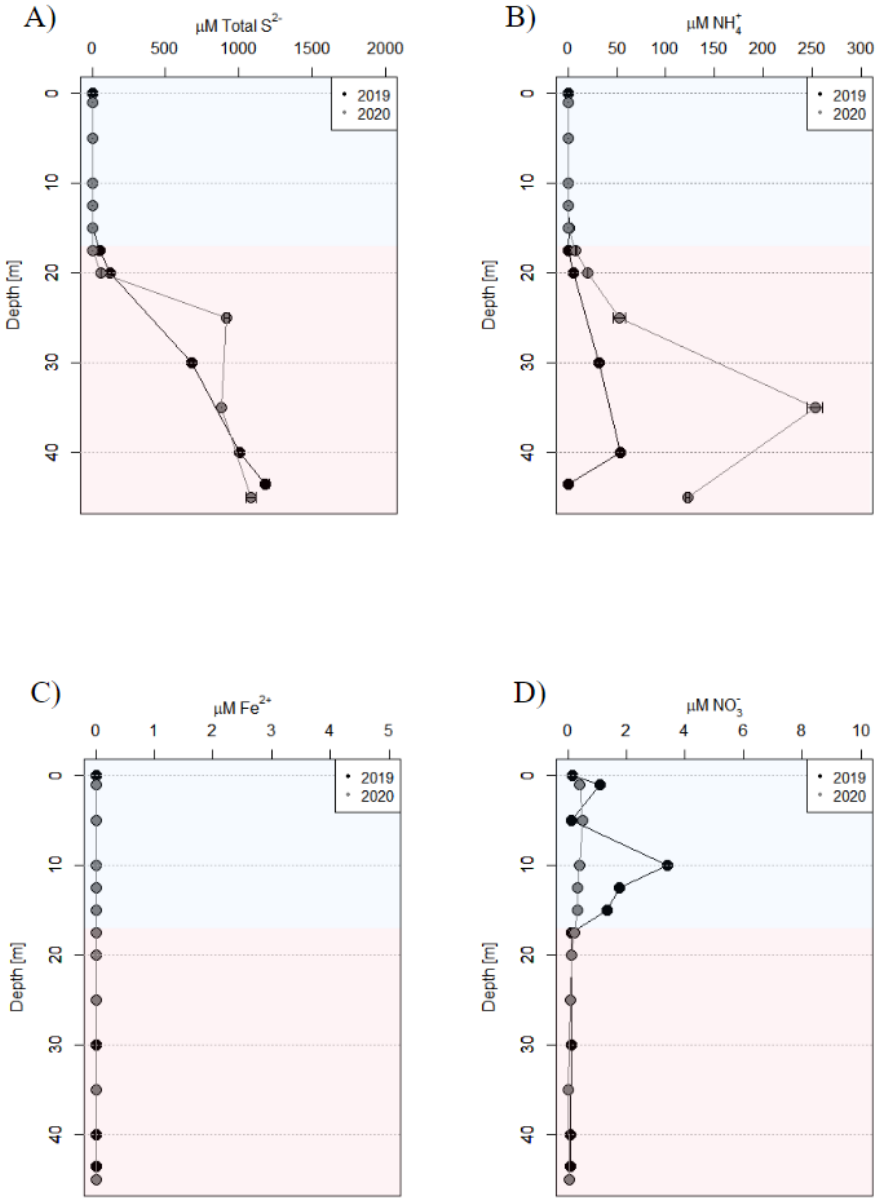

Figure 3.3: *Nutrient profiles at the D1 site in 2019 and 2020 showing TS^{2-} (A), NH_4^+ (B), Fe^{2+} (C), and $NO_3^- + NO_2^-$ (D) concentrations through the water column. Light blue shading (aerobic) and light red shading (anaerobic) represent approximate DO concentration zones.*

Secchi disk measurements were taken at the D1 site to assess the concentration of suspended particulate matter in the upper oxic environment, as an indicator of phytoplankton abundance. In 2019, measurements were 2.95 m down and in 2020 were 4.20 m down, which indicates more turbid waters in 2019 compared to 2020.

3.2.2 Fish Pen Array

To assess the potential impact of the fish pens on background water properties observed at the D1 site, CTD measurements of the potential temperature (independent of pressure effects), S, and DO concentrations collected at the D1 and F1 sites in 2019 and 2020 were compared (Fig. 3.4). In 2019, there were no significant differences in water temperature or salinity throughout the water column between the two sites (Fig. 3.4; A). In 2020, water temperature and salinity showed slight variations between the two sites throughout the water column, with the F1 site having slightly higher values in the surface and slightly lower values in the subsurface, compared to the D1 site (Fig. 3.4; C). The difference in temperature and salinity between years and each site is likely due to the 2020 sampling taking place in September, while the 2019 sampling occurred in November. Overall, there were no hydrographically significant differences between the fish pen array and the deep site for either year, except for the slight variations mentioned above.

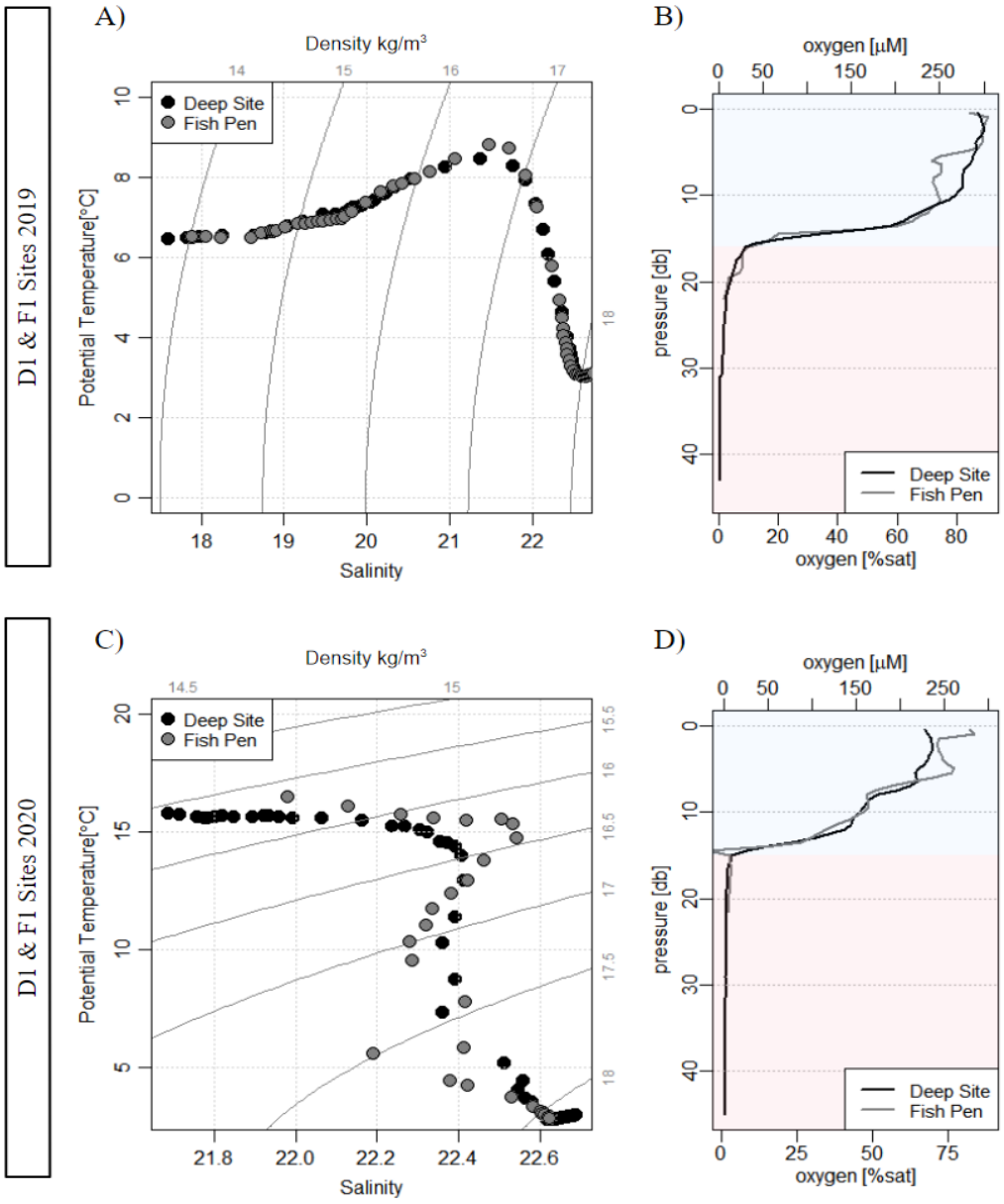

Figure 3.4: *A comparison between water properties at the D1 and F1 sites for November 2019 and September 2020. A and C) show the 2019 and 2020 TS isolines plotted against density. Isolines vary due to the difference in scale for each plot. B and D) show the 2019 and 2020 DO concentration and % saturation plotted against pressure. Light blue shading (aerobic) and light red shading (anaerobic) represent approximate DO concentration zones.*

Dissolved oxygen profiles in the upper ~22 m of the water column did not reveal significant differences between the F1 and D1 sites (Fig. 3.4; B, D). In both 2019 and 2020,

oxygen concentrations were greater than 200 µM (> 70% saturation) in the surface layer, followed by a rapid decrease to 0 µM at around 15 m depth. In September 2020, there was a shoaling of the oxycline in the upper water column, likely due to intense mixing due to high winds observed during this period (Bruce Hatcher, personal communication), with max gusts reaching 45 km/h recorded at the Port Hawkesbury station for the month of September (Environment Canada, 2022).

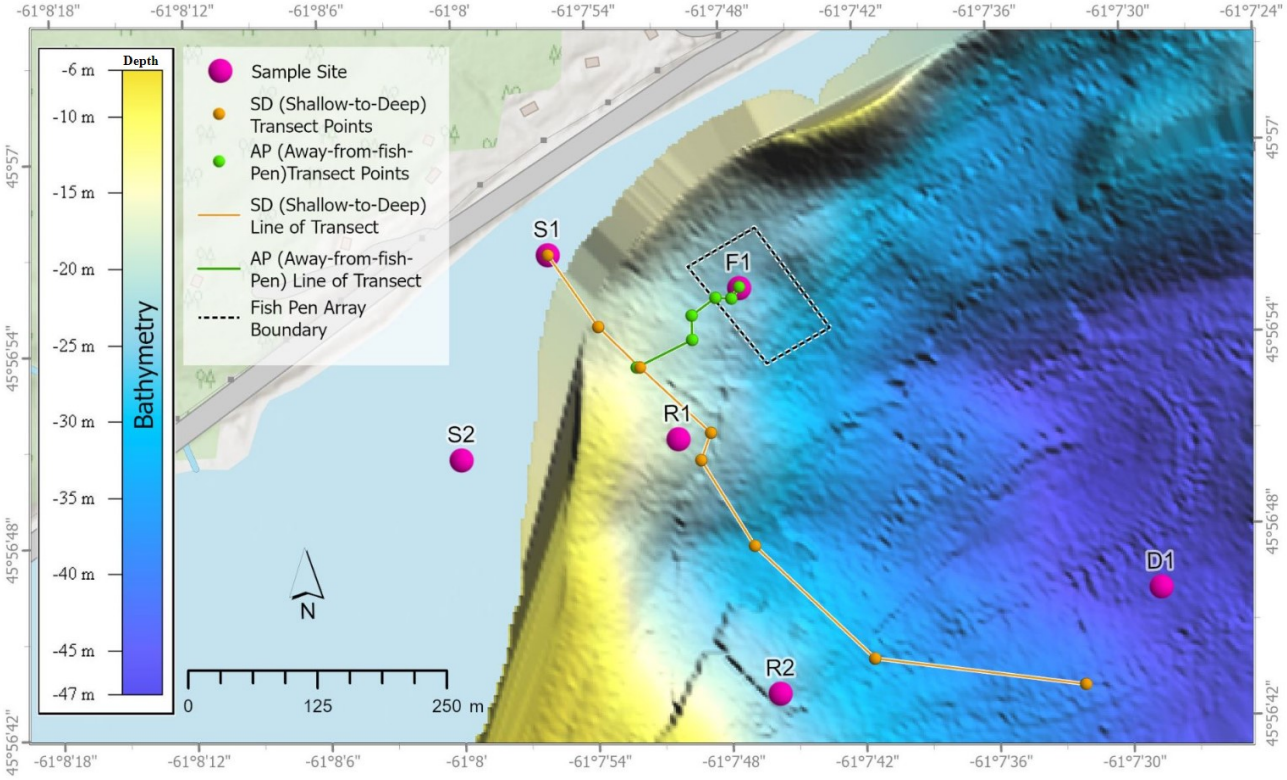

Figure 3.5: *A close-up map of the sediment grab transects with the SD Transect (orange line) moving from shallow to deep and the AP Transect (green line) moving away from the fish pen array.*

3.3 Surficial Sediment Chemistry

Concentrations of TS^{2-}, NH_4^+, Fe_2^+, bottom water, TC, TIN, and C:N ratios were measured through sediment grabs along the SD and AP Transect lines (Fig. 3.5). The concentration gradients observed represent the background concentration along the basin (SD) and the horizontal concentrations moving away from the fish pen array (AP) (Fig. 3.5-3.9).

3.3.1 Bottom Water

In 2020, bottom water concentrations (~ 1 m above the SWI) were measured along the SD and AP Transects and analyzed for TS^{2-} and NH_4^+ (Fig. 3.6). Along the SD Transect, bottom water concentrations of both TS^{2-} and NH_4^+ increased with depth and distance, starting at ~18 m depth (Fig. 3.6; A). TS^{2-} concentrations increased to ~780 μM, and NH_4^+ concentrations increased to ~210 μM by ~35 m depth. On the other hand, the AP Transect showed highly elevated TS^{2-} and NH_4^+ bottom water concentrations near the fish pen array (F1), with concentrations decreasing from ~310 μM and 19 μM, respectively, to below detection limits by 120 m distance away from the fish pen array (Fig. 3.6; B).

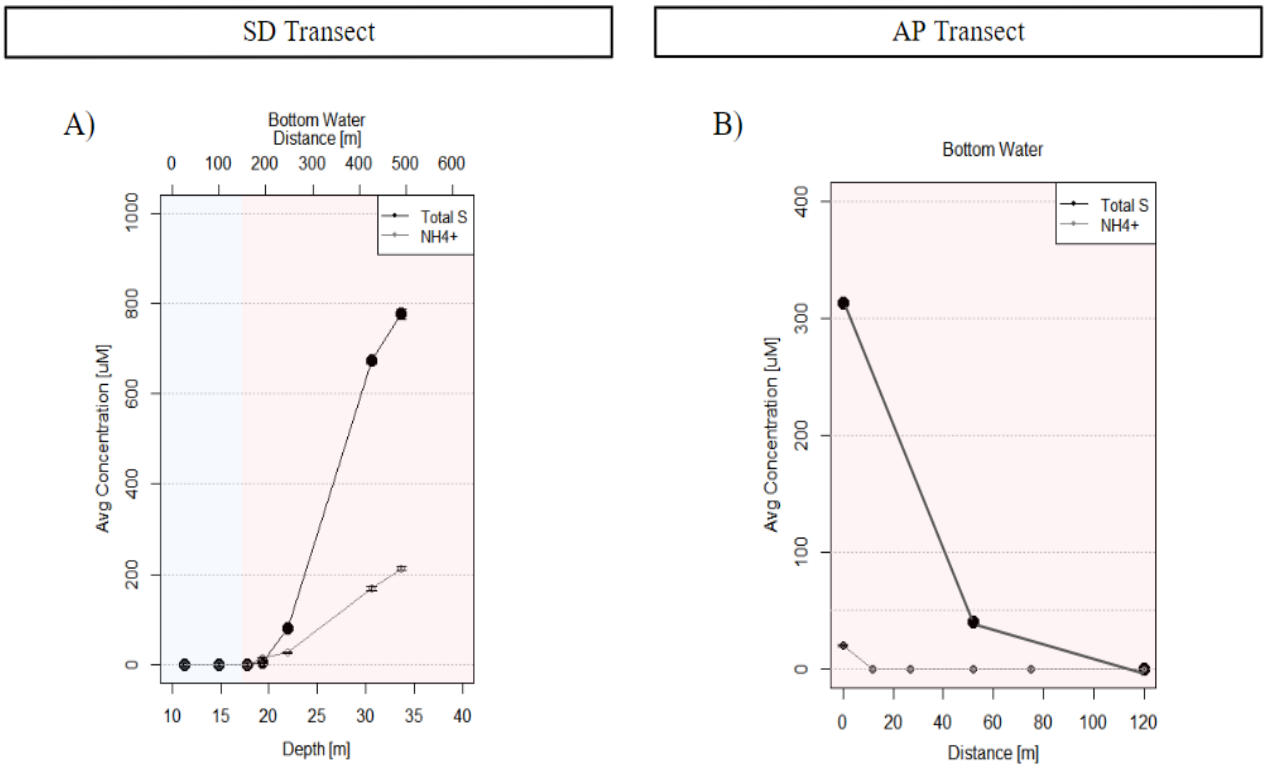

Figure 3.6: *Concentrations of TS^{2-} and NH_4^+ (mean ± SD) in samples of bottom water taken in 2020 along the SD and AP Transects through the Whycocomagh Basin. A) the SD Transect TS^{2-} and NH_4^+ concentrations gradually increase with depth and distance from the shore. B) the AP Transect TS^{2-} and NH_4^+ concentrations decreased to below detection for both dissolved nutrients by 120 m from the pen array. Light blue shading (aerobic) and light red shading (anaerobic) represent the approximate DO concentration zones.*

3.3.2 Total Sulfide

The sediment grab samples along the SD Transect revealed a pattern of increasing TS^{2-} concentrations in surface sediment with increasing water depth and distance from the nearshore end (Fig. 3.7; A). In 2019, TS^{2-} concentrations increased from ~400 to 1800 µM between 10 and 20 m depth and remained constant until 30 m where concentrations peaked at 3200 µM. Subsequently, concentrations decreased to 2400 µM by 43 m depth. In 2020, the subset of three

TS^{2-} samples collected along the SD Transect showed a more rapid increase with depth, with concentrations rising from ~1950 µM at 15 m to 3500 µM by 22 m depth.

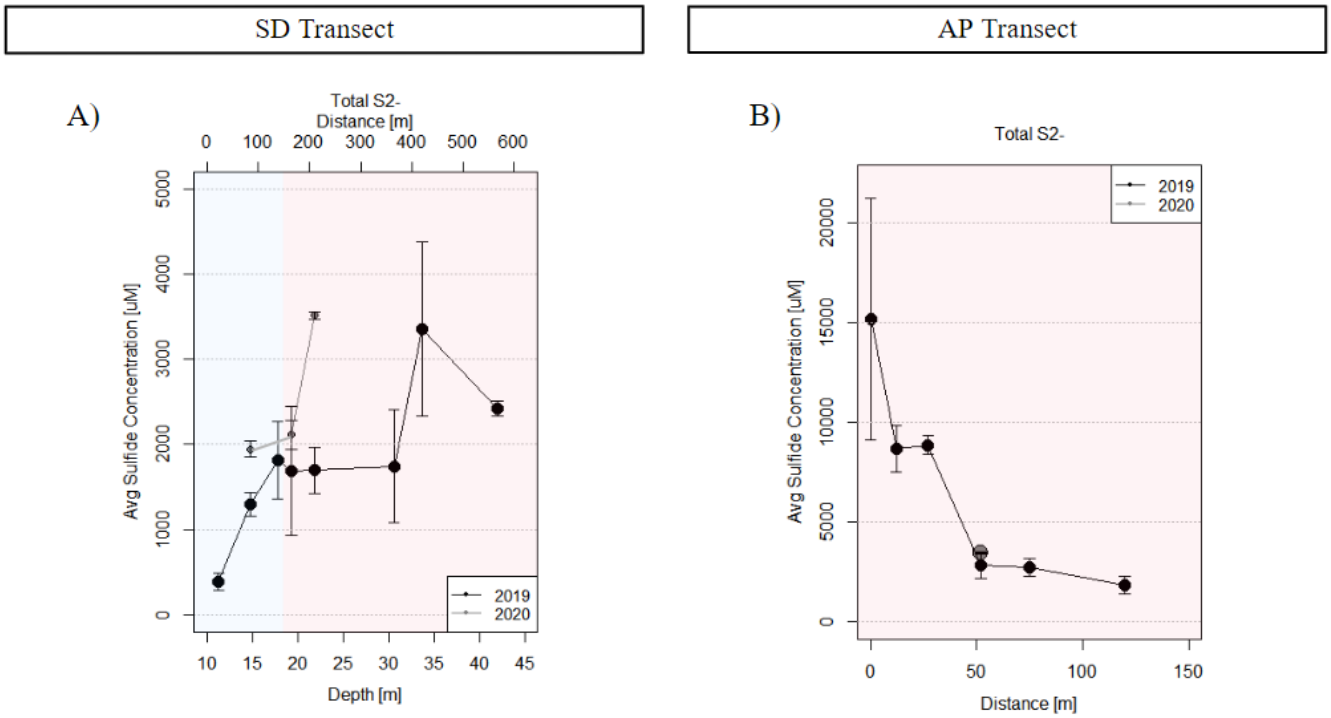

Figure 3.7: *TS^{2-} concentrations (mean ± SD) of surface sediment grab samples collected along transects through the Whycocomagh Basin in 2019 and 2020. A) the SD Transect from nearshore towards the center of the deep basin. B) the AP Transect along the 20-25 m depth contour from the center of the fish pen array out beyond 100 m. Light blue shading (aerobic) and light red shading (anaerobic) represent the approximate DO concentration zones.*

The sediment grab samples along the AP Transect showed significantly elevated surface sediment TS^{2-} concentrations near the fish pen array (F1), which decreased with increasing distance away from the pens (Fig. 3.7; B). In 2019, the TS^{2-} concentration was 15000 µM directly beneath the F1 site at 0 m, and it decreased to ~1800 µM at 120 m away - similar to the concentrations observed at a similar depth along the SD Transect (Fig. 3.7; A). In 2020, the TS^{2-} concentration for the single sample taken 50 m away from the F1 site (~3400 µM) was similar to

the 2019 levels at the same distance. TS^{2-} concentrations underneath the fish pen array were approximately 15 times higher than those observed in the rest of the basin, and samples taken more than 50 m away were below 3000 μM, in line with the background concentrations observed at the D1 site.

3.3.3 Ammonium

Surface sediment NH_4^+ concentrations along the SD Transect increased with increasing water depth and distance from the nearshore site (Fig. 3.8; A). In 2019, NH_4^+ concentrations were approximately 350 μM at 10 m and increased steadily to around 700 μM by 45 m depth. The subset of the three NH_4^+ samples taken in 2020 along the SD Transect showed a similar increase with depth and slightly higher concentrations, ranging from around 490 μM at 15 m up to ~580 μM at 22 m depth.

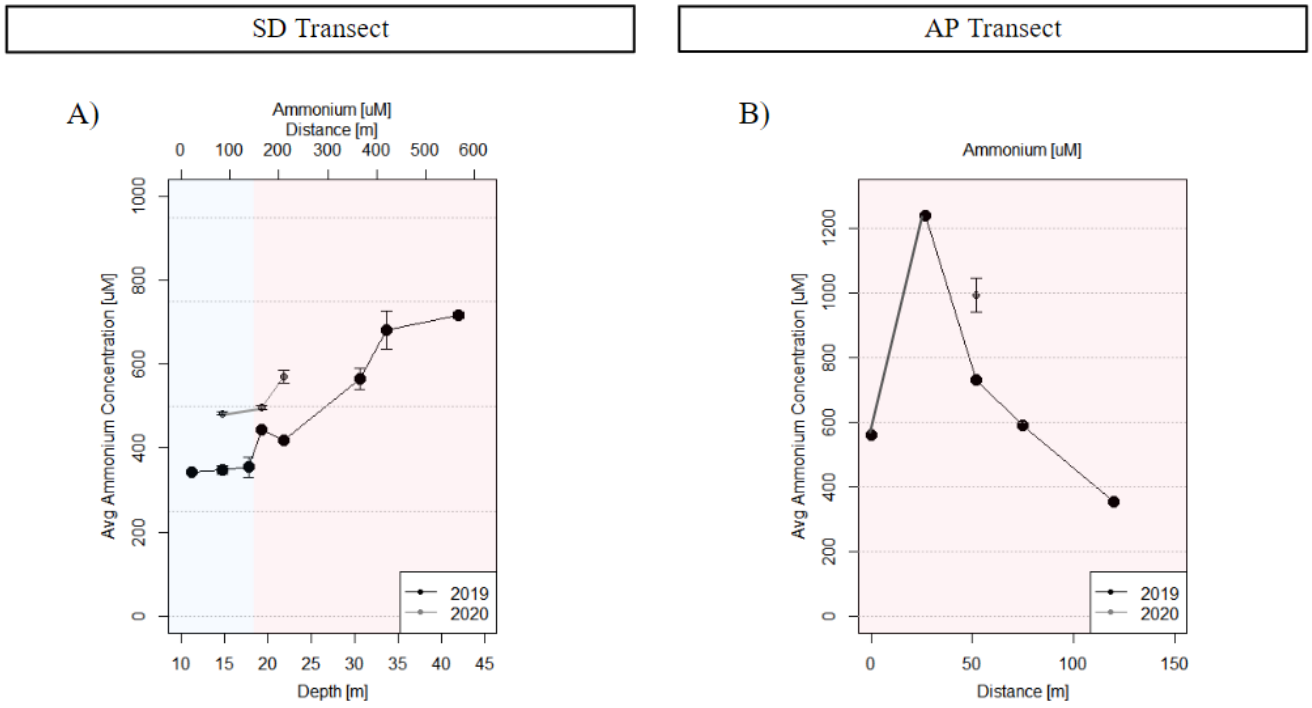

Figure 3.8: *NH_4^+ concentrations (mean ± SD) of surface sediment grab samples collected along transects through the Whycocomagh Basin in 2019 and 2020. A) the SD Transect from nearshore towards the center of the deep basin. B) the AP Transect along the 20-25 m depth contour from the center of the fish pen array out beyond 100 m. Light blue shading (aerobic) and light red shading (anaerobic) represent the approximate DO concentration zones.*

The AP Transect showed a peak in surface sediment NH_4^+ concentrations at 50 m depth near the fish pen array (F1), which decreased with increased distance from the fish pen (Fig. 3.8; B). In 2019, NH_4^+ concentrations were highest under the F1 site at 0 m with levels exceeding 1200 µM and gradually decreasing to ~380 µM by 120 m. Concentrations at 20-25 m depth were comparable to those at a similar depth along the SD Transect (between 350-420 µM). In 2020, the single NH_4^+ sample taken 50 m away from the F1 site had concentrations of ~1000 µM, which is slightly higher than levels observed at the same distance in 2019.

3.3.4 Organic Carbon and Nitrogen

In 2019, TC (%C) and TIN (%N) surface sediment grab samples were taken along the SD and AP Transects and plotted against the same range of vertical axes to compare both transect values (Fig. 3.9 and Fig. 3.10). The SD Transect values were relatively constant with depth and distance, with TC averaging 5.5 ± 0.4% and TIN 0.56 ± 0.05% (n=8). The values slightly decreased to ~4.8% and ~0.4%, respectively, by 30 m depth, and both increased back to similar values for the rest of the transect (Fig. 3.9; A, B). The slight dip in TC and TIN, and subsequent increase in C:N values at 25-30 m depth (200-325 m distance), is likely due to spatial heterogeneity. Nevertheless, the sediment material had an average C:N ratio of 9.94 ± 0.29 (n=8) (Fig. 3.9; C).

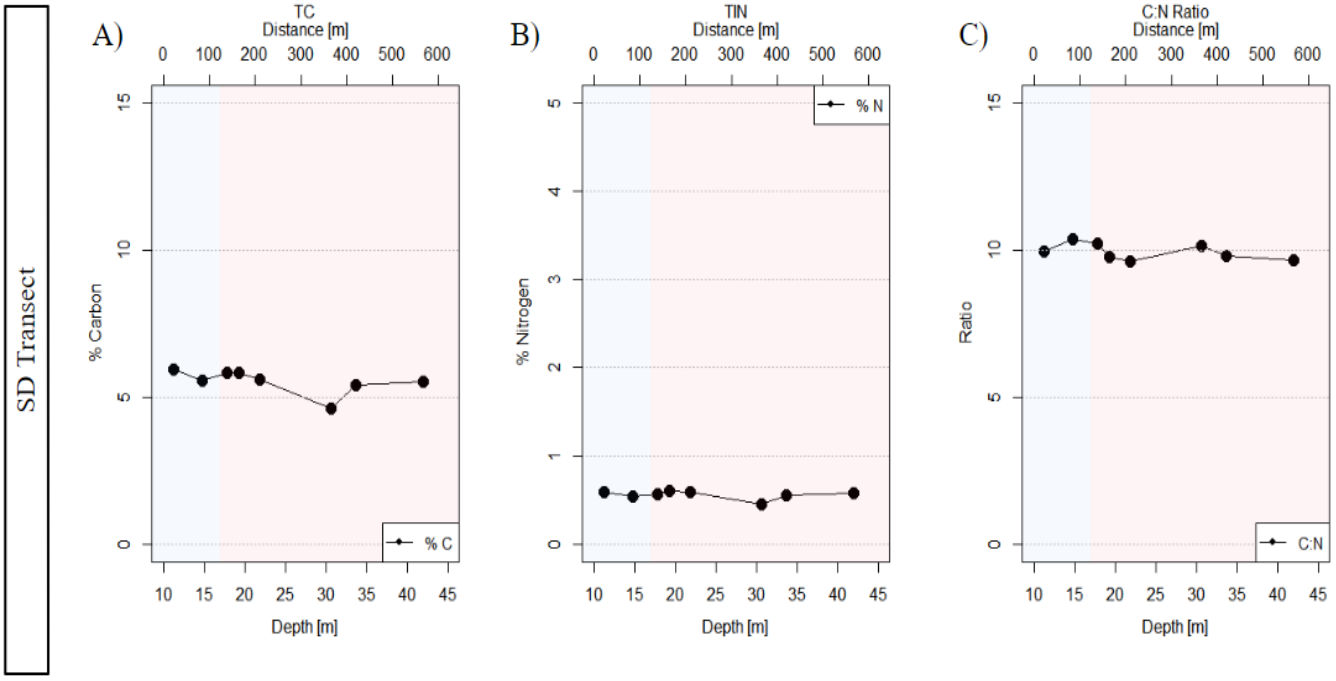

Figure 3.9: *Percent Total Carbon (A), percent Total Inorganic Nitrogen (B), and Carbon: Nitrogen ratio (C) values of the surface sediment grab samples collected along the SD Transect from the nearshore (shallow) to middle of the Whycocomagh Basin (deep). Light blue shading (aerobic) and light red shading (anaerobic) represent the approximate DO concentration zones.*

Measurements of TC and TIN (n=6) were taken along the AP Transect in 2019 and showed an increase within the first 45 m of the fish pen array and decreased after 50 m (Fig. 3.10). TC increased from ~6% to ~13%, and then leveled off to ~6% by 50 m for the rest of the transect, averaging 7.3 ± 2.6% TC (Fig. 3.10; A). Similarly, TN also increased within the first 45 m to about 1.5%, and then leveling back down to ~1% by 50 m for the rest of the transect, averaging 0.78 ± 0.34% TIN (Fig. 3.10; B). The C:N ratio inversely dipped down to ~8 by 45 m, and then leveled out around 10, with an average C:N ratio of 9.5 ± 0.64 (n=6) in the sediment material (Fig. 3.10; C). Overall, these values fell within the range reported for anoxic coastal sediments (Berner *et al.,* 1970).

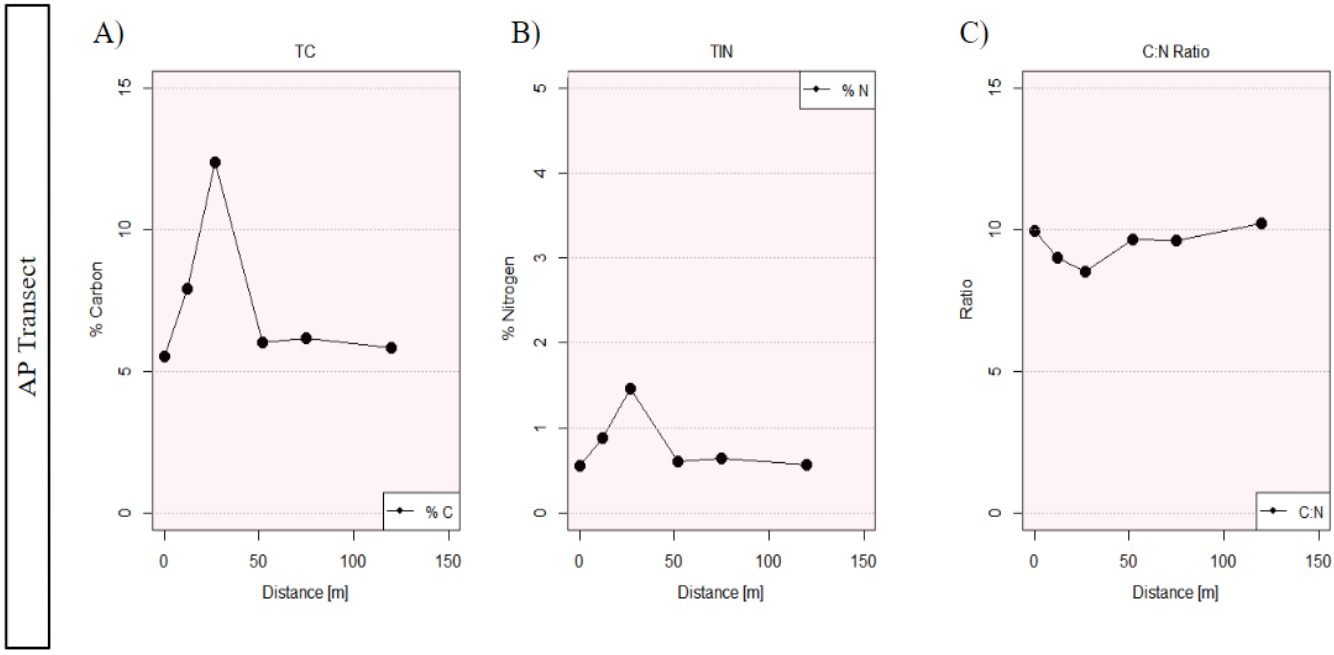

Figure 3.10: *Percent Total Carbon (A), percent Total Inorganic Nitrogen (B), and Carbon: Nitrogen ratio (C) values of the surface sediment grab samples collected along the AP Transect moving away from the fish pen array. Light red shading (anaerobic) represents the approximate DO concentration zone.*

3.4 Chemical Profiles in Sediment Cores

Porewater from sediment cores collected at the coring sites (indicated in Fig. 2.3 and Tables 2.1 and 2.2) was used to examine the vertical distributions of TS^{2-}, NH_4^+, Fe^{2+}, TC, and TN. Core profiles are labeled sequentially to the order the sample sites were sampled (*e.g.,* C1 to C12) and duplicate cores were collected in 2020. The sample sites were chosen to closely correspond to the end members of the sediment grab transects, but it should be noted that the deep site (D1) of the SD Transect could not be cored due to the winch wire on the vessel being too short to reach the bottom of the deepest point in the basin. In 2019, due to wind conditions during sampling in the Basin, only a single core was collected for geochemistry, while in 2020, duplicate cores were collected. Therefore, measurements in 2020 provide a better representation

of spatial heterogeneity for each site than in 2019. It is important to keep these factors in mind when interpreting the following results.

3.4.1 Total Sulfide

Depth profiles of TS from the sediment cores in 2019 and 2020 are plotted in Fig. 3.11. The shallow sites (S1, S2) were in slightly different locations in 2019 and 2020 but were similar in depth. In 2019, the S1 site core (C1) showed a slight increase in TS^{2-} with depth in the sediment, starting at 0 μM at the surface and increasing to ~100-200 μM by 23 cm depth (Fig. 3.11; A). In 2020, the S2 site cores (C1, C2) exhibited higher concentrations than the previous year, with TS^{2-} starting at 0 μM and increasing to ~1000 μM by 23 cm depth, then dropping to ~700 μM at 27 cm depth for core C1 (Fig. 3.11; B). It is unclear whether the difference between the two years reflects an increase in sediment sulfide or is a result of spatial heterogeneity at the scale of sampling.

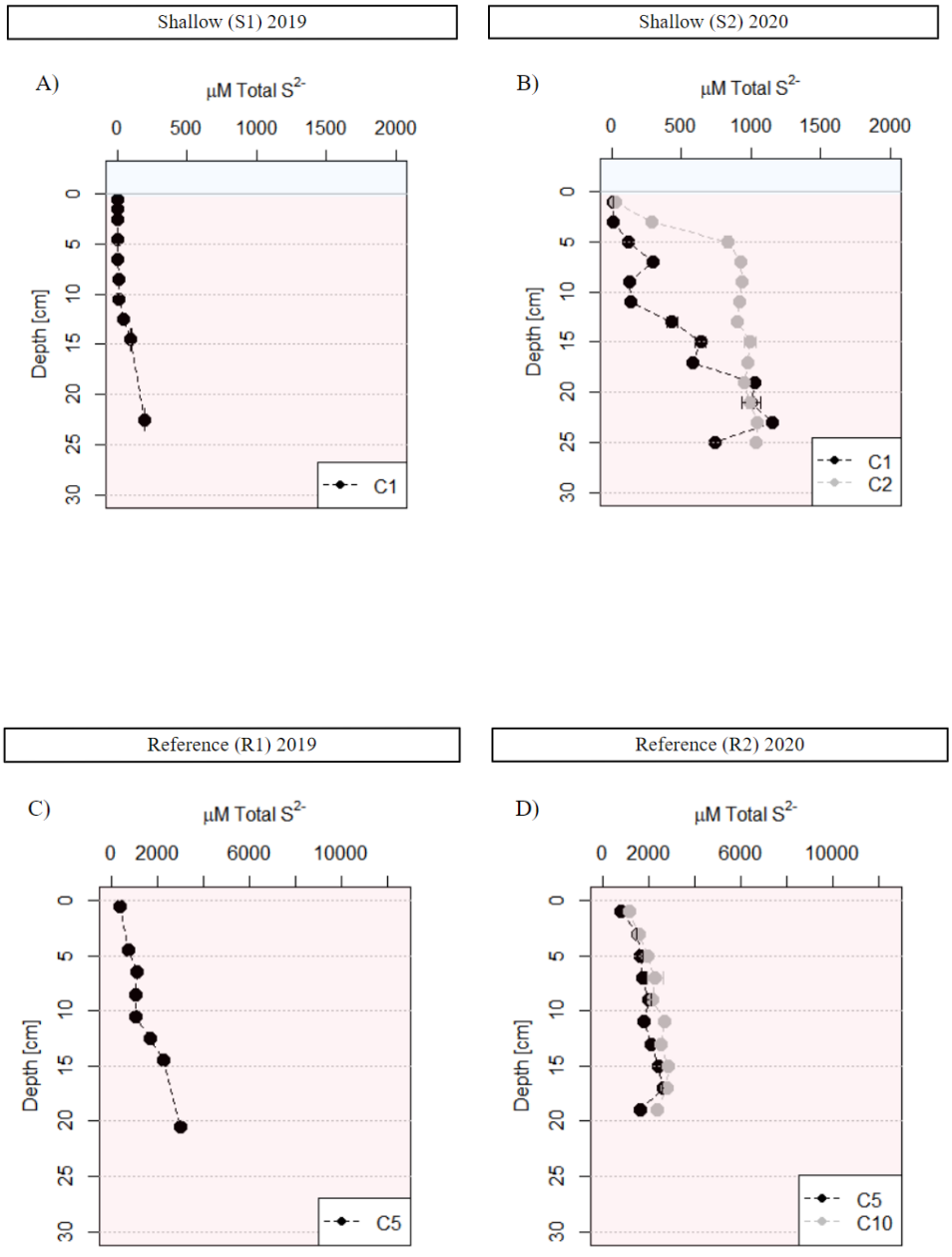
Shallow (S1) 2019
Shallow (S2) 2020
A)
B)
µM Total S2-
0 500 1000 1500 2000
Depth [cm]
0 5 10 15 20 25 30
C1
C2
Reference (R1) 2019
Reference (R2) 2020
C)
D)
0 2000 6000 10000
C5
C10

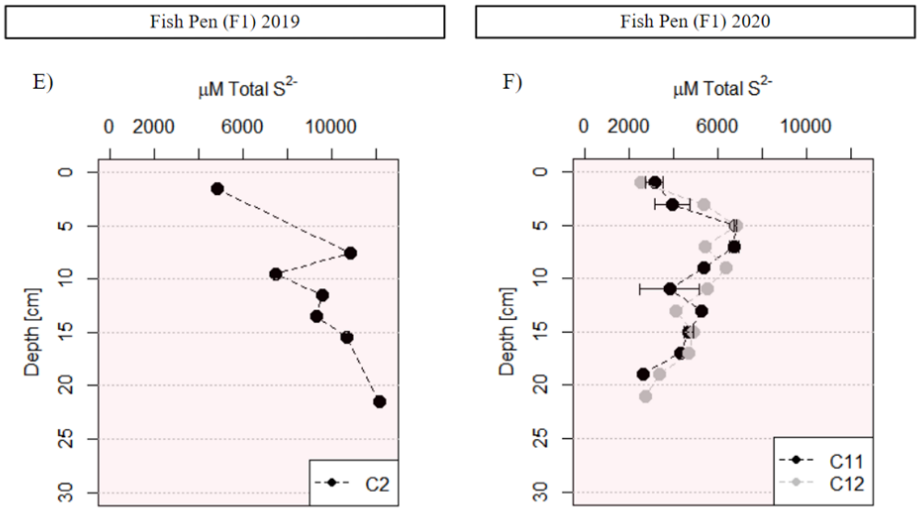

Figure 3.11: *TS^{2-} concentrations in porewater profiles through sediment cores collected at sites in the Whycocomagh Basin in 2019 and 2020. Cores were collected at five sites: S1 in 2019 and S2 in 2020 (A & B), R1 in 2019 and R2 in 2020 (C & D), and F1 in 2019 and 2020 (E & F). See Fig. 3.5 for site locations. Light blue shading (aerobic) and light red shading (anaerobic) represent the approximate DO concentration zones.*

The cores from the reference sites (R1, R2) were collected at slightly different locations in 2019 and 2020 but were taken at similar depths and distances from the fish pen site (F1). In 2019, the R1 site core (C5) showed a steady increase in TS^{2-} concentrations from ~300 µM at the surface of the sediment to ~3000 µM by 20 cm depth in the core (Fig. 3.11; C). In 2020, the R2 site cores (C5, C10) exhibited similar concentrations in the upper 10 cm as the previous year at ~900-1000 µM at 0 cm depth, with concentrations steadily increasing to ~2500 µM at 10 cm depth and slightly lower bottom concentrations than the R1 site at ~2000 µM by 20 cm depth (Fig. 3.11; D).

The sediment cores from the fish pen array site (F1) were much higher in TS^{2-} concentrations compared to the reference sites for both 2019 (fish present) and 2020 (fallow). In 2019, the F1 site core (C2) TS^{2-} concentrations were ~4800 µM near the surface and increased up to 12000 µM by 20 cm depth in the core (Fig. 3.11; E). In 2020, the F1 site cores (C11, C12)

TS^{2-} concentrations were still high but significantly lower than the previous year, starting at ~2800 μM at the surface. There was a peak of ~7000 μM at 5 cm depth, which then decreased back down to ~2800 μM by 20 cm depth in the core (Fig. 3.11; F).

3.4.2 Ammonium

Sediment depth profiles of NH_4^+ displayed a pattern similar to the TS^{2-} profiles (Fig. 3.12). In 2019, the S1 site core (C1) concentrations were ~15 μM at the sediment surface and increased to ~200 μM by 25 cm depth in the core (Fig. 3.12; A), while the S2 site cores (C1, C2) exhibited higher levels of NH_4^+, peaking above 1000 μM by 25 cm depth (Fig. 3.12; B). Also in 2019, the R1 site core (C5) increased in NH_4^+ concentration with depth in the core, starting at ~400 μM at the surface and increasing to ~1000 μM by 20 cm depth (Fig. 3.12; C). In 2020, the R2 site cores (C5, C10) NH_4^+ concentrations were slightly higher at the sediment surface, with levels of 600-800 μM at 0 cm depth in the core and increasing to 700-1300 μM by 20 cm (Fig. 3.12; D).

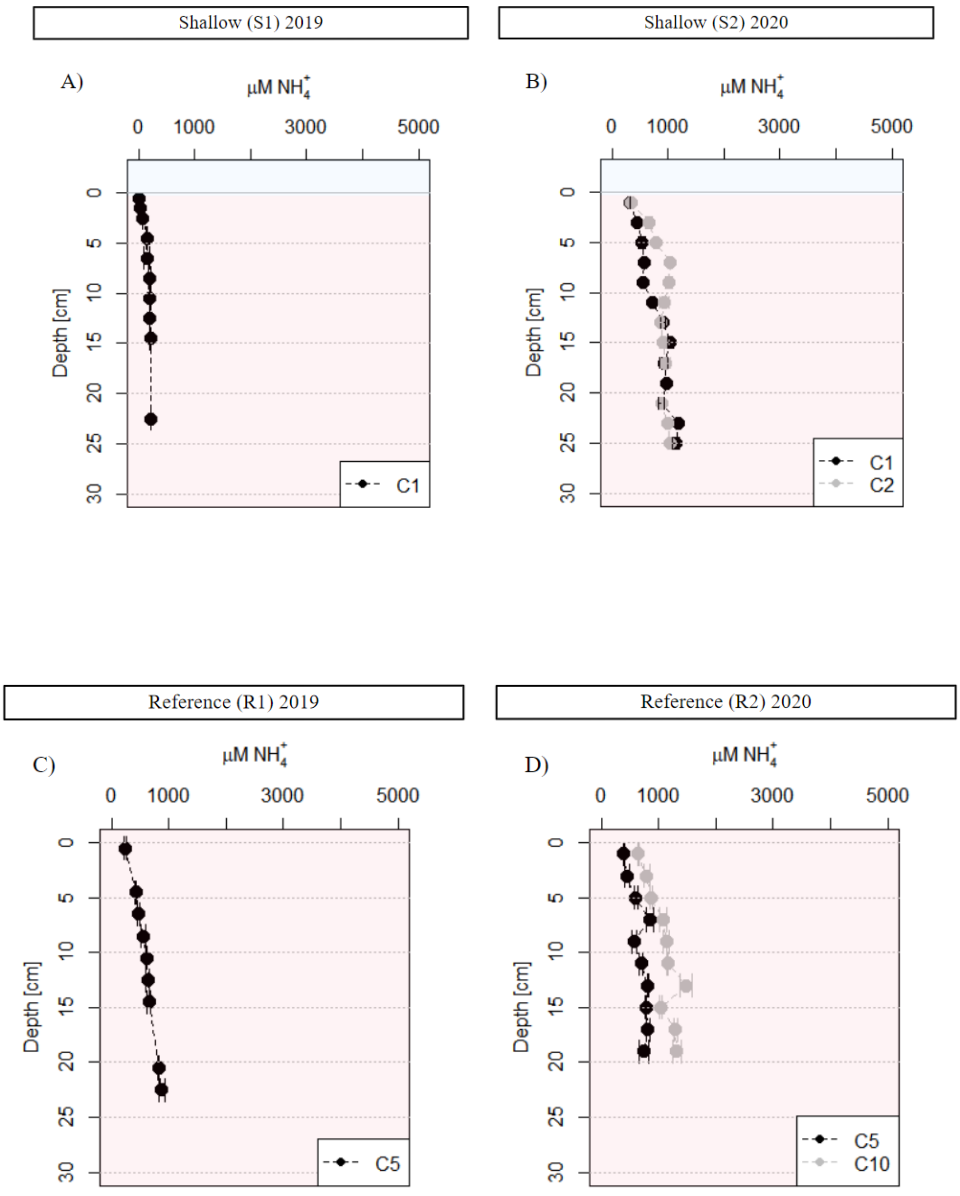
Shallow (S1) 2019
A)
µM NH_4^+
0
1000
3000
5000
Depth [cm]
0
5
10
15
20
25
30
C1
Shallow (S2) 2020
B)
µM NH_4^+
0
1000
3000
5000
Depth [cm]
0
5
10
15
20
25
30
C1
C2
Reference (R1) 2019
C)
µM NH_4^+
0
1000
3000
5000
Depth [cm]
0
5
10
15
20
25
30
C5
Reference (R2) 2020
D)
µM NH_4^+
0
1000
3000
5000
Depth [cm]
0
5
10
15
20
25
30
C5
C10

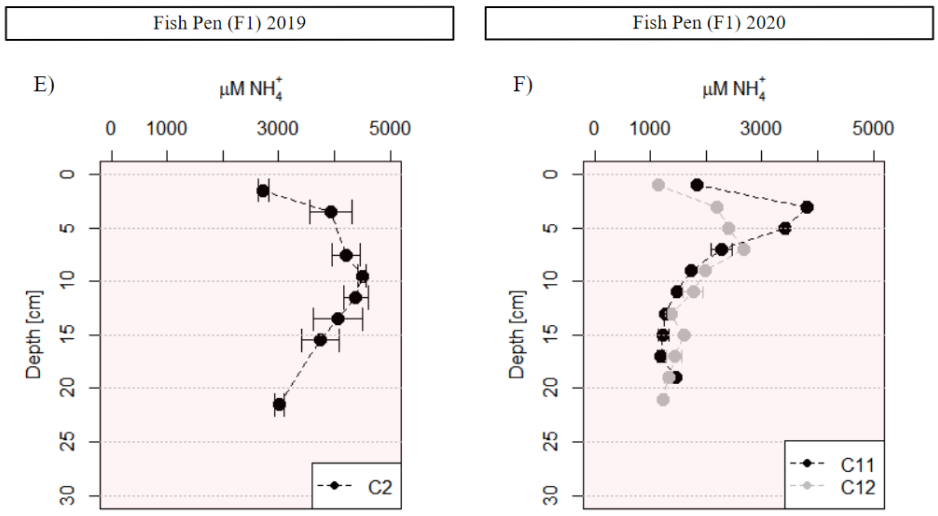

Figure 3.12: *NH_4^+ concentrations in porewater profiles through sediment cores collected at sites in the Whycocomagh Basin in 2019 and 2020. Cores were collected at five sites: S1 in 2019 and S2 in 2020 (A & B), R1 in 2019 and R2 in 2020 (C & D), and F1 in 2019 and 2020 (E & F). See Fig. 3.5 for site locations. Light blue shading (aerobic) and light red shading (anaerobic) represent the approximate DO concentration zones.*

The fish pen array site (F1) core samples had elevated NH_4^+ concentrations in comparison with the other four sites (i.e., > 1000 µM *vs.* < 1000 µM, respectively) in both years (Fig. 3.12; E, F). The F1 core NH_4^+ profiles also showed a distinct bulge of higher concentrations between 2 and 10 cm depth below the sediment surface. Concentrations tapered back to surface values near the bottom of the core profiles but showed a greater decrease with depth in the deeper sediments in 2020. In 2019, the F1 site core (C2) NH_4^+ concentrations were ~2700 µM at the sediment surface and peaked at ~4500 µM by 10 cm depth, then steadily decreased back down to ~3000 µM (Fig. 3.12; E). In 2020, the F1 site cores (C11, C12) concentrations differed substantially in the upper 7 cm (1100 µM *vs.* 1900 µM, respectively) at the surface but had a similar profile pattern to the previous year with both cores peaking at 2.5 cm (2800 µM and 3900 µM, respectively), then decreasing back down to between 1200-1400 µM by 20 cm depth (Fig. 3.12; F).

3.4.3 Iron

Figure 3.13 shows the depth profiles of dissolved Fe^{2+} concentration in the sediment cores collected at the S1 site in 2019 and the S2, R2, and F1 sites in 2020. Fe^{2+} was detected only in the surface sediments of the shallow cores (S1, S2) for both years. In 2019, the S1 site core (C1) Fe^{2+} concentrations increased from 9 μM to 28 μM in the top 5 cm and then decreased sharply to undetectable levels (<4 μM) by 9 cm depth (Fig. 3.13; A). In 2020, the S2 site cores (C1, C2) Fe^{2+} concentrations were ~5-9 μM at 0 cm and steadily decreased to levels below detection by 5 cm (Fig. 3.13; B). Dissolved Fe^{2+} concentrations measured in 2020 at the R2 site (cores C5, C10) and F1 site (only the C11 core was analyzed) were below detection through the entire 20 cm core (Fig. 3.13; C, D).

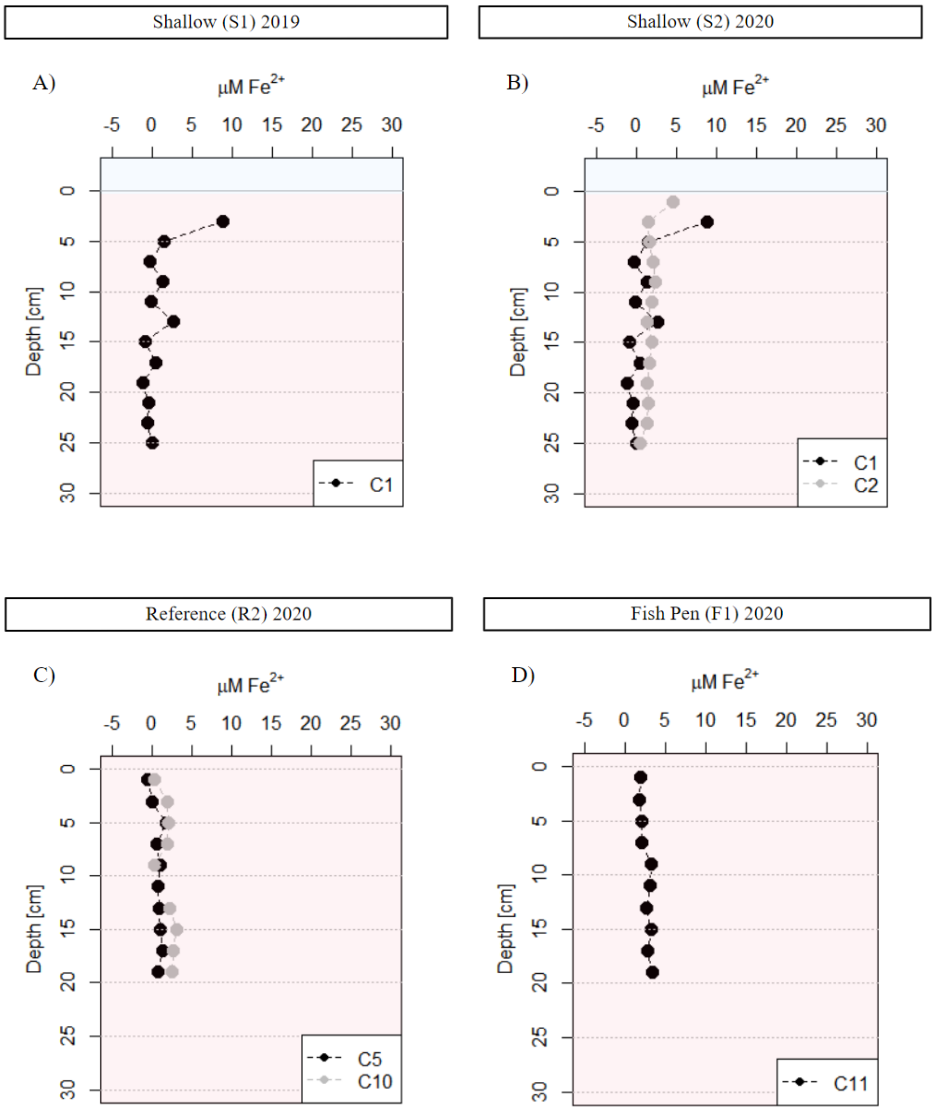

Figure 3.13: *Fe^{2+} concentrations in porewater profiles through sediment cores collected at sites in the Whycocomagh Basin in 2019 and 2020. Cores were collected at four sites: S1 in 2019 and S2 in 2020 (A & B), R2 in 2020 (C), and F1 in 2020 (D). See Fig. 3.5 for site locations. Light blue shading (aerobic) and light red shading (anaerobic) represent the approximate DO concentration zones. Sediment core porewater profiles for 2019 and 2020. Light blue shading (aerobic) and light red shading (anaerobic) represent the approximate DO concentration zones.*

3.4.4 Organic Carbon and Nitrogen

Profiles of TC (%C), TIN (%N), and C:N ratios in sediment cores were measured at the shallow (S1, S2), reference (R1, R2), and fish pen (F1) sample sites in 2019 and 2020 (Fig. 3.14-3.16). In 2019, the S1 site core (C3) averaged 4.94 ± 1.19% (TC), 0.48 ± 0.14% (TIN), and had a C:N ratio of 10.36 ± 0.69 (n=15) (Fig. 3.14; A, B, C). In 2020, the S2 site cores (C1, C2) averages were slightly higher with 5.72 ± 0.81% (TC), 0.52 ± 0.10% (TIN), and a C:N ratio of 11.06 ± 0.84 (n=13) (Fig. 3.14; A, B, C).

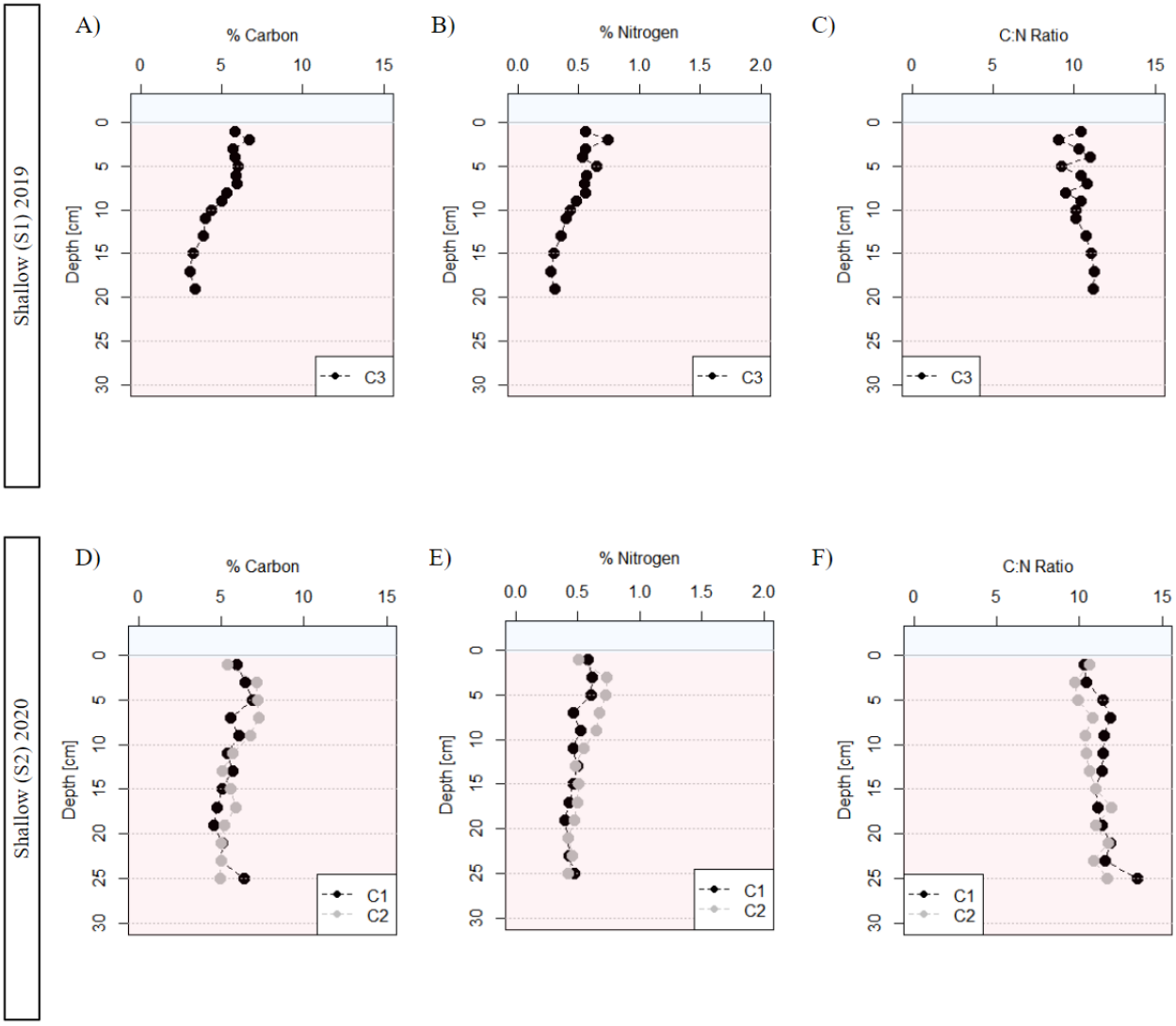

Figure 3.14: *Percent Total Carbon (A), percent Total Inorganic Nitrogen (B), and Carbon: Nitrogen ratio (C) values in porewater profiles through sediment cores collected at the S1 and S2 sites in the Whycocomagh Basin in 2019 and 2020. See Fig. 3.5 for site locations. Light blue shading (aerobic) and light red shading (anaerobic) represent the approximate DO concentration zones.*

The R1 and R2 sites TC and TIN content remained consistent between the two years (Fig. 3.15). In 2019, the R1 site core (C12) had an average TC content of 5.33 ± 0.42%, an average TN content of 0.54 ± 0.06%, and an overall C:N ratio of 9.89 ± 0.5 (n=15) (Fig. 15; A, B, C). In 2020, the R2 site cores (C5, C10) had similar content, averaging 5.31 ± 0.46% (TC), 0.52 ± 0.06% (TN), with an overall C:N ratio of 10.15 ± 0.35 (Fig. 3.15; D, E, F).

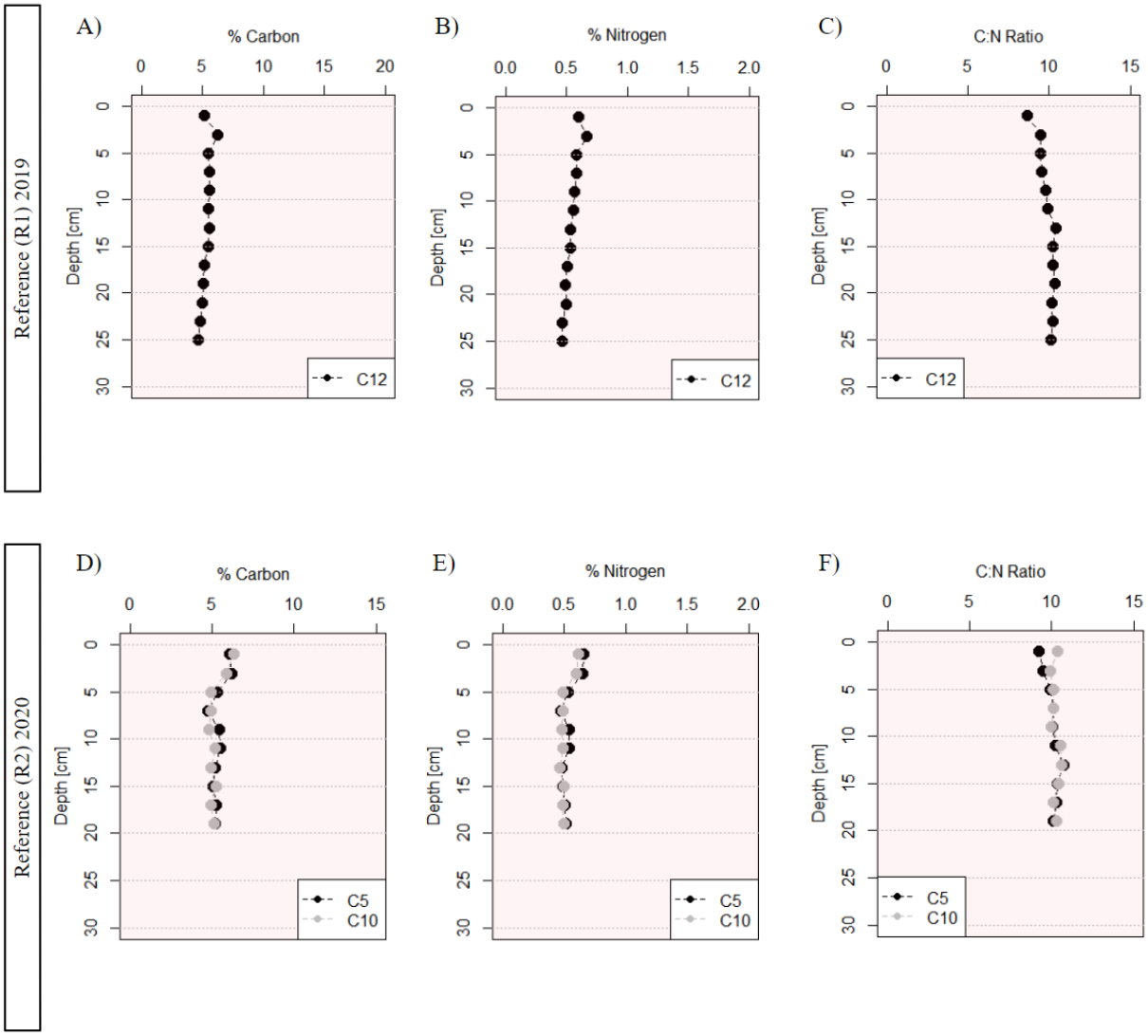

Figure 3.15: *Percent Total Carbon (A), percent Total Inorganic Nitrogen (B), and Carbon: Nitrogen ratio (C) values in porewater profiles through sediment cores collected at the R1 and R2 sites in the Whycocomagh Basin in 2019 and 2020. See Fig. 3.5 for site locations. Light blue shading (aerobic) and light red shading (anaerobic) represent the approximate DO concentration zones.*

The fish pen site (F1) exhibited higher TC and TN concentrations in the upper sediment for both years, as shown in Figure 3.16. In 2019, the F1 site core (C10) had TC concentrations of 20% and TN concentrations of 2% at the surface, both decreasing to around 5% and 0.5% by a depth of 15 cm, respectively. The whole core averages for TC and TN were 9.05 ± 5.3% and 0.89 ± 0.48%, respectively, with a C:N ratio of 9.92 ± 0.48 (n=15) (Fig. 3.16; A, B, C). In 2020,

the F1 site cores (C11, C12) had slightly lower values with TC and TN concentrations of 10% and 1.0%, respectively, at the surface, before returning to average values of 5% and 0.5%, respectively, by a depth of 5 cm. The whole core averages for TC and TN were 5.75 ± 1.39% and 0.57 ± 0.17%, respectively, with a C:N ratio of 10.28 ± 0.55 (n=10) (Fig. 3.16; D, E, F).

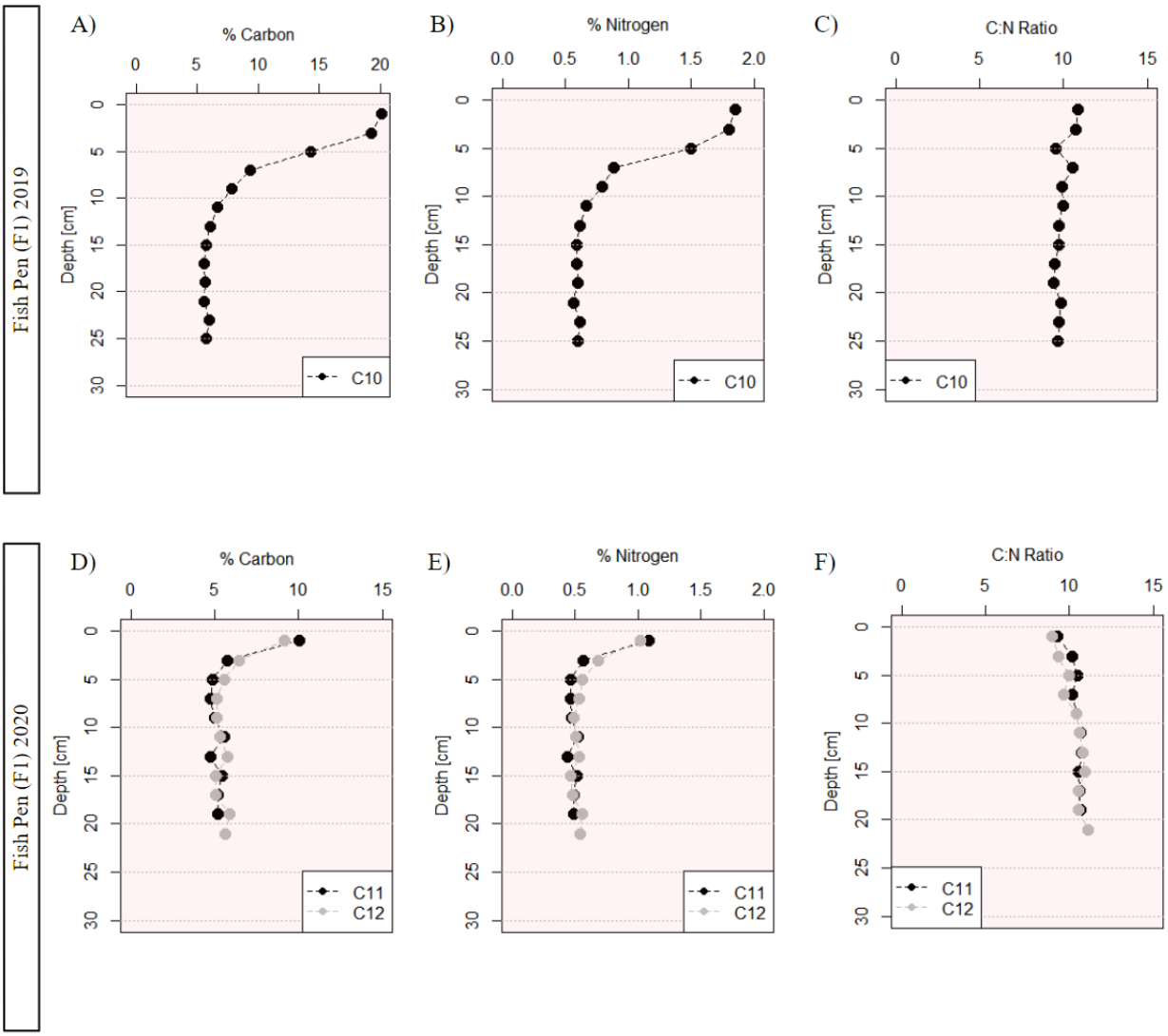

Figure 3.16: *Percent Total Carbon (A), percent Total Inorganic Nitrogen (B), and Carbon: Nitrogen ratio (C) values in porewater profiles through sediment cores collected at the F1 site in the Whycocomagh Basin in 2019 and 2020. See Fig. 3.5 for site locations. Light blue shading (aerobic) and light red shading (anaerobic) represent the approximate DO concentration zones.*

3.4.5 Porosity

Porosity values were measured only for sediment cores collected in 2019 at the S1, F1, and R1 sites (Fig. 3.17). All sites showed similar porosity values in the top 5 cm, starting at around 0.95% and then steadily decreasing to 0.85-0.90% by 10 cm depth in the core. Below this depth, porosity at the S1 site exhibited a sharp decrease to 0.75% between 12-15 cm depth. Porosity at the R1 site gradually decreased to approximately 0.78% at 23 cm, with a significant decrease down to 0.60% at 25 cm depth. Sediment porosity at the F1 site maintained porosity values between 0.80-0.90% down to 25 cm depth in the core.

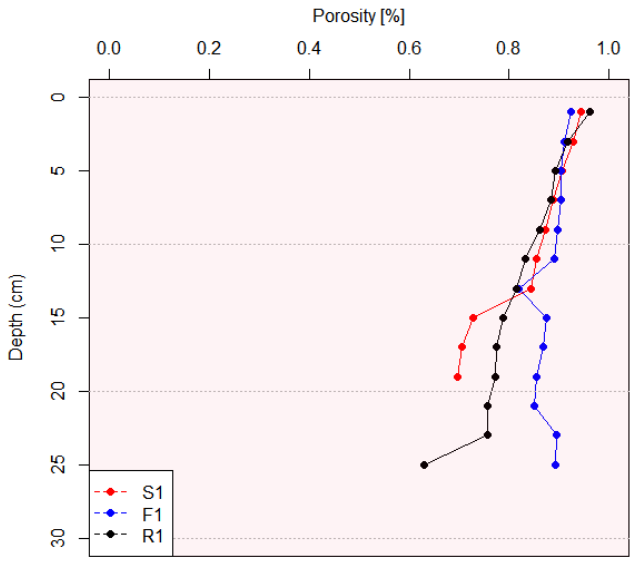

Figure 3.17: *2019 porosity values for the S1, F1, and R1 sites. Light red shading (anaerobic) represents the approximate DO concentration zone.*

3.5 Microsensor Profiles

3.5.1 Dissolved Oxygen

Dissolved Oxygen (DO) profiles were taken only from a sediment core at the S1 (2019) and S2 (2020) sites (Fig. 3.18) since the sediments at the other sites were collected below permanently anoxic water (Punshon *et al.*, 2022). DO concentrations in the core collected at the S1 site were highest at the SWI (0 cm) at 200 µM and decreased to 0 µM by 0.2 cm depth in the core (Fig. 3.18; A). At the S2 site, each of the three DO profiles were approximately 350 µM at the SWI and each rapidly declined to 0 µM by 0.4 cm depth (Fig. 3.18; B).

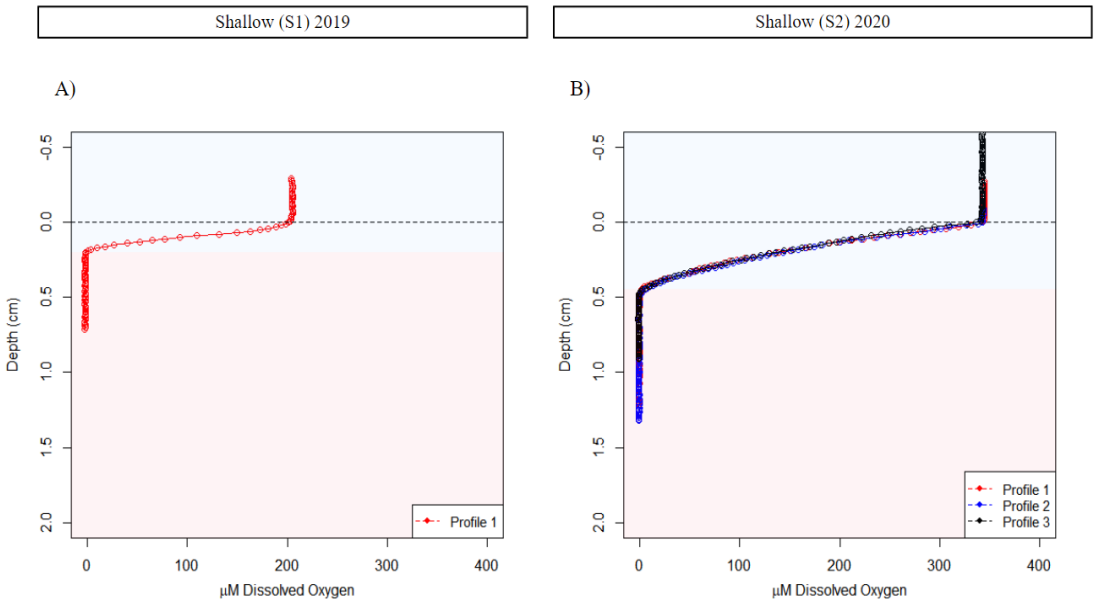

Figure 3.18: *Microsensor profiles of DO concentrations through sediment cores collected in the Whycocomagh Basin at the A) S1 site (one profile in 2019) and B) S2 site (3 profiles in 2020). Light blue shading (aerobic) and light red shading (anaerobic) represent the approximate DO concentration zones.*

3.5.2 pH

The pH microsensor profiles were measured along the same profiles as the DO concentrations which were used to calculate the sediment core TS^{2-} concentrations. The pH values were measured in the surface sediments (top 5 cm) at the sample sites for each micro-profile in both 2019 and 2020 (Fig. 3.19). In 2019, pH ranged from 6.7-8.2 across the three sample sites (Fig. 3.19; A). The lowest pH of 6.7 was observed at the S1 site from 0.5 to 1.5 cm depth. At the F1 site, the pH increased from 7 to 7.4 in the upper 1 cm, then decreased to ~6.9 at 4 cm depth. The R1 site had the highest pH, starting at 8.2 at 0 cm and steadily decreasing to ~7.7 at 4 cm depth. In 2020, pH values were more similar among the three sites ranging from 6.7-7.5 (Fig. 3.19; B). The S2 site showed an increase in pH to 7.5 in the top 1 cm depth in the core, followed by a slight decrease down to 7.1 by ~1.5 cm depth. The F1 site profile was almost identical in both years, with a pH of ~6.7 from the top to bottom of the core. The R2 site core profile was markedly different than the R1 site sampled in 2019 and showed a significant decrease from the previous year with a pH ranging from 7.0-7.2 within 5 cm depth.

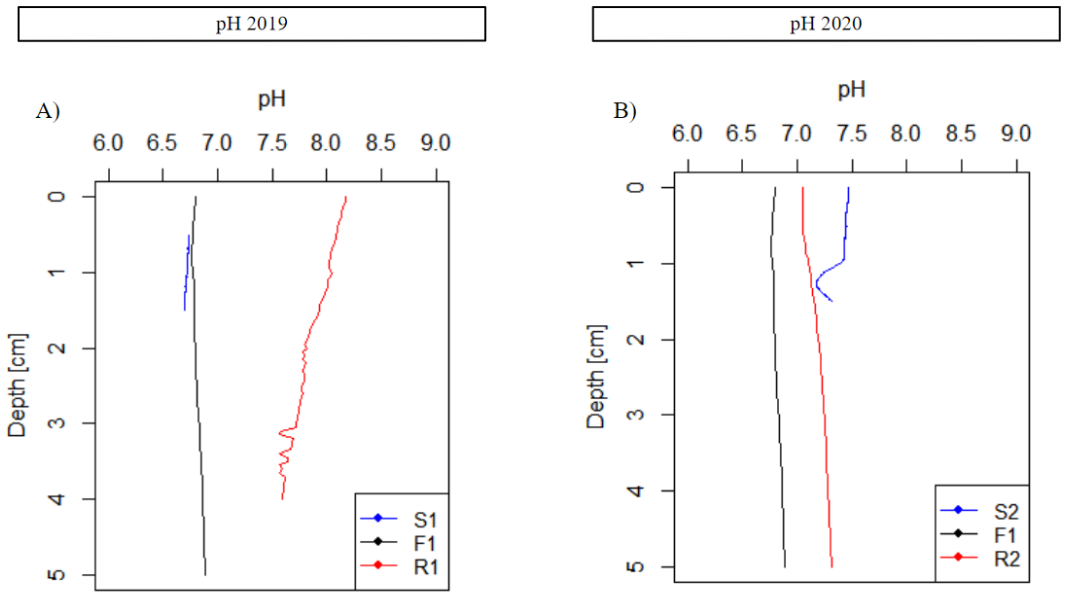

Figure 3.19: *Microsensor pH profiles for the A) 2019 S1, F1, and R1 sites and B) 2020 S2, F1, and R2 sites.*

3.5.3 Total Sulfide

Sediment core profiles were used to measure TS^{2-} concentrations in the top 2 cm at all sites for both 2019 and 2020 (Fig. 3.20), except for the S1 site which was not analyzed in 2019. In 2020, the S2 site showed an increase in TS^{2-} concentrations from 0-400 µM by 0.4 cm depth (Fig. 3.20; A). The F1 site, which reared adult trout in 2019, maintained steady TS^{2-} concentrations at ~11,500 µM from 0-2 cm depth (Fig. 3.20; B). However, in 2020 when the F1 site was fallow, profiles of bottom TS^{2-} concentrations decreased by about 1,000 µM, starting at ~4,500 µM at 0 cm and gradually increasing to ~10,500 µM by 2 cm depth (Fig. 3.20; C). At the R1 site in 2019, TS^{2-} concentration profiles were ~400 µM at 0 cm and increased to 2,500 µM by

2 cm depth (Fig. 3.20; D). In 2020, the R2 site profiles were slightly higher, with TS^{2-} concentrations of ~1,000 μM at 0 cm increasing to ~4,000 μM by 2 cm depth (Fig. 3.20; E).

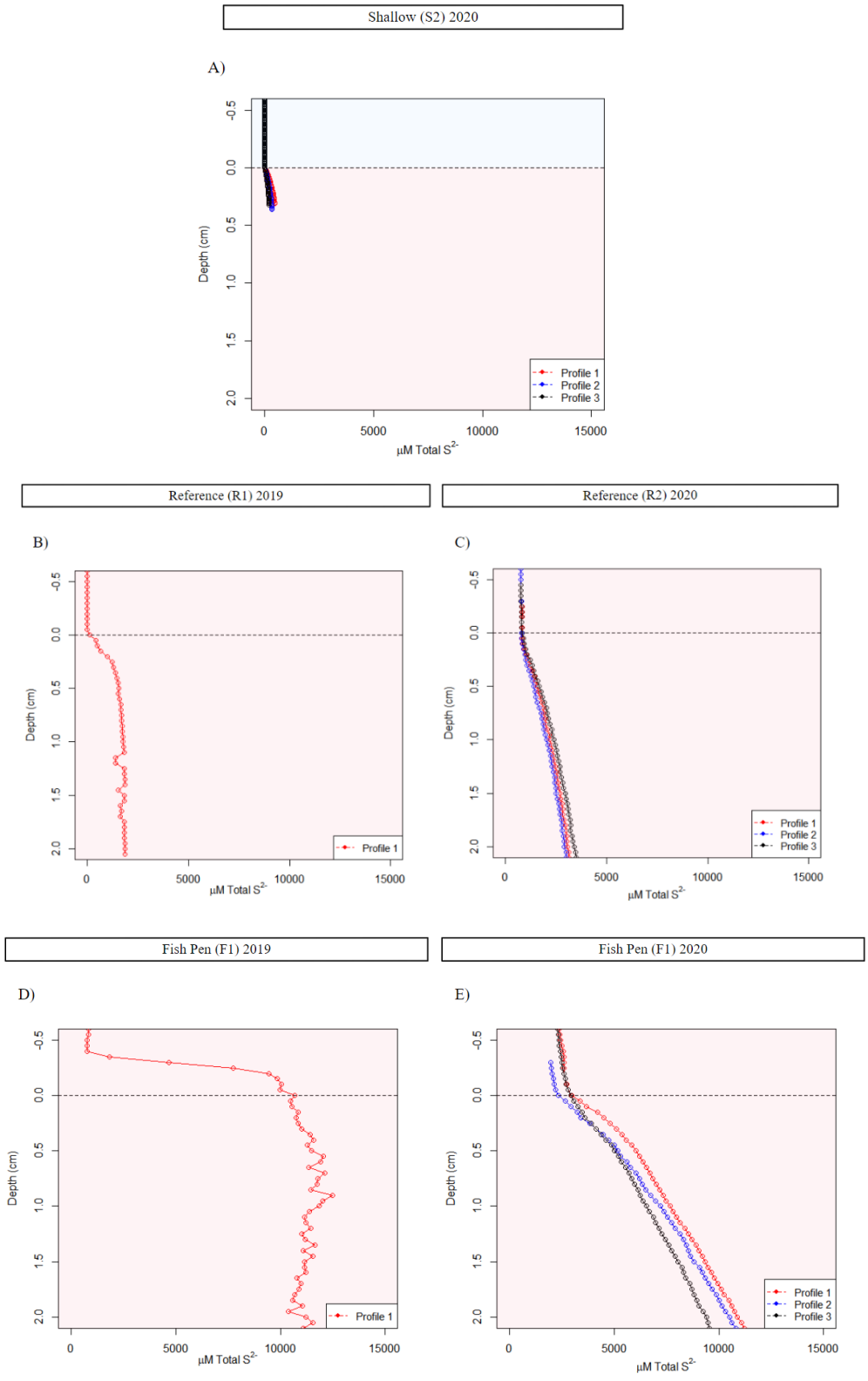

Figure 3.20: *Microsensor TS^{2-} concentration profiles in sediment at sites A) S2 (2020), B) R1 (2019), C) R2 (2020), D) F1 (2019), and E) F1 (2020). Triplicate profiles were taken in the 2020 core samples. Light blue shading (aerobic) and light red shading (anaerobic) represent the approximate DO concentration zones.*

CHAPTER 4
DISCUSSION

4.1 Chemistry of the Whycocomagh Basin

The Whycocomagh Basin offers an ideal case study to investigate the effects of organic enrichment on benthic biogeochemical processes in a permanent, anoxic ecosystem. The isolation of the Whycocomagh Bay from the rest of the Bras d'Or Lakes (BdOL) by the shallow, Little Narrows sill (~15 m depth) creates minimal tidal influence, with a near-surface exchange circulation of less than 100 $m^3 s^{-1}$, and significant wave heights < 0.6 m (Petrie & Budgen, 2002). Further isolation of the Whycocomagh Basin from the eastern Whycocomagh Bay due to the Mid Bay sill (~7 m depth) contributes to the persistent thermocline and halocline (*i.e.,* pycnocline) observed at ~10-15 m depth (see Fig. 3.1). This restricts the ventilation of bottom waters and has created a permanent anoxic zone from ~20-48 m depth (Parker *et al.,* 2007). These physical conditions were evident at the deep site (D1) which was stratified during both November 2019 and September 2020. Surface temperature and salinity were lower in 2019 at 6 °C and 18 PSU than in 2020 at 16 °C and 22 PSU, respectively. This is likely due to the difference in sampling months between years, but subsurface values remained constant below the thermo- and haloclines at ~3 °C and 22.7 PSU (Fig. 3.1). These values are in line with past observations, though bottom water salinity was slightly less saline than previous years (Krauel, 1975; Strain & Yeats, 2002; Punshon *et al.,* 2022). Nonetheless, this demonstrates the control the pycnocline has on the depth of the anoxic zone and suggests good ventilation down to ~14 m depth, with deeper waters largely isolated from the surface layer.

The hydrography of a system strongly influences the development of hypoxic and anoxic conditions and can greatly affect the response to increased organic matter (OM) input (Gray *et al.,* 2002). Gurbutt & Petrie (1995) and Manning *et al.* (2019) reported the residence time of the waters of the Whycocomagh Basin to be ~0.7 years for the surface waters and ~2 years for the subsurface waters, with exceedingly low bottom current velocities of ~0.3 cm s^{-1} (Gurbutt & Petrie, 1995). The bathymetry of the 48 m deep Basin has a parabolic shape, which influences the horizontal transport of materials, specifically near the bottom of the Basin. This shape, and the other attributes of the Basin (described above), leaves vertical mixing as the primary exchange between the surface and subsurface waters, and influences exchange processes across the pycnocline. This natural separation between the surface (oxic) and subsurface (anoxic) waters in the Basin influences both biological and physical factors. The rapid attenuation of light through the upper 5 m of the turbid water column in both 2019 and 2020, as well as the chlorophyll maximum at ~10 m depth (also observed by Punshon *et al.*, 2022), indicates high phytoplankton activity in the upper surface layer, where nutrient concentrations are typically higher. Eutrophy refers to the state of high nutrient availability and biological productivity in aquatic systems. In eutrophic coastal estuaries, high inputs of nutrients and organic matter (OM) typically contribute to eutrophic conditions throughout the water column (Gray *et al.,* 2002). However, in the Whycocomagh Basin, eutrophic conditions are primarily restricted to the bottom sub-surface waters at >20 m depth, driven by inputs of OM to the bottom layer. This is further indicated by dissolved oxygen (DO) concentrations in the surface water near saturation in November 2019 (300 μM; ~90% saturation) and in September 2020 (~240 μM; ~75% saturation), which were consistent with the maximum value observed in October 2017 (245 μM) by Punshon *et al.* (2022). Below the pycnocline, DO concentrations at this site have been

consistently undetectable for approximately fifty years since 1975 (Krauel, 1975; Strain *et al.,* 2002; Manning *et al.,* 2019; Punshon *et al.,* 2022). In September 2020, the oxycline shoaled into the upper water column, such that penned fish were affected and the pens had to be moved out of the Basin. This shallowing of the oxycline was likely caused by local upwelling due to the strong offshore winds observed during this period. Maximum gusts of 45 km/h were recorded at the Port Hawkesbury station for the month of September 2020 (Environment Canada, 2022).

The major biogeochemical pathways of nutrients and redox-sensitive solutes in the subsurface water column and sediments of the Whycocomagh Basin closely follow the redox cascade of respiration processes, as originally described by Froelich *et al.* (1979; Fig. 1.1). In anoxic waters, the natural abundance of sulfate makes it the preferred electron acceptor of anaerobic microbes, producing TS^{2-} that accumulates in dissolved form in stagnant environments if there are no available oxidation reactions or sinks such as mineral precipitation on the adjacent sediments. Because NH_4^+ is a preferred source of nitrogen for phytoplankton in the upper, oxic part of the water column and is taken up through nitrification resulting in the absence of NH_4^+ above the pycnocline. However, the absence of nitrification processes occurring below the pycnocline leads to an increase in NH_4^+ concentrations in the anoxic zone due to microbial mediated ammonification. By comparing the present water column concentrations of TS^{2-} and NH_4^+ to historical levels observed in the Basin, it is evident that both compounds have experienced a significant increase over the past 50 years (Krauel, 1975; Strain *et al.,* 2002; Punshon *et al.,* 2022). Specifically, since 1995, TS^{2-} levels have shown a tenfold increase (Punshon *et al.,* 2022). Furthermore, during periodic upwelling events, the redox potential discontinuity (RPD) layer has been observed to extend to the bottom of the fish pens, as communicated by Bruce Hatcher and Robin Stewart (personal communication).

At the D1 site in the middle of the Basin, TS^{2-} concentrations were similar in 2019 and 2020, reaching ~1100 μM by 45 m depth. This is within the range observed at 44 m depth by Punshon *et al.* (2022) at ~1000 μM. In contrast, NH_4^+ concentrations in the near-bottom waters at the D1 site differed by an order of magnitude between the two study years, being considerably lower in 2019 (50 μM) than in 2020 (250 μM) at 35 m depth, with the latter more similar to bottom water concentrations observed by Punshon *et al.* (2022) at ~290 μM. Analytical or sampling errors, including potential inaccuracies in the dilution factor or spatial heterogeneity, cannot be completely ruled out for the 2019 NH_4^+ data, particularly when considering the low concentration compared to measured values in 2017 (Punshon *et al.,* 2022) and in 2020. However, the lower concentrations may also indicate a greater degree of microbial processing of OM occurring earlier in the autumn season (September 2020) than later (November 2019). In both sample years, however, NH_4^+ concentrations in the bottom water declined at 35-45 m depth, rather than increasing down toward the sediment-water interface (SWI). This decrease near the SWI was also observed by Punshon *et al.* (2022) in October 2017, but it was not nearly as sharp a decrease as observed in both months of this study. With a calculated residence time of greater than 2 years for bottom water exchange in the Basin (Gurbutt & Petrie, 1995; Manning *et al.,* 2019) and TS^{2-} concentrations increasing with depth throughout the water column to the SWI, NH_4^+ concentrations were expected to follow a similar trend, but they did not.

The reason for this inversion of the NH_4^+ trend near the seabed is unknown. It is possible that there are unidentified sink processes for NH_4^+ occurring in the Basin, such as the presence of an anoxic biofilm of aggregated microorganisms that use NH_4^+ for protein assimilation (Sawayama, 2006). Testing this hypothesis requires benthic sediment profiles to observe how NH_4^+ concentrations change across the SWI, but this was not possible at the D1 site due to the

length of the winch wire on the vessel used for coring operations. The inversion of NH_4^+ could also be a result of horizontal mixing transporting OM away from the fish pens and, or from periodic physical mixing of bottom water by dense water intrusion events entering from the Whycocomagh Bay to the west of Indian Island over a 14 m deep sill (refer to Fig. 2.2). In both these cases, however, one would expect a corresponding decrease in TS^{2-} concentrations in the lower water column towards the SWI, which was not observed. Despite this discrepancy, the resemblance of current profiles of TS^{2-} and NH_4^+ concentrations in bottom water to past observations, along with the notable increase in these concentrations over the past few decades, are most likely attributable to heightened anaerobic decomposition of settling of OM within the Basin (Punshon *et al.,* 2022).

Throughout the entire water column in the deep Basin, nutrient profiles of dissolved iron (Fe^{2+}) concentrations, as well as nitrate and nitrite ($NO_3^- + NO_2^-$), remained below detection limits (2 μM and .4 μM, respectively). There were no noticeable vertical trends observed, except for a small peak of $NO_3^- + NO_2^-$ (~3.8 μM) at 10 m depth, followed by a decrease down to 0 μM for the rest of the water column. This pattern aligns with the expected behavior, as nitrification processes primarily occur in the upper oxic zone, via oxidation, while denitrification processes consume nitrate and nitrite in anoxic waters through reduction, typically at the redox potential discontinuity layer (RPD) (Berner, 1974).

A similar peak of Fe^{2+} in the upper oxic zone was also expected but was either not captured due to the sampling resolution of the Niskin bottle samples (taken approximately every 5 m) or absent because of Fe^{2+} precipitation with TS^{2-} in the anoxic zone, resulting in the formation of iron sulfide (FeS) minerals. In the anoxic zone, iron reduction generates dissolved Fe^{2+} which typically diffuses upward and re-oxidizes to form Fe^{3+} upon encountering oxygen

(Fig. 4.1). The Fe^{3+} quickly precipitates into iron oxides (FeO_3) and sinks back into the anoxic zone, where it is reduced again. Consequently, anoxic water columns often display a distinct dissolved iron peak just below the oxycline due to intense iron cycling (Berner, 1970).

However, in the Whycocomagh Basin, the relatively high TS^{2-} concentrations near the RPD layer might bind with Fe^{2+} to form stable FeS, which could then sink through the water column and eventually be buried. This process may prevent the typical dissolved iron cycling at the RPD layer, which leads to a peak in Fe^{2+}. If there is sufficient available Fe^{2+} for TS^{2-} to precipitate with, it could effectively reduce TS^{2-} accumulation in the sediments and decrease the demand for sulfide oxidation processes (Schendel *et al.,* 2004; Cranford *et al.,* 2020).

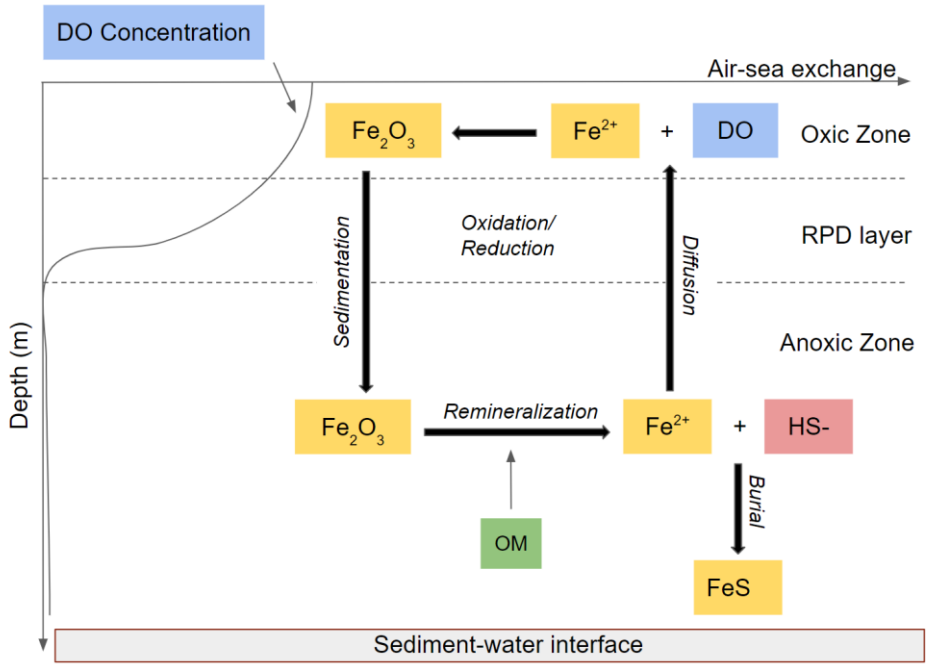

Figure 4.1: *Iron cycling diagram exhibiting the diffusion and precipitation processes that typically occur where the oxic/anoxic zones meet.*

The sediments in the Whycocomagh Basin undergo a transition to a more reduced state with increasing depth, mirroring the pattern observed in the water column. Along the SD Transect, concentrations of TS^{2-} and NH_4^+ in bottom water and surface-grab porewater increased with depth, indicating progressively more reduced sediments (Figs. 3.7 and 3.8). At the shallow end of the transect (10-17 m depth), both TS^{2-} and NH_4^+ concentrations in bottom waters were 0 μM, but they steadily rose to 790 μM and 200 μM, respectively, near the deep end (~33 m depth). Porewater concentrations of TS^{2-} and NH_4^+ also exhibited an upward trend, increasing from ~500-390 μM at the shallow end to around 3500 μM and 700 μM, respectively, by the deep end. The sediment grab samples collected along the SD Transect showed consistent average total carbon (TC) and total inorganic nitrogen (TIN) values with depth, measuring 5.54% C and 0.56% N, respectively. This resulted in a carbon-to-nitrogen (C:N) ratio of approximately 10:1 (Fig. 3.9). The observed C:N ratio is consistent with ratios found in coastal waters (Berner *et al.*, 1970), indicating efficient metabolism of organic matter (OM) in the sediments of the Whycocomagh Basin.

As a result of anaerobic respiration, OM in the sediments is effectively metabolized, and the byproducts of anaerobic respiration accumulate in the porewater. These byproducts gradually diffuse into the overlying bottom water when the sediments become saturated (Berner *et al.*, 1970). The degradation processes of OM strongly depends on the C:N ratio, with easier degradation and remineralization occurring when the ratio is below 10. Higher ratios may indicate the presence of more recalcitrant carbon (Knapp & Bromley-Challoner, 2003). Therefore, inputs of high-quality OM with low C:N ratios can contribute to eutrophication in already nutrient-rich ecosystems by providing excess nutrient inputs (Gray *et al.,* 2002).

To provide a more detailed understanding of the sediment geochemistry in the Whycocomagh Basin, and the changes in the redox state with water depth, a comparison was made between sediment cores from shallow sites (S1 and S2) and references sites (R1 and R2). The shallow site cores were collected beneath oxygenated bottom waters at depths of 10-11 m, while the references site cores were collected beneath permanent, anoxic bottom waters at depths of 25-30 m. Both sites exhibited similar TC and TIN values of 5% C and 0.5% N, but their porewater geochemistry differed (Figs. 3.14 and 3.15).

In the shallow site cores (C1 in 2019, C1 and C2 in 2020), a thin oxic layer was present from the sediment surface down to 0.25 cm in 2019 and 0.5 cm in 2020. Below these oxic layers, Fe^{2+} porewater concentrations were detected and increased, peaking at ~30 μM in 2019 and 5-10 μM in 2020 within the upper ~5-8 cm, after which concentrations declined to below detection. This pattern is characteristic of bioturbated sediments with active iron cycling and likely due to the binding of Fe^{2+} to upward diffusing TS^{2-} and the formation of iron-sulfide minerals (Thamdrup *et al.,* 1994). Following the depletion of Fe^{2+}, TS^{2-} concentrations started to increase, reaching 200 μM in 2019 and ~1000 μM in 2020. Similarly, NH_4^+ concentrations increased with depth, reaching ~200 μM in 2019 and over 1000 μM in 2020. It is unclear whether more reduced profiles observed in the 2020 cores (*e.g.,* higher TS^{2-} and NH_4^+, and lower Fe^{2+}) compared to 2019 are due to spatial or temporal variability. In contrast to the shallow site sediment cores, the reference site cores (C5 in 2019, C5 and C10 in 2020) exhibited highly reduced conditions with no evidence of aerobic mineralization. Concentrations of TS^{2-} and NH_4^+ exceeded 2000 μM and 1000 μM, respectively, in these cores.

Despite differences in depth and scale, the redox processes in the Whycocomagh Basin exhibit similarities with other strongly stratified, anoxic water bodies, such as the Black Sea - the

largest permanently anoxic, land-locked basin in the world (Anderson & Raiswell, 2004; Hiscock & Millero, 2006). The Black Sea is approximately 22 million years old (Ryan *et al.,* 1997) and exhibits hydrographic qualities similar to the Whycocomagh Basin, although on a much larger scale of 2000 m depth compared to the Whycocomagh Basin's 48 m depth (Anderson & Raiswell, 2004; Hiscock & Millero, 2006; Murray *et al.,* 1991). Both waters have experienced anthropogenic impacts since the 1970s (Krauel, 1975; Tugrul *et al.,* 2014). The surface salinity of both the Black Sea and the Whycocomagh Basin is lower (17-18 PSU) than subsurface waters (21-23 PSU) due to freshwater input from rivers and tidal connections to seawater sources (Krauel, 1975; Tugrul *et al.,* 2014).

While the Black Sea and the Whycocomagh Basin share characteristics such as low bottom water currents (~0.5 m^{-3} s^{-1} and 0.3 m^{-3} s^{-1}, respectively), there are notable differences between the two waters. The depth of the RPD layer, where concentrations of DO, TS^{2-}, and other redox-sensitive compounds intersect in the water column, occurs at different depths. In the Black Sea, the RPD layer lies at ~150–200 m below the surface waters, while in the Whycocomagh Basin, it occurs at ~15-20 m depth (Krauel, 1975; Haklidir & Kapkin, 2005; Baykara *et al.,* 2007). The Black Sea has a deep-water residence time of ~387 years compared to an ~2-year residence time in the Whycocomagh Basin (Murray *et al.,* 1991; Gurbutt & Petrie, 1995; Manning *et al.,* 2019).

Despite the longer residence time in the Black Sea, its TS^{2-} and NH_4^+ concentrations near the seafloor are lower than those observed in the Whycocomagh Basin. Concentrations of TS^{2-} and NH_4^+ in the bottom waters of the Black Sea are reported to be ~400 μM and ~100 μM, respectively, near the seafloor at a depth of 2000 m (Kuypers *et al.,* 2003; Haklidir & Kapkin, 2005; Baykara *et al.,* 2007). In contrast, the Whycocomagh Basin exhibits significantly higher

concentrations, with TS^{2-} reaching 3200 μM and NH_4^+ ranging from 200-300 μM. These elevated concentrations are noteworthy even when compared to other anoxic, brackish waters with limited mixing (Mente *et al.,* 2006). This indicates that factors other than residence time play a role in determining the sulfide and ammonium concentrations in these two anoxic water bodies.

The differences in TS^{2-} and NH_4^+ concentrations between the Black Sea and the Whycocomagh Basin may be influenced by various factors, including OM inputs. The Black Sea, known for its higher levels of iron deposition under anoxic/euxinic bottom waters, as mentioned in Anderson & Raiswell's (2004) review, may contribute to lower TS^{2-} concentrations due to the high reactivity of iron with sulfide compared to oxic sediments. In the Black Sea's anoxic sediments, there are distinct terminal processes of OM mineralization. Sulfate reduction primarily occurs in the upper 2–4 m, while methanogenesis takes place below the sulfate zone (Jorgensen *et al.,* 2004). Below the sulfidic water column, Jorgensen *et al.* (2004) proposed a diffusion model to explain the interaction between excess reactive iron in the deep waters and the hydrogen sulfide (H_2S) derived from methane. According to this model, the majority of the methane derived H_2S diffusing up from the sediments reacts with the excessive iron from the water column. This combination of methane-driven sulfate reduction and the presence of a deep H_2S sink ultimately leads to the formation of isotopically heavy pyrite in the sediment. Therefore, the input of OM, coupled with the presence of iron and the specific processes of OM remineralization, may contribute to the observed differences in TS^{2-} and NH_4^+ concentrations between the Black Sea and the Whycocomagh Basin.

4.2 Carbon and Sulfur Cycling in Sediments Beneath Fish Pens: Influence of Accumulated Farm Waste in the Whycocomagh Basin

Coastal waters, including fjords in the Baltic Sea, where fish farms are situated at similar depths to the Whycocomagh Basin, often experience seasonal anoxia. However, the presence of sufficient water currents in these areas help to create well-oxygenated conditions around the farms and re-suspend settled particles (Holmer & Kristensen, 1992; Mente *et al.,* 2006). Typically, impacts from fish farms in well-oxygenated waters are limited to an area within 70 m of the fish pen arrays (Mente *et al.,* 2006; Giles, 2008). The accumulation of waste from fish farms can lead to a shift toward anaerobic metabolism in the sediments beneath them, resulting in elevated concentrations of TS^{2-} that can negatively affect benthic infauna communities (Holmer & Kristensen, 1992). However, in the Whycocomagh Basin, where anoxic conditions prevail and TS^{2-} concentrations already exceed harmful levels, the impact of fish farming above an anoxic basin on the benthic ecosystem is not fully understood. In these environments, which are already dominated by microbial processes and devoid of benthic macrofauna, the consequences of fish farming remain unclear.

Fish farms have been found to significantly enhance the metabolism of nutrient-rich, eutrophic sediments, promoting anaerobic processes that can be up to 10 times higher during the farming seasons (Holmer & Kristensen, 1992). When OM decomposes in the water column, only a fraction of it (around 10-20%) reaches the sediment surface, where further degradation drives sediment diagenesis and benthic fluxes (Emerson & Hedges, 2008). The OM derived from fish feed undergoes decomposition similar to other types of organic inputs in the sediment and can be

utilized by benthic organisms if present (Boyd *et al.,* 2010). In the Whycocomagh Basin, characterized by limited bottom water exchange and a decreasing gradient of macrofauna diversity from the oxic to anoxic waters, porewater fluxes primarily occur through diffusion and are influenced by the degradation of OM accumulating on the sediment-water surface (Krost *et al.,* 1994). These fluxes are typically higher within the proximity of the fish farm due to increased organic input.

Observations in the Whycocomagh Basin indicate increased sedimentation near the fish pen array (F1 site) compared to reference sites (R1, R2), as reflected in higher bottom porosity values in the sediments under the F1 site (~0.9% *vs.* ~0.6% in reference sites) (Fig. 3.17). Surface sediment grab samples and porewater profiles from sediment cores were consistent with this, revealing localized and significantly higher concentration gradients of TS^{2-} and NH_4^+ (~100s of meters) within the general farm area, compounded by the already elevated concentrations in the Basin. This can strongly be attributed to the accumulation of fish feed and waste piling on the sediment floor (Punshon *et al.,* 2022). The horizontal and vertical sediment distribution patterns of OM and anaerobic respiration by-products point to substantial enrichment (up to an order of magnitude) beneath the fish pen array, with a nearly 50% decrease observed after a year of fallowing. Similar findings from other fish farm studies (Kempf *et al.,* 2002; Schendel *et al.,* 2004) suggest that the majority of OM pollutants become sequestered directly in the sediments and remain localized, particularly in low-energy (low turbulence) fish farm environments.

The spatial variation of OM accumulation near the pen array is evident from the TC and TIN values obtained from sediment grabs along the AP Transect, which followed a constant depth contour from the fish pen array toward the middle of the Whycocomagh Basin (Fig. 3.10;

B). These values reached a peak (12.5% C and 2.5% N) with a corresponding decrease in the C:N ratio from 10:1 to 8:1 at a distance of 25-30 m away from the fish pen array. Beyond 50 m, the C:N ratio increased back to 10:1. This peak in values within the first 50 m of the transect could suggest that the breakdown of excess OM is more readily degraded around the fish pen array. The background ratios of OM in the Basin differ from those observed beneath the fish pen array, possibly due to the input of high-quality OM with a low C:N ratio coming from the fish feed, However, the exact C:N ratio of the OM originating from the fish feed is unknown. Beyond 50 m, the decline in OM values away from the pen array aligns with the spatial gradient reported by Kempf *et al.* (2002). Their study observed a fourfold increase in TC and TIN (27.5% C and 3.63% N) beneath a trout farm in the English Channel. At control stations located 300 m away, despite strong tidal influence (2.5-5.3 m), values decreased significantly (6.03% C and 0.22% N).

The concentrations of TS^{2-} and NH_4^+ from sediment grab porewater and bottom water concentrations along the AP Transect gradually decreased with increasing distance. The highest porewater concentrations of TS^{2-} and NH_4^+ were found beneath the fish pen array (~15000 μM and 1000 μM, respectively), and decreased to ~1100 μM and less than 500 μM, respectively, at distances of 100-150 m from the fish pen array (Fig. 3.7; B). Similarly, the bottom water concentrations of TS^{2-} and NH_4^+ also decreased with distance from the pen array along the transect, dropping to 0 μM by 120 m (Fig. 3.6: B).

The vertical distribution of OM accumulation and reduction processes in the sediment cores showed a trend of increasing-to-decreasing concentrations with increasing depth. The cores collected under the fish pen array in 2020 showed nearly complete recovery in the top 0-10 cm after a year of fallowing (Fig. 4.2). However, the surface values remained elevated, likely due to

the presence of fish feed and feces in 2019. In both years, the fish pen array exhibited the highest TC and TIN values compared to the reference sites, particularly in the top 0-10 cm, with concentrations approaching reference values by a depth of 15 cm (Fig. 4.2). These findings highlight the significant impact of fish farming on biogeochemical processes. The introduction of additional organic matter particulates from fish farming activities is efficiently mediated through microbial respiration in the sediments, effectively breaking down the particulates into carbon and other byproducts.

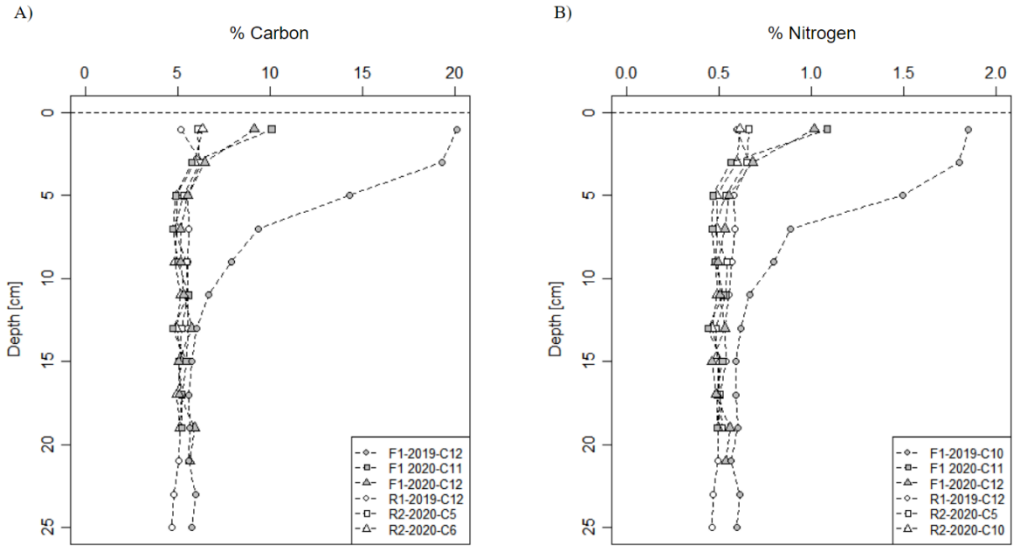

Figure 4.2: *Depth profile comparison of Total Carbon (A) and Total Inorganic Nitrogen (B) from the sediment cores collected at the Fish Pen site (F1) and Reference sites (R1, R2) in 2019 and 2020.*

The comparison of C:N ratios between the Whycocomagh Basin and a seasonally eutrophic fjord in Denmark provides valuable insights into the impact of fish farming on sediment TC and TIN levels. Holmer & Kristensen (1992) conducted a study beneath a Rainbow trout farm during mid-production and found that the highest TC and TIN values were

concentrated in the top 0-2 cm depth, with a C:N ratio ranging from 5.7-7.0. In contrast, the C:N ratios in their control stations resembled those typical of marine-estuary and coastal ecosystems, ranging from 7.7-9.8 (Burdige, 2007), which are closer to the ratios observed in the Whycocomagh Basin. These results suggest a greater preference of bacteria for nitrogen, which could be influenced by the spatial and temporal hydrographic properties of the water, affecting the dispersion of OM between different sites. Notably, even after fish harvest, the sediments studied by Holmer & Kristensen (1992) maintained low C:N ratios, indicating the continued dominance of OM waste from the fish farm as the primary substrate for decomposers.

After a year of fallowing at the fish pen site, the sediment core porewater concentrations of TS^{2-} and NH_4^+ decreased. However, concentrations were still considerably higher under the fish pen array compared to the reference sites (Fig. 4.3), suggesting no available loss processes aside from diffusion. This indicates that diffusion alone was insufficient to effectively reduce the sulfide and ammonium levels in the sediments beneath the fish pen array. Surprisingly, sediment core TS^{2-} porewater concentrations were consistent at the reference sites for both years, despite their different locations. The primary mechanism available for benthic sulfide removal in the Whycocomagh Basin would be diffusion into the water column over time, where it would be oxidized by Fe^{2+} to form FeS minerals or scavenged. However, available Fe^{2+} is likely removed higher in the water column (Berner, 1970).

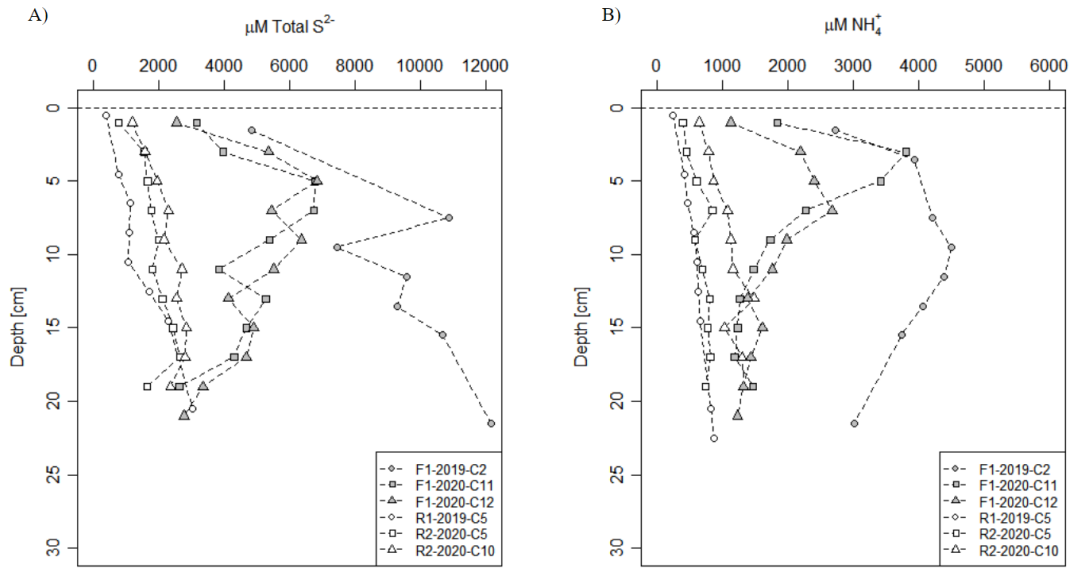

Figure 4.3: *A) TS^{2-} and B) NH_4^+ sediment core porewater concentrations collected at the Fish Pen site (F1) and Reference sites (R1, R2) in 2019 and 2020.*

The sediment cores revealed that the highest concentrations of NH_4^+ porewater were found at a depth of 10 cm beneath the fish pen array in 2019. Although these concentrations remained elevated in 2020, they decreased to levels similar to the bottom concentrations observed at the reference sites. Similarly, Schendel *et al.* (2004) reported significant levels of NH_4^+ in the top few cm of sediments along a horizontal transect away from a trout farm off the east coast of British Columbia. They observed a threefold increase in NH_4^+ concentrations beneath the farm, despite the strong influence of tidal flushing. The presence of elevated NH_4^+ levels near the fish pen array is expected, as it is the primary component of *Salmonid* urine. Merceron *et al.* (2002) also highlighted the potential for under or overestimation of NH_4^+ levels due to circadian fluctuations associated with feeding.

Coastal sediment pH profiles can be complex, primarily due to changes in OM content (Forja *et al.,* 2004). The pH values slightly decreased between years at both the pen array and reference sites, indicating a more acidic environment. This shift toward acidity is typical of anoxic sediment porewaters as high concentrations of TS^{2-} and NH_4^+ resulting from OM decomposition tend to lower the pH toward 6.9 (Ben-Yaakov, 1973; Berner *et al.,* 1970). Schaanning & Hansen (2005) identified a critical pH threshold of 7.1 below which methane gas production increases under fish pens. According to the empirical relationship between pH and TS^{2-}, Hargrave (2010) found that this threshold can be reached at TS^{2-} concentrations of 5000-6000 μM. It is worth noting that if TS^{2-} concentrations were to precipitate with Fe^{2+}, this would result in a more alkaline pH level (Ben-Yaakov, 1973).

Studies conducted in temperate regions, such as Canada, have shown that fish farm-derived particles primarily settle in the sediment, with higher concentrations near the farms and lower concentrations at greater distance (Kempf *et al.,* 2002; Doglioli *et al.,* 2004; Schendel *et al.,* 2004; Mente *et al*., 2006). This localized impact could be attributed to the limited dispersal of pelleted food commonly used in temperate regions, in contrast to alternatives like trash fish (bycatch species with no market value) commonly used in subtropical regions, which have wider particle dispersal rates (Wu *et al.,* 1994). However, Wu *et al.* (1994) found that even with the use of trash fish feed, concentrations of byproducts of OM were more pronounced in the sediments beneath the farms compared to the water column. Sediment concentrations decreased with distance and did not extend beyond 1 km away from the farm sites. Similar observations were made in the Whycocomagh Basin on a smaller and local scale (less than 100 m), where the sediments beneath the fish pen array served as a net sink for increased OM inputs, and

concentrations did not increase beyond the vicinity of the fish pen array, as indicated by the horizontal and vertical distributions in the sediments.

The results of this section suggest that the removal of accumulated OM through microbial activity at the sediment-water interface is significant during fallowing periods. These findings align with the observations of Aure & Stigebrandt (1990), who noted that in areas with low water current, the accumulation of fish farm waste eventually reaches a state of equilibrium with the rate of decomposition, which is proportional to the amount of OM present. In anoxic environments where macrofauna are typically absent due to eutrophication, microbial activity plays a crucial role. Herwig *et al.* (1997) observed elevated populations of bacteria at the sediment-water interface near fish farms. Schendel *et al.* (2004) observed elevated concentrations of colony-forming bacteria in suspended particles (flocs) near fish pens, located just above the sediment-water interface, a phenomenon commonly observed in the Whycocomagh Basin. These findings emphasize the intricate nature of biogeochemical processes and emphasize the importance of adopting a site-specific approach when evaluating the influence of fish farming on sediment chemistry.

Although excess OM near the We'koqma'q Aquaculture Farm was remineralized during the fallowing period, the byproducts of anaerobic respiration remained elevated. This is attributed to slow removal processes, which involve diffusion into the overlying water and eventual exchange with the upper surface mixed layer. In contrast, in oxic overlying water columns, rapid exchange processes occur across the sediment-water interface, facilitating reoxidation processes, bioturbation, and bio-irrigation (Hedges *et al.,* 1997).

4.3 Remineralization and Sulfur Cycling Rate Estimates

To estimate sediment recovery and remineralization processes from 2019 to 2020, depth inventories for the fish pen array (F1) and the reference sites (R1, R2) were calculated from sediment core porewater concentrations in the top 20 cm for TC, TIN, TS^{2-}, and NH_4^+ (Table 4.1). To account for bulk porosity (φ) at each depth, (Eq. 4) was used:

$$\text{Inventory} = \int_0^{20cm} \varphi \ [C]_i \ dz \qquad \text{(Eq. 4)}$$

where (C_i) is the concentration of the solute in question (TS^{2-} or NH_4^+) and (dz) gives the depth integrated inventory for the solute species. The inventory for solids was also accounted for in (Eq. 5):

$$\text{Inventory} = \int_0^{20cm} (1-\varphi)\rho_s \ [C]_i \ dz \qquad \text{(Eq. 5)}$$

where ($1-\varphi$) represents the solid volume fraction and (ρ_s) is the bulk sediment density.

Table 4.1: *Depth integrated inventories (mmol m^{-2} d^{-1}) of Total Carbon (TC), Total Inorganic Nitrogen (TIN), Total Sulfide (TS^{2-}), Ammonium (NH_4^+), and TS^{2-}: NH_4^+ and C:N ratio concentrations of sediment cores collected in 2019 and 2020.*

Site	Depth Inventory					
	TC (mmol m^{-2})	**TIN (mmol m^{-2})**	**TS^{2-} (mmol m^{-2})**	**NH_4^+ (mmol m^{-2})**	**TS^{2-}: NH_4^+ (-)**	**C:N (-)**
F1 Site (2019)	365000	30800	1560	665	2.36	11.85
F2 Site (2020) *	215500 ± 3535.53	18300 ± 282.84	841 ± 19.80	335.5 ± 34.65	2.52 ± 0.32	11.78 ± 0.01
R1 Site (2019)	199000	20400	259	96	2.70	9.75
R2 Site (2020) *	193000 ± 4242.64	19100 ± 707.11	354.5 ± 50.20	155.5 ± 44.55	2.33 ± 0.34	10.11 ± 0.15

*2020 sediment concentrations were averaged between cores

The depth inventories were compared for the fish pen and reference sites (Fig. 4.5). TC, TIN, TS^{2-}, and NH_4^+ were highest in 2019 underneath the fish pen array (labeled Pen) but decreased by almost half after a year of fallowing. TC and TIN decreased by ~150 mmol C m^{-2} and ~125 mmol N m^{-2} by 2020, reaching similar concentrations to the reference (labeled Ref.) sites. TS^{2-} and NH_4^+ inventories also decreased by half at the fish pen array after fallowing, however, levels were still elevated by more than half (~535 mmol TS^{2-} and ~84 mmol NH_4^+ m^{-2}) compared to the reference sites. Based on the inventories above, if the fallowing period was extended by an additional 10-months, an approximately 2-year fallowing period might further decrease solute concentrations toward reference levels.

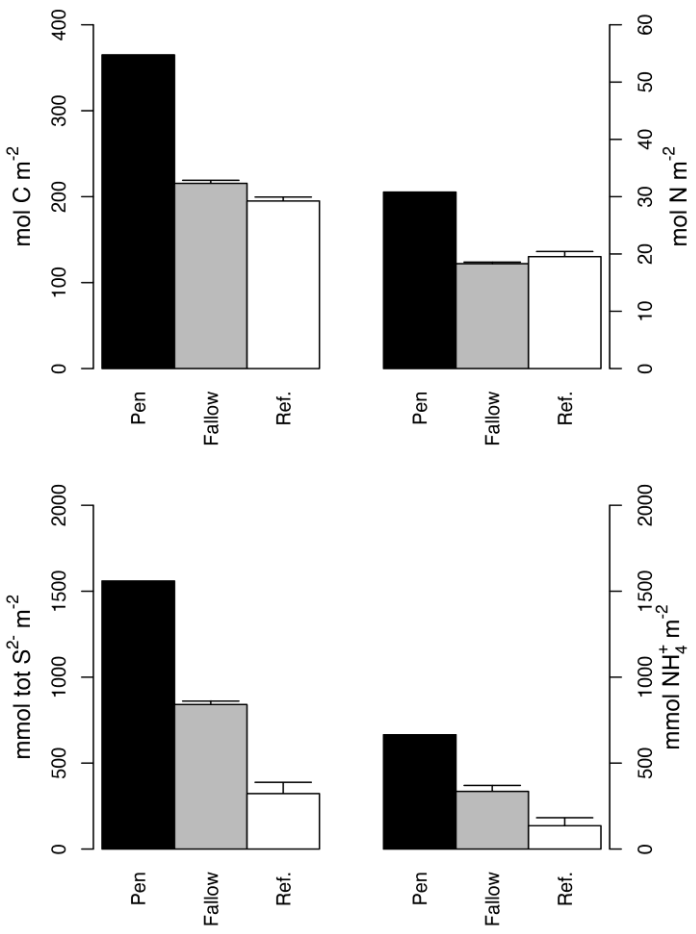

Figure 4.5: *Depth integrated inventories of TC, TIN, TS^{2-}, and NH_4^+. Pen represents the F1 site when it was stocked in 2019, Fallow represents the F1 site in 2020 when it was fallowed, and Ref. is an average of the reference sites (R1 and R2) between years.*

Comparing the depth inventories between 2020 and 2019 can provide an estimate of remineralization and sediment recovery rates after one year of fallowing at the F1 site. This can be calculated by the following mass balance equation:

$$Rate = \frac{\left(\int_0^{20} C_{(t_1)} dz - \int_0^{20} C_{(t_0)} dz \right)}{(t_1 - t_0)} \quad \text{(Eq. 6)}$$

where $\int_0^{20} C_{(t_1)}$ and $\int_0^{20} C_{(t_0)}$ are the inventories of the chemical species in question (TS^{2-} or NH_4^+) and (t_1-t_0) is the number of days that passed between sampling in 2019 and 2020 (total of 294 days). The results of these calculations are summarized in Table 4.2. The TC remineralization rate of fish waste during the fallowing period was estimated to be 508 mmol m^{-2} d^{-1}, while the TIN remineralization rate was 42 mmol m^{-2} d^{-1}. This suggests a C:N remineralization rate of 12 (508/42). Recovery rates of 2.4 and 1.1 mmol m^{-2} d^{-1} were determined for TS^{2-} and NH_4^+.

Table 4.2: *Depth integrated remineralization rates (mmol m^{-2} d^{-1}) of Total Carbon (TC), Total Inorganic Nitrogen (TIN), Total Sulfide (TS^{2-}), Ammonium (NH_4^+), and TS^{2-}: NH_4^+ and C:N ratio concentrations of sediment cores between sampling periods (294 calendar days) collected in 2019 and 2020.*

Process	Symbol	Rate	SD	Units
1. Carbon Remineralization	C_{rem}	508	12	mmol C m^{-2} d^{-1}
2. Nitrogen Remineralization	N_{rem}	42	1	mmol N m^{-2} d^{-1}
3. Net Sulfide Removal	ΔTS^{2-}	2.4	0.1	mmol TS^{2-} m^{-2} d^{-1}
4. Net Ammonium Removal	ΔNH_4^+	1.1	0.1	mmol NH_4^+ m^{-2} d^{-1}

*1. Calculated TC mineralization to C02 = twice the rate of sulfate reduction 2. Calculated TIN mineralization 3. Calculated diffusional flux of TS^{2-} from sediment to water column 4. Calculated diffusional flux of NH_4^+ from sediment to water column.

In addition, using a mass balance equation (Eq. 6), the stoichiometry of sulfate reduction can be used to estimate the sulfate reduction rate from the TC remineralization rate (Rosenfeld 1979):

$$(CH_2O)(NH_3)_{(0.08)} + 0.5(SO_4^{2-}) \rightarrow (CO_2) + 0.5(TS^{2-}) + 0.08(NH_4^+) \quad \text{(Eq. 7)}$$

By assuming 0.5 moles of SO_4^{2-} are required to oxidize 1 mole of C, the sulfate reduction rate can be estimated to be 254 mmol m^{-2} d^{-1} (508 mmol C/2). This estimate should be

considered as an upper bound limit since it assumes that all C remineralization is occurring through sulfate reduction. However, it is possible that some fraction of this estimate of remineralization could be caused by methane (CH_4) through methanogenesis since it has been observed that eutrophic marine sediments are generally characterized by coinciding sulfate depletion/methane production near the sediment surface (Boudreau & Westrich, 1984; Jorgensen *et al.,* 2001). According to Punshon et al. (2022), there was a notable saturation of CH_4 concentrations in the Whycocomagh Basin, observed across a depth range of approximately 20-45 m. This finding implies that a portion of the observed remineralization processes could be attributed to methane production. The reaction between sulfate and methane (Eq. 8) shows how they coexist:

$$CH_4 + SO_4^{2-} \rightarrow HCO_3^- + HS^- + H_2O \qquad \text{(Eq. 8)}$$

The partitioning of carbon remineralization between sulfate reduction and methanogenesis can be estimated by considering the ratio of sulfide to ammonium production. According to (Eq. 7), if carbon remineralization was entirely due to sulfate reduction, the ratio of TS^{2-} to NH_4^+ production in the sediment would be approximately 6 (Rosenfeld, 1979). However, the ratio of TS^{2-} to NH_4^+ in the sediments was only ~2.4 (Table 4.2). This suggests another process (i.e., methanogenesis) is also producing NH_4^+. If methanogenesis is represented by following reaction:

$$(CH_2O)(NH_3)_{(0.08)} + 0.5(H_2O) \rightarrow (CO_2) + 0.5(CH_4) + 0.08(NH_3) \qquad \text{(Eq. 9)}$$

the ratio of sulfide to ammonium production can be given by (Eq. 10):

$$\left(\frac{\Delta totS^{2-}}{\Delta NH_4^+}\right) = \frac{(0.5 \times R_{SO4})}{(NC \times R_{SO4}) + (NC \times R_{CH4})} \qquad \text{(Eq. 10)}$$

where (*NC*) is the to nitrogen to carbon ratio (1:12), and (R_{SO4}) and (R_{CH4}) are the carbon remineralization rates due to sulfate reduction and methanogenesis, respectively. The total rate of carbon remineralization is given by (Eq. 11):

$$C_{rem} = R_{SO4} + R_{CH4} \quad \text{(Eq. 11)}$$

By rearranging the following expression for R_{SO4} and substituting (Eq. 11) into (Eq. 12), the rate for sulfate reduction can then be given by:

$$R_{SO4} = \frac{\left(\frac{\Delta TS^{2-}}{\Delta NH_3} \times NC \times C_{rem}\right)}{0.5} \quad \text{(Eq. 12)}$$

With a TS^{2-} to NH_4^+ ratio of 2.4 (Table 4.2), and a NC ratio of 0.08 (Eq. 10), remineralization estimates would equal 195 mmol m^{-2} d^{-1} of C from sulfate reduction (R_{SO4}) and 313 mmol m^{-2} d^{-1} by methanogenesis (R_{CH4}). According to the stoichiometry in (Eq. 7) and (Eq. 9), this works out to a sulfate reduction rate (*SRR*) of 97.5 mmol m^{-2} d^{-1} (195/2) and a methane production rate (*MPR*) of 156 mmol m^{-2} d^{-1}(313/2). It is important to note that these estimates may be conservative, as they do not account for the potential adsorption of NH_4^+ to sediment particles, nor the consumption of TS^{2-} through anaerobic methane oxidation (Burdige, 2007). Both of these processes are likely to occur in the sediments to some extent. Nevertheless, the findings suggest that the *SRR* during the approximately one-year fallowing period was between 97.5 – 254 mmol m^{-2} d^{-1}, while the *MPR* was between 0 – 156 mmol m^{-2} d^{-1}.

Keeley *et al.* (2019) conducted a study in Norway to investigate benthic respiration and microbial waste production in a shallow, well dispersed coastal seabed. They collected sediment cores from stations located near and far from a fish farm during production and post-fallow periods. The results revealed that fish farming had a significant impact on OM and

carbon/nitrogen remineralization rates, particularly in the vicinity of the fish pens. In the top 5 cm of sediment cores collected more than 50 m from the pens, TC and TIN values peaked at 359 ± 100 mmol C m^{-2} d^{-1} and ~40 mmol N m^{-2} d^{-1}, respectively, during mid-production. This increase in values, similar to the peak observed near the fish pen array in the Whycocomagh Basin, could be attributed to the higher degradability of the C:N ratios in the fish feed. Post-fallow remineralization rates of TC and TIN were relatively low across the entire site, ranging from 5-50 mmol C m^{-2} d^{-1} and 2-5 mmol N m^{-2} d^{-1}, respectively. These findings underscore the significant role of fish farming in enhancing OM and carbon/nitrogen remineralization rates, even in well-dispersed sites. Interestingly, the Whycocomagh Basin, characterized by low water dispersal and a permanent anoxic environment, exhibited comparable levels of TC and TIN remineralization beneath the fish pen array (Table 4.2). This suggests that despite challenging environmental conditions, the Whycocomagh Basin could be a potentially productive site for fish farming.

Comparisons with the literature indicate that the observed processes in the Whycocomagh Basin fall within the boundaries observed in aquaculture-impacted sediments. For instance, in the study by Holmer & Kristensen (1992) at the primary station beneath the fish farm, macrofauna were absent throughout the farming period, and anoxic conditions were indicated by the presence of a mat of *Beggiatoa spp.* and black sediment at the sediment-water interface. The study showed significantly higher carbon remineralization during the production period (525-619 mmol m^{-2} d^{-1}) compared to control stations (24-70 mmol m^{-2} d^{-1}), and no changes were observed in sediments more than 30 m from the farm. The highest depth-integrated *SRR* was observed in the upper 4 cm beneath the fish pens (234-310 mmol m^{-2} d^{-1}) during the farming season, which decreased considerably post-harvest (33-77 mmol m^{-2} d^{-1}) but remained

elevated compared to the control stations. The extent of enrichment effects were 4-10 times higher than in low-flow dispersal sites, as observed in other studies (Brooks & Mahnken, 2003; Brooks *et al.,* 2003; Giles, 2008).

The findings in the Whycocomagh Basin align with a study conducted by Krost *et al.* (1994) in the Western Baltic Sea, which is a shallow, low current, and seasonally anoxic fjord. The study revealed a notable impact on the sediments beneath a rainbow trout fish farm during the production months. They reported higher *SRR* (101.6 mmol m^{-2} d^{-1}) and TC remineralization (~100-150 mmol m^{-2} d^{-1}) rates beneath the farm compared to outside the pen margins (0-27.6 mmol m^{-2} d^{-1}). In sites with shallow water depth and high dispersal, such as the one studied by Keeley *et al.,* (2019), zones of influence extended up to 600-1100 m, and they suggested that reference stations at distances of 1.5-2 km would have been more appropriate. Shallow, dispersive sites are relatively resilient to enrichment effects, but water current and sediment resuspension can lead to larger dispersive impacts and accumulation footprints compared to non-dispersive sites.

Site-specific models calibrated to field data and variable parameters of a particular location can help interpret future scenarios and identify the most effective fallowing period to restore rates to background levels. Brigolin *et al.* (2009) calibrated an integrated deposition model (DEPOMOD), used for particle-tracking through the water column, and a reactive-transport model to an independent field dataset collected at a well-flushed, steady-state, Atlantic Salmon farm located off the shores of Scotland. The model observed a higher flux of OM during the harvest season, with TC remineralization rates within the same order of magnitude as that observed in the Whycocomagh Basin (821 mmol C m^{-2} d^{-1}). The simulation showed that a significant portion of OM (88%) remained within the computational area (400 m x 300 m), and

concentrations of fish farm-derived OM, NH_4^+, and TS^{2-} were higher under the perturbed site in both the simulation and field data. These findings confirm that elevated point-source organic loading can be returned to background concentrations by fallowing, and geographic differences between sites in high hydrographic dispersal conditions can play a role in the extent of enrichment effects and dispersion of OM.

The response of sediment chemical remediation, whether over several months or years, is highly influenced by site-specific water properties and movement (Keeley *et al.,* 2019). Low-flow muddy substrates, like those in the Whycocomagh Basin, tend to have more constrained enrichment effects. In contrast, high dispersal sites with sandy substrates have less definitive boundaries, facilitating greater solute distribution (Keeley *et al.,* 2013; Keeley *et al.,* 2019). These factors can affect a site's capacity to withstand OM enrichment, leading to a subjective assessment of the extent of the impact of OM enrichment. For a site to be considered sustainable, it must maintain a functional benthos and have a high assimilation capacity for microbes to degrade OM before adverse effects impact natural biogeochemical processes (Keeley *et al.,* 2019). Although fallowing a fish pen site for one year led to a significant decrease in all aspects beneath the Whycocomagh Basin's fish pen array, the rates were still higher than background levels at the deep and reference sites. This suggests that a longer fallowing period, such as two years, may be necessary. As the We'koqma'q First Nation Aquaculture Farm plans to increase fish farm sites, developing a site-specific model for the Whycocomagh Basin could help assess the rates of TS^{2-} accumulation and determine if the proposed location or increased fish pen stocks would lead to TS^{2-} levels that could potentially harm the benthic and oxycline environments.

4.4 Reactive Transport Model

To answer the question on how the elevated TS^{2-} rates are developing in the Basin, a simple, 1-D reactive-transport model was developed to examine how the fish farm may alter bottom water sulfide concentrations and impact the sulfur cycling at the basin scale. Reactive-transport models provide a way of integrating geochemical, physical, and spatial coupled processes from focused field research to simulate natural rates and scale these interactions to a parameterized environment (Steefel *et al.,* 2005). In a marine environment, estimating elemental and nutrient fluxes at the sediment-water interface can be challenging due to the complexity of the transport processes involved and the limited nature of collecting direct measurements without disrupting the sediment processes (Regnier *et al.,* 2011). While sediment reactive transport models have not yet been extensively developed for aquaculture industries, a few notable exceptions exist (see Brigolin *et al.,* 2009 and Bravo & Grant, 2018). Such models have the potential to forecast the sensitivity of the local environment to potential aquaculture farming scenarios, which could improve site leasing, operations, and sustainable fish-rearing practices.

Here, a reactive-transport model calibrated with water column samples collected near the end of the 2019 and 2020 harvesting seasons, is utilized to simulate potential long-term farming scenarios and observe how fish farm-derived OM deposition can impact the concentration of TS^{2-} below the redoxcline in the Whycocomagh Basin. To achieve this, two sets of model experiments were conducted. The first model increased the number of pens above the current farming depth (~8 m) to examine the effect on sulfide levels in the anoxic zone. The second model increased the farming depth to assess how this may alter the depth distribution of sulfide in the basin.

4.4.1 Governing Equations and Reactions

The model domain was constructed using bathymetry data from the Canadian Hydrological Society Non-Navigational (NONNA) 10 m bathymetric database (Government of Canada, 2022) and was processed using the R package 'marmap' (Pante *et al.,* 2013) to map the Whycocomagh Basin (Fig. 4.6). the basin geometry was approximated as a paraboloid with a radius of 500 m, based on the assumption that the Basin has a parabolic shape (y = ax^2).

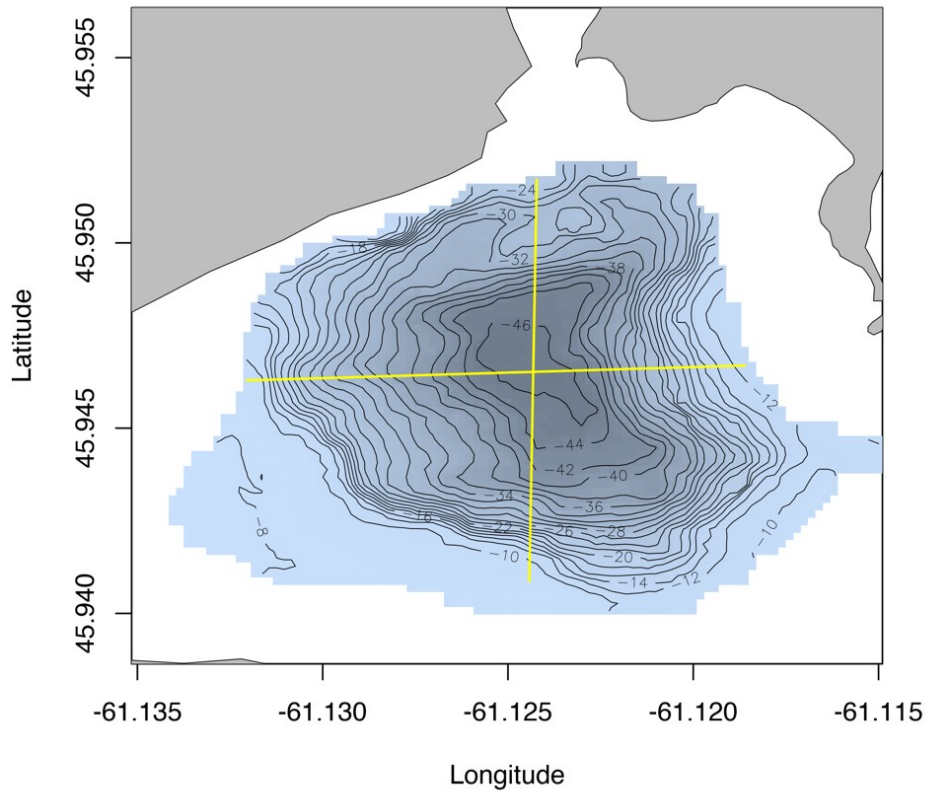

Figure 4.6: *Bathymetric representation of the Whycocomagh Basin with a light-blue shaded depth contour with two intersecting cross-sections. The red line denotes the North to South transect. The yellow line denotes the West to East transect.*

A comparison of the idealized model geometry, which assumes a parabolic shape, with the actual bathymetry in both the east-west and north-south directions is shown (Fig.4.7). Although the 1-D domain cannot capture the full spatial heterogeneity of the Basin or the complex biogeochemical cycling throughout the Basin, the implementation of a parabolic shape appears to capture much of the volume of the Basin. It should be noted that any differences between the real bathymetry and the model may have some impact on the model calculations, although they are relatively small.

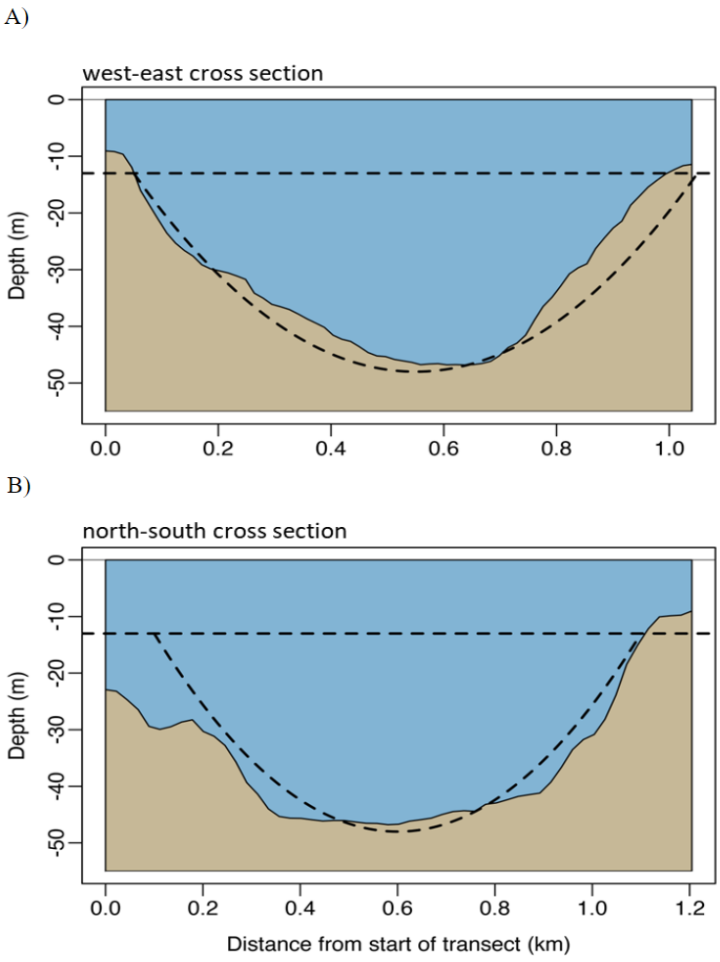

Figure 4.7: *The anoxic portion cross-sections of the basin. A) North-south cross-section. B) West-east cross-section.*

Boundary conditions were applied to the model domain with the upper boundary at 13 m, starting just above the typical redoxcline depth and extending down toward the lower boundary layer at the sediment-water interface (SWI) at 48 m depth, representing a 35 m deep anoxic basin (Fig. 4.8). The model domain is divided into 35 boxes of increasing volume, each with a height of 1 m and increasing cross-sectional area, which was calculated using the 'marmap' package.

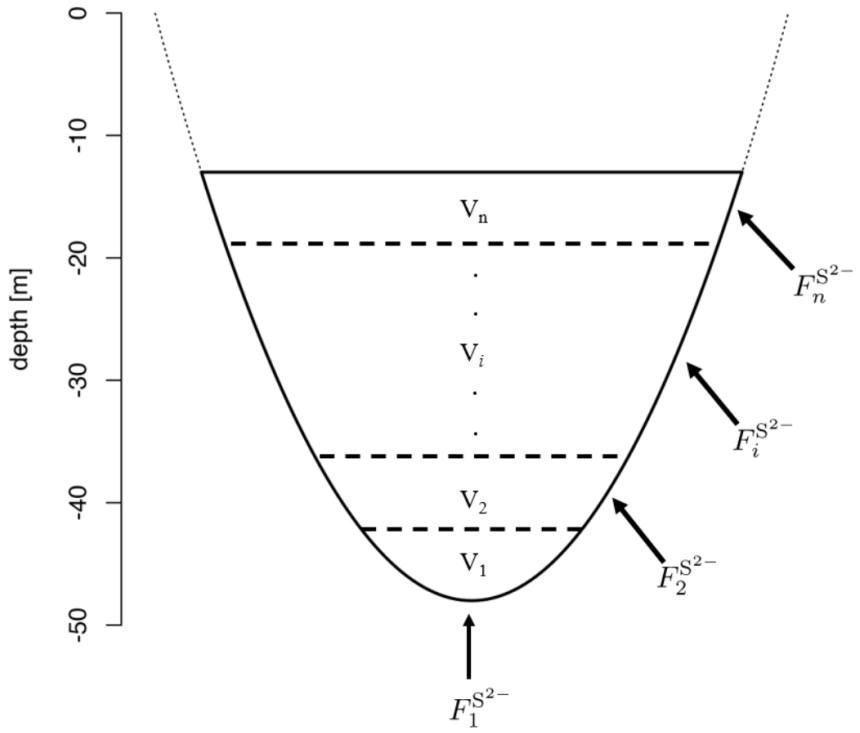

Figure 4.8: *Model formulation of the Whycocomagh Basin. V_1 to V_n represents the total volume of each layer. F_1 to F_n of S^{2-} represents flux of sulfide from the sediment.*

The model was developed without accounting for direct nutrient inputs from sources such as rainfall or river effluent. To maintain simplicity, advective currents were kept constant since they occur in the oxic portion of the Basin. The model assumption was made that the redoxcline

is primarily influenced by physical factors, rather than biological and chemical factors, due to the relatively constant temperature and salinity throughout all seasons below 20 m.

To predict changes to the Whycocomagh Basin's TS^{2-} concentrations, 0 µM concentration were assumed for the surface conditions since the upper surface is oxic. The max estimate of the sum of all sulfate reduction byproducts (i.e., aerobic sulfide oxidation, iron sulfide (FeS) precipitation, and anaerobic methane oxidation) were assumed to be collectively lost to diffusion into the water column and completely removed at the redoxcline via aerobic oxidation. Therefore, model TS^{2-} concentrations start at 0 µM near the upper boundary and increase with depth toward the lower boundary. Based on past macrofaunal surveys and the anoxic nature of the Whycocomagh Basin, no bioturbation or bio-irrigation was assumed to occur in the sediments (Krauel, 1975; Strain & Yeats, 2002; Punshon *et al.,* 2022). The parameters are summarized in Table 4.3.

Table 4.3: *Parameter values used in the model simulations.*

Parameter	Initial Conditions	Boundary Conditions	Units
Temperature	4	V_1 - V_n	°C
Salinity	21	V_1 - V_n	PSU
Avg. TS^{2-}	0	Upper	mmol m^{-3}
Avg. TS^{2-}	2400	Lower	mmol m^{-3}
Dispersion Coeff.	$2.7 \times 10^{0.8}$	V_1 - V_n	m^{-3} yr^{-1}
Diffusion Coeff.	0.03	V_1 - V_n	m^{-2} yr^{-1}
K_{sox}	90	V_1 - V_n	µM yr^{-1}

To determine the TS^{2-} concentrations in the anoxic zone of the Whycocomagh Basin, the following mass balance equation was used:

$$\frac{\Delta[TS^{2-}]}{\Delta t} = \frac{(Flux_{in} - Flux_{out})}{\Delta V} + \Sigma Reactions \qquad \text{(Eq. 13)}$$

where the left-hand side represents the change in TS^{2-} with time ($\Delta[TS^{2-}]/\Delta t$) in the Whycocomagh Basin. This equation is balanced by the difference in transport of sulfide, both in and out of the basin ($(Flux_{in} - Flux_{out})/\Delta V$), as well as any reactions ($\Sigma Reactions$) that may produce and consume sulfide.

Assuming TS^{2-} is mainly produced in the sediments and transported to the water column via diffusion, the flux across the sediment-water interface was considered. The TS^{2-} is then assumed to diffuse upward through the water column and transported out of the basin, assuming a residence time for deep-water exchange of 2 years, as given by Manning *et al.* (2019). To model the TS^{2-} concentration, the mass balance equation (Eq. 14) was discretized assuming a volumetric version of the mass balance reactive diffusion equation (Soetaert & Meysman, 2012):

$$\frac{d[TS^{2-}]_i}{dt} = \frac{\Delta_i\left(E \cdot \Delta[TS^{2-}]_i\right)}{\Delta V_i} + \frac{1}{\Delta V_i} \int F_{TS^{2-}}^{swi}\, \delta S - k_{sox}(z)[TS^{2-}]_i \qquad \text{(Eq. 14)}$$

where ($\frac{d[TS^{2-}]_i}{dt}$) represents the change in sulfide concentration over time in each box, (E) is the volumetric dispersion coefficient, and ($F_{TS^{2-}}^{swi}$) is the flux across the sediment-water interface, which is integrated over the surface area of sediment in each grid volume (ΔV_i). Additionally, $k_{sox}(z)$, a depth dependent, first order rate constant, is used to parameterize sulfide loss processes occurring near the redoxcline, representing a combination of TS^{2-} oxidation and mineral precipitation loss processes.

The modeled solute transport used a dispersion coefficient with a dispersivity of 2.7 x 10^8 m^{-3} yr^{-1} over a 2-year residence time. A diffusion coefficient for total sulfide (0.03 m^{-2} yr^{-1}) was used with a temperature (T) of 4 °C and salinity (S) of 21 PSU of the Basin per day per year. To

assess the effectiveness of the dispersion coefficient used in the model, a dye-tracer model experiment was conducted (Fig. 4.9). The initial tracer concentration was set to 1 mmol in each grid box and the decrease in concentration was set over the span of a 2-year residence time (Manning *et al.,* 2019). The dispersion coefficient was then manually adjusted to fit the residence time.

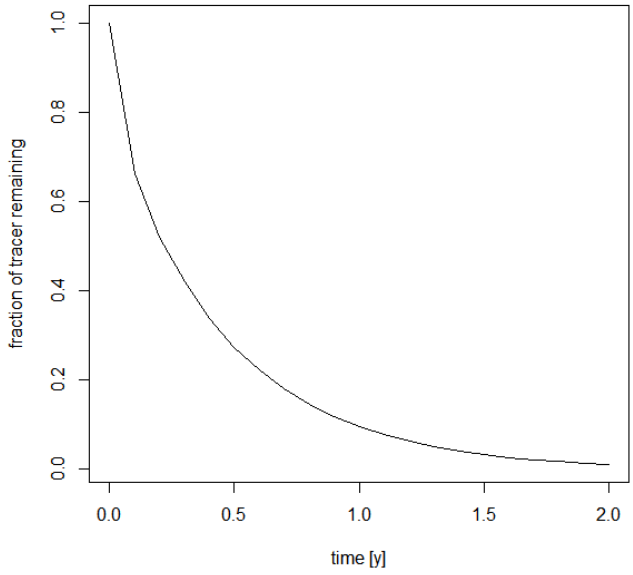

Figure 4.9: *Passive tracer used to simulate the residence time of water in the Whycocomagh Basin.*

The sulfide flux across the sediment-water-interface was assumed to be controlled by transport across the diffusive boundary layer, which is typical of cohesive sediments in low energy environments (Boudreau et al., 1984), and given by the following mass transfer equation:

$$F_{TS^{2-}}^{swi} = \frac{D_{TS^{2-}}}{DBL}\left([TS^{2-}]_{sed} - [TS^{2-}]_i \right) \quad \text{(Eq. 15)}$$

where ($D_{TS^{2-}}$) is the diffusion coefficient for sulfide and was calculated using the R package "marelac" based on the measured salinity and temperature for each grid box (V_i). A reactive diffusion model was set up and solved in the R package "ReacTran" (Soetaert *et al.,* 2012). Sulfide produced in the sediments is mass transported to the water column across the SWI and the diffusive boundary layer (*DBL*), where diffusion is the only transport process. The thickness of the *DBL* was assumed to be approximately 1 mm based on Jørgensen & Revsbech (1985). The rate of removal of sulfide from the sediment ($\frac{D_{TS^{2-}}}{DBL}$) was calculated by dividing the diffusion coefficient by the *DBL* and multiplying the difference between the sulfide concentration in the sediment ($[TS^{2-}]_{sed}$) and the sulfide concentration in the water column ($[TS^{2-}]_i$).

The concentrations of TS^{2-} just below the SWI $[TS^{2-}]_{sed}$ were set to sediment-surface grab sample concentrations from the SD Transect. The $[TS^{2-}]_i$ is the modeled concentration in the i-th (V_i) grid box. For each fish pen added, $[TS^{2-}]_{sed}$ concentrations were set to the TS^{2-} measured from sediment-surface grab samples collected near the fish pen array in 2019 obtained from the AP Transect when fish were present. The excess sediment TS^{2-} flux from the fish pens was incorporated as an additional sediment flux injected into each grid box at a specified depth, scaled by the area of pens at that water depth.

A sinusoidal shape of the sulfide removal rate constant ($k_{sox}(z)$) was used to shape the TS^{2-} water column profile in the basin, with the highest values near the upper boundary layer and the lowest values near the lower boundary layer (Fig. 4.10). This constant represents the parameterization of the sulfide loss processes occurring near the upper boundary of the model as the oxycline/redoxcline is approached and reflects the greater sulfide removal processes assumed to be occurring at the upper boundary layer.

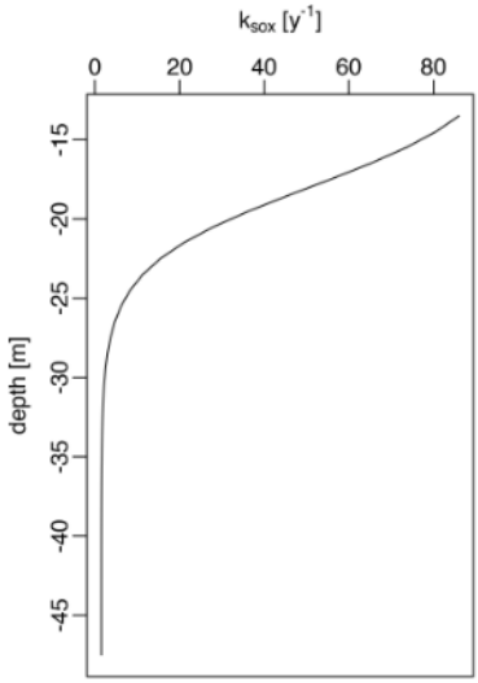

Figure 4.10: *Rate constant k_{sox} decreasing with depth as the sulfide oxidation rate decreases with decreasing oxygen concentration.*

These processes would likely include aerobic sulfide oxidation from DO mixing down into the sulfidic zone and the precipitation of FeS (or FeS_2) minerals produced by Fe^{2+} reduction encountering the TS^{2-} diffusing up from below. However, explicitly modeling these processes would require measurements of the mixing processes occurring in the upper layers of the water column and independent estimates of Fe^{2+} reduction rates, which were beyond the scope of this study. To parameterize these loss processes, the removal rate constant *($k_{sox}(z)$)* was assumed to be a sinusoidal function with depth. The specific values of (k_{sox}) at variable depths are unknown, so a gaussian function with depth was used for parameterization (Eq. 16):

$$k_{sox}(z) = y_0 \times \frac{e^{-\frac{(z-z_L)}{aL}}}{1 + e^{-\frac{(z-z_L)}{aL}}} \quad \text{(Eq. 16)}$$

where (y_0), (z_L), and (a_L) are the fitted parameters at each water depth. To determine these values, a baseline simulation without sulfide loss processes was performed and compared to the sulfide water column concentrations measured in 2019 and 2020. It was found that the model accurately represented the bottom water sulfide but overpredicted sulfide near the upper boundary. The values of (y_0) and (a_L) were then adjusted to recreate the shape of the sulfide profile near the upper boundary.

4.4.2 Model Simulation and Findings

Figure 4.11(A) shows the model simulation for the situation on the farm in 2019, where 70 fish pens were located in water depths of 20-25 m. On the other hand, Figure 4.11(B) shows the model simulation for the same number of pens in 2019, but in deeper waters with a depth of 48 m. The TS^{2-} concentrations were determined using direct measurements via water column seawater taken beneath the fish pen array.

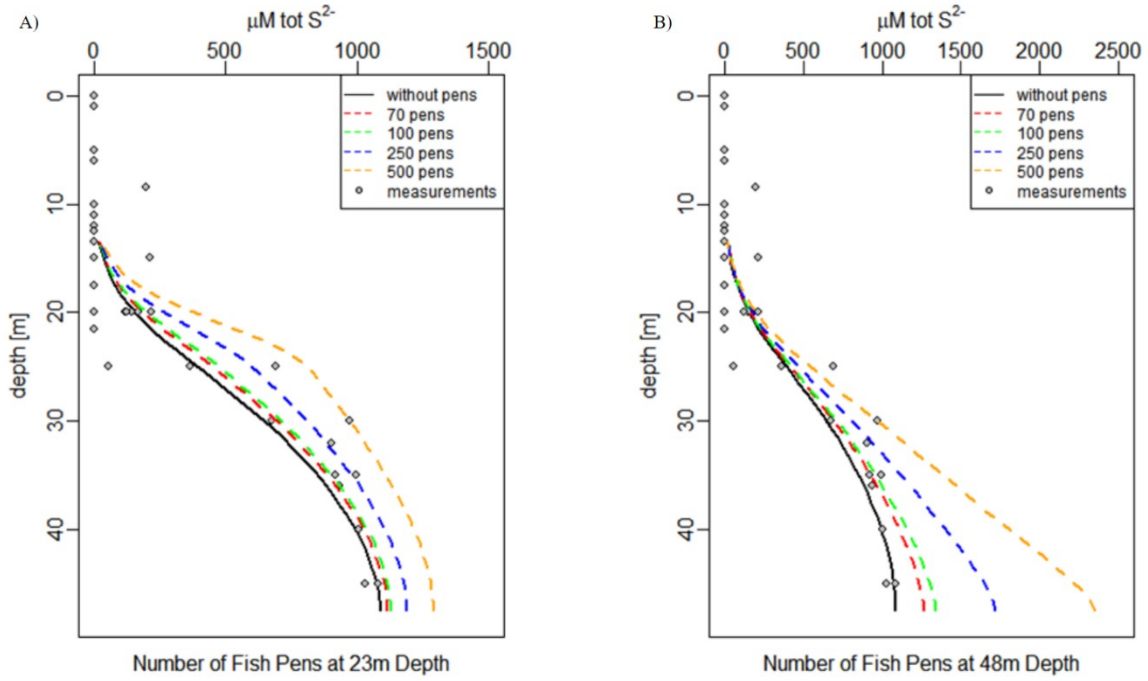

Figure 4.11: *The measured sample concentrations (represented by dots) are compared to the baseline simulation without fish pens (represented by the black line), along with simulated profiles of total sulfide. The simulated profiles depict the variations in total sulfide concentrations with different numbers of fish pens located above 23 m depth (A) and 48 m depth (B), shown by colored dashed lines.*

For the first model experiment, TS^{2-} concentrations were simulated for a range of fish pen numbers, based on their corresponding concentration estimates, and compared to water column

measurements with no fish pens (black line) (Fig. 4.11; A). The simulated concentrations followed a similar distribution with depth, increasing more rapidly in the upper boundary layer closer to the oxycline (from the anoxic zone (13 m) down to 30 m depth), with each increase in the number of pens. Between 70-100 fish pens, concentrations stabilized around background concentrations steadily with depth, with bottom concentrations of around 1100 μM at 40 m. Between 250-500 pens, concentrations began to deviate from background concentrations between 13-30 m, increasing laterally toward 700-900 μM and then more vertically up to 1250 μM by 40 m.

In the second model experiment, the simulated number of fish pens was placed above 48 m depth against water column measurements with no fish pens (Fig. 4.11; B). TS^{2-} concentrations remained similar to background levels down to 20 m depth. At 22 m depth, concentrations began to increase away from background concentrations in the lower boundary layer up to ~1200 μM with 70-100 pens, similar to the highest lower boundary concentrations in the first model. With 250-500 pens, concentrations deviated from background levels by 20 m with lower boundary concentrations up to 1500-2400 μM.

The two model experiments shed light on how the altered sediment dynamics and sulfide production from the fish farm waste affect the concentration of sulfide in the water column of the anoxic zone. The first experiment showed an increase in sulfide concentrations the upper boundary layers when fish pens were placed in shallower waters (23 m), while the second experiment showed a greater increase in the lower boundary layer when fish pens were placed in deeper waters (48 m). From these two different simulations, the results show that when fish pens are placed in shallower waters, sulfide concentrations in the upper boundary layers increase, while in deeper waters, concentrations increase in the lower boundary layer. This has important

implications for the shoaling of the oxycline, which occurs between ~15-20 m depth. The oxycline is the depth range where oxygen concentrations drop rapidly, and sulfide concentrations rise, creating a zone of transition between the oxic and anoxic zones. Elevated TS^{2-} levels in the shoaling zone of the oxycline can cause it to move upward, resulting in the expansion of the anoxic zone, which can have negative ecological consequences.

The second model experiment, with pen arrays in deeper water (48 m), showed that TS^{2-} concentrations did not significantly increase until well below the oxycline/redoxcline, which could be a potential solution to the issue of shoaling. Although sulfide concentrations were much higher in the deep waters compared to the first model, it is likely that TS^{2-} would be effectively stored and increase only in the bottom water, releasing slowly from only diffusion and reducing the overall extension of the anoxic flux to the oxycline beneath the pens. This finding is consistent with the results of Giles (2008), who used a Bayesian network of 64 studies to examine the quantitative relationships between benthic impact parameters and various fish farm characteristics. The study found that benthic impact parameters were primarily a function of farm volume, food C:N ratios, water depth, current flow, and sediment composition. The spatial trends observed in the study, with higher concentrations of sulfide confined within 40-70 m from the farms and deeper farms (>30 m) having considerably lower concentrations compared to shallower ones (<15 m), were similar to those observed in the Whycocomagh Basin model experiements.

For both model experiments, it is important to note that the models are based on specific conditions in the Whycocomagh Basin and are not directly applicable to other locations. Additionally, the models do not take into account the rise in bottom sulfide levels over the last few decades (see section 2.2.1) or consider the effects of fish farming on eutrophication of the

overlying estuary. While TS^{2-} concentrations seem to only be increasing from OM deposition surrounding the fish farm area, increased farm effluents could also be contributing to eutrophication of the surface waters, leading to increased primary production, in addition to accumulating effluents stemming from the Whycocomagh sewage treatment facility from the watershed into the Basin.

Based on the information provided, the 1-D reactive-transport models used in this study were developed specifically for the Whycocomagh Basin and were designed to model the TS^{2-} sediment flux from the deep water. Although the models only provide information on how TS^{2-} is changing in the bottom water, they are expected to offer insights into the sulfur cycling dynamics in the Basin. These insights can be used by the We'koqma'q Fish Farm to assess potential scenarios for sulfide accumulation and ultimately improve productivity and sustainable harvest within the Whycocomagh Bay, Bras d'Or Lakes.

CHAPTER 5

CONCLUSION

The goal of this thesis was to investigate the impact of a fish farm on sediment geochemistry and the rates of natural sulfide production in the Whycocomagh Basin. In particular, the study aimed to address two main questions: 1) How does accumulated farm waste affect sediment carbon and sulfur cycling in the Basin? 2) How do the altered sediment dynamics and sulfide production, due to fish farm waste, affect sulfide concentrations in the water column of the anoxic zone?

To address the first question, three distinct total sulfide (TS^{2-}) monitoring techniques were employed in November 2019 and September 2020 to assess the flux of TS^{2-} and nutrient concentrations across the sediment-water interface originating from the fish farm in the Whycocomagh Basin. Sampling took place at three different locations: the center of a fish pen array, an undisturbed reference site, and a deep site. The sampling was conducted both at the end of a fish rearing cycle and after approximately one-year of fallowing. The results consistently showed higher TS^{2-} concentrations within 50-100 m of the fish pen array, indicating the influence of organic matter (OM) loading from farm inputs. The presence of elevated TS^{2-} concentrations and nutrients in the surface sediments beneath the fish pen array suggested a direct association with OM loading from farm inputs. The fish pen array with reared fish exhibited the highest concentrations of TS^{2-} during the first year of the study. Although

concentrations remained elevated in the second year, there was evidence of recovery and a decrease to background levels after the fallowing period.

Despite variations among the sampling techniques, each method showed increased OM enrichment and sulfide production in the sediments beneath the fish farm, decreasing to background levels with increased distance from the farm. While examining the impact of the fish farm on sediment geochemistry, it was observed that sulfide and ammonium concentrations were significantly elevated beneath the pen array. These elevated concentrations did not extend beyond the immediate vicinity of the farm, indicating a localized influence. Furthermore, along the SD Transect, an increase in TS^{2-} concentrations was consistently observed with greater depth and distance from the farm, which aligns with previous research findings (Punshon et al., 2022). Interestingly, contrary to expectations, the presence of the fish farm did not have a significant impact on chemistry in the water column. Instead, the majority of the C:N material and concentrations were concentrated in the top 0-2 cm of sediment beneath the fish pen array.

These findings shed light on the spatial distribution of sulfide and ammonium concentrations, emphasizing the localized and depth-related patterns of their impact. Sediments often follow an organic enrichment gradient, with aquaculture impacts decreasing with increased distance from the source (Karakassis et al., 2002). Accordingly, most monitoring efforts measure eutrophication extents relative to distant reference sites. The sedimentation levels outside ~50 m along the AP Transects at similar depths from the fish pen array showed lowering concentrations toward background levels observed along the SD Transect at similar depth. This suggests that OM enrichment is being successfully metabolized by microbes within the margins of the fish pen array and that nutrient enrichment is more localized and concentrated beneath the farm,

suggesting that the increase in concentrations is likely influenced by the fish farm since they have increased production since beginning in 2011.

To address the second question regarding the altered sediment dynamics and sulfide production due to fish farm waste, this study employed a reactive-transport model specific to the Whycocomagh Basin. Through model experiments, the impact of different fish pen scenarios on TS^{2-} concentrations was assessed and it was demonstrated that TS^{2-} concentrations remained close to background levels for scenarios involving 70-100 pens at the farming depth in 2019 (~23 m). However, deviations from the background concentrations were observed when more than 100 fish pens were added or when pens were located in deeper waters (48 m). These deviations led to elevated concentrations of TS^{2-} in the water column near the oxycline/RPD layer when the pens were placed in shallow waters (~23 m), and elevated concentrations of TS^{2-} near the sediment-water interface when the pens were placed in deep waters (48 m).

While these findings suggest potential implications of increased TS^{2-} concentrations for both model scenarios, placing the fish pen arrays in deeper waters appears to keep sulfide levels near the lower-boundary layer instead of rising near the oxycline. It is important to note that the Basin environment appears to be microbially dominated and capable of effectively remineralizing OM. It is this efficient microbial activity that likely contributes to the Whycocomagh Basin's ability to regulate sulfide concentrations. By employing a reactive-transport model, these findings could offer valuable insights for the potential monitoring of anoxic fish farms.

Total free sulfide monitoring is a widely employed biogeochemical tool for assessing the impact of OM deposition in the sediments (Cranford et al., 2020). The reliability and sensitivity of its measurements as an indicator align with other biotic and abiotic indicators commonly used.

Moreover, its cost effectiveness and practicality make it a readily employable tool for aquaculture farm management (Hargrave et al., 2008). Nevertheless, free sulfide is a volatile and highly reactive substance, particularly in the presence of dissolved oxygen (DO). Although certain aspects of the low-energy, anoxic environment of the Whycocomagh Basin facilitated sampling, such as the absence of benthic fauna and bottom water currents, which rendered diffusive fluxes as the main representation of the system, variations in concentration observed across the different measurement methods are likely attributable to sampling artifacts and inherent limitations associated with each approach.

Sediment grab samples provided generalized measurements in the top 5-10 cm but lacked spatial resolution as the use of a single point-measurement cannot accurately represent the entire grab. While sediment core porewater samples allowed for deeper and undisturbed profiling, cross-sectioning of the sediment during sampling could potentially alter sediment properties, including the diffusive boundary layer thickness, which may impact fluxes (Giles, 2008). Microsensor measurements offered fine-scale resolution scales below the sediment-water interface (top 2-5 cm) but require high replication for representative results (Giles, 2008). Sample limitations in keeping anoxic conditions also differed among methods primarily from controlling sulfide during transport, storage, and analysis techniques. Variability of samples collected in the field could also be reflected by situations out of this study's control, such as the transport and storage of samples from the Basin to the lab, the ability to stabilize the boating vessel to collect samples, changes in the locations of the fish pens over existing sample sites, as well as wind and human error involved with collection.

To assess the resilience of the Basin ecosystem to nutrient enrichment and gauge long-term trends, monitoring of the vertical trends of the water column and the sediment beneath the

fish farm is crucial, and future research should emphasize the importance of long-term, monthly monitoring to account for seasonal cycles, fish stocking impacts, and interannual variability. Harvesting dates and total fish food input during these months would be of interest given seasonal alterations in farm production, which seem to affect remineralization rates. Considering the dynamic nature of fish farm sediments across different farming stages, understanding the role of microbial communities as environmental proxies at the sediment-water interface and the pseudo-benthos in OM remediation throughout the Whycocomagh Basin could provide valuable insights. For example, the genus *Sulfurovum,* which is dominant in highly sulfidic conditions, such as mid- and post-harvest farming stages, has a high correlation with sulfide levels in sediment and water environments (Choi *et al.,* 2022).

This study provided insights into the effects of a fish farm on sediment geochemistry and sulfide production in the Whycocomagh Basin and the potential of naturally occurring anoxic basins, like the Whycocomagh Basin, as suitable locations for fish farming without disrupting existing organisms. The growing demand for aquaculture has led to increased eutrophication and excess organic matter accumulation, exerting pressure on coastal ecosystems (Middleburg & Levin, 2009). TS^{2-} concentrations resulting from sulfate reduction by sulfate-reducing bacteria are a critical variable for current aquaculture Environmental Management Programs (EMPs) to assess undesirable shifts at farming sites from aerobic to anaerobic dominated systems. However, these standards prove ineffective when applied to farm sites situated above naturally occurring anoxic environments.

Considering the absence of benthic macrofauna and the limited dispersal of OM in the Whycocomagh Basin, it is plausible that naturally occurring, stratified, anoxic systems could serve as suitable environments for surface water aquaculture without significant disruption to

existing organisms. Moreover, continuous monitoring, consideration of microbial communities, and extending the fallowing period to two harvesting seasons could aid in the recovery of concentration levels to background levels, aligning with the principles of Netukulimk. It is hoped these findings can contribute to the understanding of complex interactions between fish farming in variable ecosystems and to sustainable aquaculture practices.

BIBLIOGRAPHY

Alexander, D. R., Kerekes, J. J., & Sabean, B. C. (1986). Description of Selected Lake Characteristics and Occurrence of Fish Species in T81 Nova Scotia Lakes. Proceedings of the Nova Scotian Institute of Science, 36(2), 63-106.

Anderson, T. F., & Raiswell, R. (2004). Sources and mechanisms for the enrichment of highly reactive iron in euxinic Black Sea sediments. American Journal of Science, 304(3), 203–233.

Anttila, K., Lewis, M., Prokkola, J. M., Kanerva, M., Seppänen, E., Kolari, I., & Nikinmaa, M. (2015). Warm acclimation and oxygen depletion induce species-specific responses in salmonids. The Journal of experimental biology, 218(10), 1471-1477.

Atlantic Zone Monitoring Program (AZMP). (2022). https://www.dfo-mpo.gc.ca/science/data-donnees/azmp-pmza/index-eng.html

Aure, J., & Stigebrandt, A. (1990). Quantitative estimates of the eutrophication effects of fish farming on fjords. Aquaculture, 90(2), 135-156.

Barton, L. L., Fardeau, M. L., & Fauque, G. D. (2014). Hydrogen sulfide: a toxic gas produced by dissimilatory sulfate and sulfur reduction and consumed by microbial oxidation. The metal-driven biogeochemistry of gaseous compounds in the environment, 237-277.

Bauer, J. E., Cai, W. J., Raymond, P. A., Bianchi, T. S., Hopkinson, C. S., & Regnier, P. A. (2013). The changing carbon cycle of the coastal ocean. Nature, 504(7478), 61-70.

Baykara, S. Z., Figen, E. H., Kale, A., & Veziroglu, T. N. (2007). Hydrogen from hydrogen sulphide in Black Sea. International journal of hydrogen energy, 32(9), 1246-1250.

Belley, R., & Snelgrove, P. V. (2016). Relative contributions of biodiversity and environment to benthic ecosystem functioning. Frontiers in Marine Science, 3, 242.

Ben-Yaakov, S. (1973). pH Buffering of pore water of recent anoxic marine sediments 1. Limnology and Oceanography, 18(1), 86-94.

Berner, R. A. (1970). Sedimentary pyrite formation. American journal of science, 268(1), 1-23.

Berner, R. A., Scott, M. R., & Thomlinson, C. (1970). Carbonate alkalinity in the pore waters of anoxic marine sediments 1. Limnology and Oceanography, 15(4), 544-549.

Berner, R. A. (1974). Kinetic models for the early diagenesis of nitrogen, sulfur, phosphorus, and silicon in anoxic marine sediments. The sea, 5, 427-450.

Berner, R. A. (1985). Sulphate reduction, organic matter decomposition and pyrite formation. Philosophical Transactions of the Royal Society of London. Series A, Mathematical and Physical Sciences, 315(1531), 25-38.

Biermann, F., Kanie, N., & Kim, R. E. (2017). Global governance by goal-setting: the novel approach of the UN Sustainable Development Goals. Current Opinion in Environmental Sustainability, 26-27, 26-31.

Bjerg, J. T., Damgaard, L. R., Holm, S. A., Schramm, A., & Nielsen, L. P. (2016). Motility of electric cable bacteria. Applied and environmental microbiology, 82(13), 3816-3821.

Boesen, C., & Postma, D. (1988). Pyrite formation in anoxic environments of the Baltic. American Journal of Science, 288(6), 575-603.

Böttcher, M. E., Thamdrup, B. O., & Vennemann, T. W. (2001). Oxygen and sulfur isotope fractionation during anaerobic bacterial disproportionation of elemental sulfur. Geochimica et Cosmochimica Acta, 65(10), 1601-1609.

Braman, R. S., & Hendrix, S. A. (1989). Nanogram nitrite and nitrate determination in environmental and biological materials by vanadium (III) reduction with chemiluminescence detection. Analytical chemistry, 61(24), 2715-2718.

Bravo, F., & Grant, J. (2018). Modelling sediment assimilative capacity and organic carbon degradation efficiency at marine fish farms. Aquaculture Environment Interactions, 10, 309-328.

Brigolin, D., Pastres, R., Nickell, T. D., Cromey, C. J., Aguilera, D. R., & Regnier, P. (2009). Modelling the impact of aquaculture on early diagenetic processes in sea loch sediments. Marine Ecology Progress Series, 388, 63-80.

Brodecka-Goluch, A., Siudek, P., & Bolałek, J. (2019). Impact of sampling techniques on the concentration of ammonia and sulfide in pore water of marine sediments. Oceanological and Hydrobiological Studies, 48(2), 184-195.

Brooks, K. M., & Mahnken, C. V. (2003). Interactions of Atlantic salmon in the Pacific northwest environment: II. Organic wastes. Fisheries Research, 62(3), 255-293.

Brooks, K. M., Stierns, A. R., Mahnken, C. V., & Blackburn, D. B. (2003). Chemical and biological remediation of the benthos near Atlantic salmon farms. Aquaculture, 219(1-4), 355-377.

Boudreau, B. P., & Westrich, J. T. (1984). The dependence of bacterial sulfate reduction on sulfate concentration in marine sediments. Geochimica et cosmochimica acta, 48(12), 2503-2516.

Boyd, C. E., Wood, C. W., Chaney, P. L., & Queiroz, J. F. (2010). Role of aquaculture pond sediments in sequestration of annual global carbon emissions. Environmental pollution, 158(8), 2537-2540.

Burdige, D. J. (2007). Geochemistry of marine sediments. Princeton university press.

Carstensen, J., Andersen, J. H., Gustafsson, B. G., & Conley, D. J. (2014). Deoxygenation of the Baltic Sea during the last century. Proceedings of the National Academy of Sciences, 111(15), 5628-5633.

Carter, K. (2005). The effects of dissolved oxygen on steelhead trout, coho salmon, and chinook salmon biology and function by life stage. California Regional Water Quality Control Board, North Coast Region, 10.

Choi, A., Lee, T. K., Cho, H., Lee, W., & Hyun, J. (2022). Shifts in benthic bacterial communities associated with farming stages and a microbiological proxy for assessing sulfidic sediment conditions at fish farms. Marine Pollution Bulletin, 178, 113603.

Cline, J. D. (1969). Spectrophotometric determination of hydrogen sulfide in natural waters 1. Limnology and Oceanography, 14(3), 454-458.

Cranford, P. J., Brager, L., & Wong, D. (2017). A dual indicator approach for monitoring benthic impacts from organic enrichment with test application near Atlantic salmon farms. Marine Pollution Bulletin, 124(1), 258-265.

Cranford, P., Brager, L., Elvines, D., Wong, D., & Law, B. (2020). A revised classification system describing the ecological quality status of organically enriched marine sediments based on total dissolved sulfides. Marine Pollution Bulletin, 154, 111088.

Díaz, R. J. (2010). Agriculture's impact on aquaculture: Hypoxia and eutrophication in marine waters.

Díaz, R., Rabalais, N. N., & Breitburg, D. L. (2012). Agriculture's impact on aquaculture: hypoxia and eutrophication in marine waters. Organisation for Economic Co-operation and Development. Bullock & O'Shea November 2013, 146.

DFO. (2015). Fisheries and Oceans Canada Aquaculture Monitoring Standard. www.dfo-mpo.gc.ca/aquaculture/management-gestion/AAR_Monitoring_Standard_July_2015.pdf.

DFO Maritimes Region. (2018). Review of the Proposed Marine Finfish Aquaculture Boundary Amendment, Whycocomagh Bay, Bras d'Or Lakes, Nova Scotia.

Doglioli, A. M., Magaldi, M. G., Vezzulli, L., & Tucci, S. (2004). Development of a numerical model to study the dispersion of wastes coming from a marine fish farm in the Ligurian Sea (Western Mediterranean). Aquaculture, 231(1-4), 215-235.

Emerson, S., & Hedges, J. (2008). Chemical oceanography and the marine carbon cycle. Cambridge University Press.

Environment Canada. (2022). Port Hawkesbury weather station. Retrieved from https://www.weather.gc.ca/

EPA, U. (2016). EPA 821-R-16-006 Definition and procedure for the determination of the method detection limit, revision 2. Washington, DC.

Fisheries and Coastal Resources Act (1996). SNS. <https://canlii.ca/t/556tg> retrieved on 2023-07-04

Forja, J. M., Ortega, T., DelValls, T., & Gómez-Parra, A. (2004). Benthic fluxes of inorganic carbon in shallow coastal ecosystems of the Iberian Peninsula. Marine Chemistry, 85(3-4), 141-156.

Forster, S., Glud, R. N., Gundersen, J. K., & Huettel, M. (1999). In situ study of bromide tracer and oxygen flux in coastal sediments. Estuarine, Coastal and Shelf Science, 49(6), 813-827.

Froelich, P., Klinkhammer, G., Bender, M., Luedtke, N., Heath, G., Cullen, D., Dauphin, P., Hammond, D., Hartman, B., & Maynard, V. (1979). Early oxidation of organic matter in pelagic sediments of the eastern equatorial Atlantic: Suboxic diagenesis. Geochimica et Cosmochimica Acta, 43(7), 1075-1090. https://doi.org/10.1016/0016-7037(79)90095-4

Gardner, W. S., McCarthy, M. J., Carini, S. A., Souza, A. C., Lijun, H., McNeal, K. S., ... & Pennington, J. (2009). Collection of intact sediment cores with overlying water to study nitrogen-and oxygen-dynamics in regions with seasonal hypoxia. Continental Shelf Research, 29(18), 2207-2213.

Gilbert, D., Rabalais, N. N., Diaz, R. J., & Zhang, J. (2010). Evidence for greater oxygen decline rates in the coastal ocean than in the open ocean. Biogeosciences, 7(7), 2283-2296.

Giles, H. (2008). Review article: using Bayesian networks to examine consistent trends in fish farm benthic impact studies. Aquaculture, 274, pp. 181-195.

Government of Canada. (2015). Government of Canada Aquaculture Activities Regulations. www.laws.justice.gc.ca/PDF/SOR-2015-177.pdf

Government of Canada. (2021). Aquaculture Activities Regulations (AAR)

Government of Canada. (2022). Canadian Non-Navigational (NONNA) 10 m Resolution Bathymetric Database.

Gray, J. S., Wu, R. S. S., & Or, Y. Y. (2002). Effects of hypoxia and organic enrichment on the coastal marine environment. Marine ecology progress series, 238, 249-279.

Guenther, E. A., Johnson, K. S., & Coale, K. H. (2001). Direct ultraviolet spectrophotometric determination of total sulfide and iodide in natural waters. Analytical Chemistry, 73(14), 3481-3487.

Gurbutt, P. A., & Petrie, B. (1995). Circulation in the Bras d'Or Lakes. Estuarine, Coastal and Shelf Science, 41(6), 611-630.

Haklıdır, M., & Kapkın, Ş. (2005). Black Sea, a hydrogen source. In Proceedings International Hydrogen Energy Congress and Exhibition IHEC.

Hammond, D. (2001). Pore water chemistry. Academic Press.

Hargrave, B. T., Holmer, M., & Newcombe, C. P. (2008). Towards a classification of organic enrichment in marine sediments based on biogeochemical indicators. Marine Pollution Bulletin, 56(5), 810-824.

Hargrave, B. T. (2010). Empirical relationships describing benthic impacts of salmon aquaculture. Aquaculture Environment Interactions, 1(1), 33-46.

Harris, D., Horwáth, W. R., & Van Kessel, C. (2001). Acid fumigation of soils to remove carbonates prior to total organic carbon or carbon-13 isotopic analysis. Soil Science Society of America Journal, 65(6), 1853-1856.

Hedges, J. I., Keil, R. G., & Benner, R. (1997). What happens to terrestrial organic matter in the ocean?. Organic Geochemistry, 27(5-6), 195-212.

Herwig, R. P., Gray, J. P., & Weston, D. P. (1997). Antibacterial resistant bacteria in surficial sediments near salmon net-cage farms in Puget Sound, Washington. Aquaculture, 149(3-4), 263-283.

Hiscock, W.T., & Millero, F.J. (2006). Alkalinity of the anoxic waters in the Western Black Sea. Deep-Sea Research II, 53: 1787–1801.

Holmer, M., & Kristensen, E. (1992). Impact of marine fish cage farming on metabolism and sulfate reduction of underlying sediments. Marine ecology progress series. Oldendorf, 80(2), 191-201.

Holmer, M., Wildish, D., & Hargrave, B. (2005). Organic enrichment from marine finfish aquaculture and effects on sediment biogeochemical processes. Environmental effects of marine finfish aquaculture, 181-206.

Jeroschewski, P., Steuckart, C., & Kühl, M. (1996). An amperometric microsensor for the determination of H2S in aquatic environments. Analytical Chemistry, 68(24), 4351-4357.

Jørgensen, B. B. (1977). The sulfur cycle of a coastal marine sediment (Limfjorden, Denmark) 1. Limnology and oceanography, 22(5), 814-832.

Jørgensen, B. B., & Revsbech, N. P. (1985). Diffusive boundary layers and the oxygen uptake of sediments and detritus 1. Limnology and oceanography, 30(1), 111-122.

Jørgensen, B. B., Böttcher, M. E., Lüschen, H., Neretin, L. N., & Volkov, I. I. (2004). Anaerobic methane oxidation and a deep H2S sink generate isotopically heavy sulfides in Black Sea sediments. Geochimica et Cosmochimica Acta, 68(9), 2095-2118.

Kapranov, S. V., Karavantseva, N. V., Bobko, N. I., Ryabushko, V. I., & Kapranova, L. L. (2021). Element contents in three commercially important edible mollusks harvested off the southwestern coast of Crimea (Black Sea) and assessment of human health risks from their consumption. Foods, 10(10), 2313.

Karakassis, I., Tsapakis, M., Hatziyanni, E., Papadopoulou, K. N., & Plaiti, W. (2000). Impact of cage farming of fish on the seabed in three Mediterranean coastal areas. ICES Journal of Marine Science, 57(5), 1462-1471.

Karakassis, I., Tsapakis, M., Smith, C. J., & Rumohr, H. (2002). Fish farming impacts in the Mediterranean studied through sediment profiling imagery. Marine Ecology Progress Series, 227, 125-133.

Karstensen, J., Fiedler, B., Schütte, F., Brandt, P., Körtzinger, A., Fischer, G., ... & Wallace, D. (2015). Open ocean dead zones in the tropical North Atlantic Ocean. Biogeosciences, 12(8), 2597-2605.

Keeley, N. B., Cromey, C. J., Goodwin, E. O., Gibbs, M. T., & Macleod, C. M. (2013). Predictive depositional modelling (DEPOMOD) of the interactive effect of current flow and resuspension on ecological impacts beneath salmon farms. Aquaculture Environment Interactions, 3(3), 275-291.

Keeley, N., Valdemarsen, T., Woodcock, S., Holmer, M., Husa, V., & Bannister, R. (2019). Resilience of dynamic coastal benthic ecosystems in response to large-scale finfish farming. Aquaculture Environment Interactions, 11, 161-179.

Kelley, R. B., Andersen, T., Foss, A., Hjellvik, V., & Skjelbred, B. (2019). Impact of fish farming on water quality and sedimentation in a Norwegian fjord. Aquaculture Environment Interactions, 11, 41-52.

Kelley, D. E., Richards, C., & Layton, C. (2022). oce: an R package for Oceanographic Analysis. *Journal of Open Source Software*, *7*(71), 3594.

Kempf, M., Merceron, M., Cadour, G., Jeanneret, H., Méar, Y., & Miramand, P. (2002). Environmental impact of a salmonid farm on a well flushed marine site: II. Biosedimentology. Journal of Applied Ichthyology, 18(1), 51-60.

Kirchman, D. L. (2021). Dead zones: the loss of oxygen from rivers, lakes, seas, and the ocean. Oxford University Press.

Knapp, J. S., & Bromley-Challoner, K. C. A. (2003). Recalcitrant organic compounds. Handbook of water and wastewater microbiology, 559-595.

Krauel, D. P. (1975). The physical oceanography of the Bras d'Or Lakes 1972-1974. Research and Development Directorate, Marine Ecology Laboratory, Bedford Institute of Oceanography.

Kristensen, E., Connolly, R. M., Otero, X. L., Marchand, C., Ferreira, T. O., & Rivera-Monroy, V. H. (2017). Biogeochemical cycles: Global approaches and perspectives. Mangrove ecosystems: A global biogeographic perspective: structure, function, and services, 163-209.

Krost, P., Chrzan, T., Schomann, H., & Rosenthal, H. (1994). Effects of a floating fish farm in Kiel Fjord on the sediment. Journal of Applied Ichthyology, 10(4), 353-361.

Kuypers, M. M., Sliekers, A. O., Lavik, G., Schmid, M., Jørgensen, B. B., Kuenen, J. G., ... & Jetten, M. S. (2003). Anaerobic ammonium oxidation by anammox bacteria in the Black Sea. Nature, 422(6932), 608-611.

Lakshmi, A. (2021). Coastal ecosystem services & human wellbeing. *Indian Journal of Medical Research*, *153*(3), 382. https://doi.org/10.4103/ijmr.ijmr_695_21

Lambert, T. (2002). Overview of the Ecology of the Bras d'Or Lakes with Emphasis on Fish. Proceedings of the Nova Scotian Institute of Science (NSIS). 42. 10.15273/pnsis. v42i1.3591.

Madden, R. J., MacMillan, J. L., & Apaloo, J. (2010). Examining the occurrence of wild rainbow trout in the Bras d'Or Lakes, Nova Scotia: using scale pattern analysis to differentiate hatchery and wild populations. In Conserving wild trout. Proceedings of the Wild Trout X symposium, Bozeman, Montana, USA (pp. 176-186).

Manning, C. C., Stanley, R. H., Nicholson, D. P., Loose, B., Lovely, A., Schlosser, P., & Hatcher, B. G. (2019). Changes in gross oxygen production, net oxygen production, and air-water gas exchange during seasonal ice melt in Whycocomagh Bay, a Canadian estuary in the Bras d'Or Lake system. Biogeosciences, 16(17), 3351-3376.

Mente, E., Pierce, G. J., Santos, M. B., & Neofitou, C. (2006). Effect of feed and feeding in the culture of salmonids on the marine aquatic environment: a synthesis for European aquaculture. Aquaculture International, 14, 499-522.

Merceron, M., Kempf, M., Bentley, D., Gaffet, D., Le Grand, J., & Lamort-Datin, L. (2002). Environmental impact of a salmonid farm on a well flushed marine site: I. Current and water quality. Journal of Applied Ichthyology, 18(1), 40-50. https://doi.org/10.1046/j.1439-0426.2002.00306.x

Middelburg, J. J., & Levin, L. A. (2009). Coastal hypoxia and sediment biogeochemistry. Biogeosciences, 6(7), 1273-1293.

Millero, F. J., Plese, T., & Fernandez, M. (1988). The dissociation of hydrogen sulfide in seawater 1. Limnology and Oceanography, 33(2), 269-274.

Monroy, P., Hernández-García, E., Rossi, V., and López, C. (2017). Modeling the dynamical sinking of biogenic particles in oceanic flow, Nonlin. Processes Geophys., 24, 293–305.

Murray, J. W., Top, Z., & Özsoy, E. (1991). Hydrographic properties and ventilation of the Black Sea. Deep Sea Research Part A. Oceanographic Research Papers, 38, S663-S689.

Ni, W., Li, M., Ross, A. C., & Najjar, R. G. (2019). Large projected decline in dissolved oxygen in a eutrophic estuary due to climate change. Journal of Geophysical Research: Oceans, 124, 8271–8289.

Njiru, M., Nyamweya, C., Gichuki, J., Mugidde, R., Mkumbo, O., & Witte, F. (2012). Increase in anoxia in Lake Victoria and its effects on the fishery. Anoxia, 99-128.

Paerl, H. W., Valdes, L. M., Peierls, B. L., Adolf, J. E., & Harding, L. W. (2006). Anthropogenic and climatic influences on the eutrophication of large estuarine ecosystems. *Limnology and Oceanography*, *51*(1 II), 448–462. https://doi.org/10.4319/LO.2006.51.1_PART_2.0448

Parker, M., Westhead, M., Doherty, P., & Naug, J. (2007). Ecosystem overview and assessment report for the Bras d'Or Lakes, Nova Scotia. Canadian Manuscript Report of Fisheries and Aquatic Sciences, 2789.

Pante, E., & Simon-Bouhet, B. (2013). marmap: a package for importing, plotting and analyzing bathymetric and topographic data in R. PLoS one, 8(9), e73051.

Pearson, T. H. (1978). Macrobenthic succession in relation to organic enrichment and pollution of the marine environment. Oceanography and marine biology: an annual review, 16, 229-311.

Pease, B. (1974). Effects of Log Dumping and Rafting on the Marine Environment of Southeast Alaska: Final Report for Period July 1, 1972-August 30, 1973 (Vol. 22). Pacific Northwest Research Station, US Department of Agriculture, Forest Service.

Petrie, B., & Bugden, G. (2002). The physical oceanography of the Bras d'Or Lakes. Proceedings of the Nova Scotian Institute of Science (NSIS), 42(1).

Poulos, S. E. (2020). The Mediterranean and Black Sea Marine System: An overview of its physico-geographic and oceanographic characteristics. Earth-Science Reviews, 200, 103004.

Prosper, K., McMillan, L. J., Davis, A. A., & Moffitt, M. (2011). Returning to Netukulimk: Mi'kmaq cultural and spiritual connections with resource stewardship and self-governance. The International Indigenous Policy Journal, 2(4).

Province of Nova Scotia. (2021). Standard Operating Procedures for the Environmental Monitoring of Marine Aquaculture in Nova Scotia.

Punshon, S., Azetsu-Scott, K., & Hatcher, B. G. (2022). Carbon cycling and redox chemistry in an anoxic marine basin, Bras d'Or Lake, Nova Scotia. Proceedings of the Nova Scotian Institute of Science (NSIS), 52(2), 203.

Ramírez-Pérez, A. M., De Blas, E., & García-Gil, S. (2015). Redox processes in pore water of anoxic sediments with shallow gas. Science of the Total Environment, 538, 317-326.

Regnier, P., Dale, A. W., Arndt, S., LaRowe, D. E., Mogollón, J., & Van Cappellen, P. (2011). Quantitative analysis of anaerobic oxidation of methane (AOM) in marine sediments: A modeling perspective. Earth-Science Reviews, 106(1-2), 105-130.

Rosenberg, R., & Diaz, R. J. (1993). Sulfur bacteria (Beggiatoa spp.) mats indicate hypoxic conditions in the inner Stockholm Archipelago. Ambio, 32-36.

Rosenberg, R., Nilsson, H. C., & Diaz, R. J. (2001). Response of benthic fauna and changing sediment redox profiles over a hypoxic gradient. Estuarine, Coastal and Shelf Science, 53(3), 343-350.

Rosenfeld, J. K. (1979). Interstitial water and sediment chemistry of two cores from Florida Bay. Journal of Sedimentary Research, 49(3), 989-994.

Ryan, W. B., Major, C. O., Pitman, W. C., Shimkus, K. S., Moscalenko, V., Jones, G. A., ... & Seyir, H. Y. (1997). An abrupt drowning of the Black Sea shelf at 7.5 kyr BP.

Sandberg, L. A. (1991). Forest Policy in Nova Scotia: The Big Lease, Cape Breton Island, 1899-1960. Acadiensis, 20(2), 105–128. http://www.jstor.org/stable/30302934

Sawayama, S. (2006). Possibility of anoxic ferric ammonium oxidation. Journal of bioscience and bioengineering, 101(1), 70-72.

Schendel, E. K., Nordström, S. E., & Lavkulich, L. M. (2004). Floc and sediment properties and their environmental distribution from a marine fish farm. Aquaculture research, 35(5), 483-493.

Seeberg-Elverfeldt, J., Schlüter, M., Feseker, T., & Kölling, M. (2005). Rhizon sampling of porewaters near the sediment-water interface of aquatic systems. Limnology and oceanography: Methods, 3(8), 361-371.

Seitaj, D., Sulu-Gambari, F., Burdorf, L. D., Romero-Ramirez, A., Maire, O., Malkin, S. Y., ... & Meysman, F. J. (2017). Sedimentary oxygen dynamics in a seasonally hypoxic basin. Limnology and Oceanography, 62(2), 452-473.

Schaanning, M. T., & Hansen, P. K. (2005). The suitability of electrode measurements for assessment of benthic organic impact and their use in a management system for marine fish farms. Environmental Effects of Marine Finfish Aquaculture, 381-408.

Shaw, J., Piper, D. J. W., & Taylor, R. B. (2002). The Geology of the Bras d'Or Lakes, Nova Scotia. Proceedings of the Nova Scotian Institute of Science.

Shaw, J., Taylor, R. B., Patton, E., Potter, D. P., Parkes, G. S., & Hayward, S. (2006). Sensitivity of the coasts of the Bras d'Or Lakes to sea-level rise. Geological Survey of Canada, Dartmouth, Nova Scotia. Open File, 5397.

Soetaert, K., & Meysman, F. (2012). Reactive transport in aquatic ecosystems: Rapid model prototyping in the open source software R. Environmental Modelling & Software, 32, 49-60.

Solorzano, Lucia. (1969). Determination of Ammonia in Natural Waters by the Phenolhypochlorite Method. Limnology and Oceanography 14, no. 5 (September): 799-801.

Steefel, C. I., DePaolo, D. J., & Lichtner, P. C. (2005). Reactive transport modeling: An essential tool and a new research approach for the Earth sciences. Earth and Planetary Science Letters, 240(3-4), 539-558.

Sterling, S. M., Garroway, K., Guan, Y., Ambrose, S. M., Horne, P., & Kennedy, G. W. (2014). A new watershed assessment framework for Nova Scotia: A high-level, integrated approach for regions without a dense network of monitoring stations. Journal of Hydrology, 519, 2596-2612.

Stookey, L. L. (1970). Ferrozine---a new spectrophotometric reagent for iron. Analytical chemistry, 42(7), 779-781.

Strain, P. M., & Yeats, P. A. (2002). The Chemical Oceanography of the Bras D'Or Lakes. *Proceedings of the Nova Scotian Institute of Science (NSIS)*, *42*(1). https://doi.org/10.15273/pnsis.v42i1.3590

Subasinghe, R., Soto, D., & Jia, J. (2009). Global aquaculture and its role in sustainable development. Reviews in aquaculture, 1(1), 2-9.

Thamdrup, B., Fossing, H., & Jørgensen, B. B. (1994). Manganese, iron and sulfur cycling in a coastal marine sediment, Aarhus Bay, Denmark. Geochimica et Cosmochimica Acta, 58 (23), 5115-5129.

Tuğrul, S., Murray, J. W., Friederich, G. E., & Salihoğlu, İ. (2014). Spatial and temporal variability in the chemical properties of the oxic and suboxic layers of the Black Sea. Journal of Marine Systems, 135, 29-43.

Unisense A/S. (2020). Hydrogen Sulfide Sensor Manual (Version May 2020). Denmark.

Vaquer-Sunyer, R., & Duarte, C. M. (2010). Sulfide exposure accelerates hypoxia-driven mortality. Limnology and Oceanography, 55(3), 1075-1082.

Vistisen, B., & Vismann, B. (1997). Tolerance to low oxygen and sulfide in Amphiura filiformis and Ophiura albida (Echinodermata: Ophiuroidea). Marine Biology, 128, 241-246.

Wildish, D. J., Hargrave, B. T., & Pohle, G. (2001). Cost-effective monitoring of organic enrichment resulting from salmon mariculture. ICES Journal of Marine Science, 58(2), 469-476.

Wijsman, J. W., Middelburg, J. J., Herman, P. M., Böttcher, M. E., & Heip, C. H. (2001). Sulfur and iron speciation in surface sediments along the northwestern margin of the Black Sea. Marine Chemistry, 74(4), 261-278.

Wu, R. S. S., Lam, K. S., MacKay, D. W., Lau, T. C., & Yam, V. (1994). Impact of marine fish farming on water quality and bottom sediment: a case study in the sub-tropical environment. Marine Environmental Research, 38(2), 115-145.

Yang, B., Sheng, J., Hatcher, B. G., & Petrie, B. (2007). Numerical study of circulation and temperature-salinity distributions in the Bras d'Or Lakes. Ocean Dynamics, 57, 245-268.

APPENDIX A

A.1 Average Sediment Core Values

Summary tables of chemistry characteristics for each individual sediment core sample site collected in November 2019 and September 2020 in the Whycocomagh Basin (see Fig. 3.5). Average values are based on duplicate samples for measurements collected.

Table A.1: *Sediment core average concentrations (mean ± SD) collected in the Whycocomagh Basin at the shallow (S1) site in 2019. Refer to Fig. 3.5 for core sites.*

Core Sample ID	Sediment Depth (cm)	Latitude	Longitude	Total Sulfide (µM)	Ammonium (µM)	Iron (µM)	Nitrate+Nitrite (µM)	TC (%)	TIN (%)	C:N Ratio	Porosity (%)
C1-1	0.5	45.94736	-61.13331	0.00	14.56 ± 0.17	9.54	2.22	-	-	-	-
C1-1.1	1.5	45.94736	-61.13331	0.00	31.75 ± 1.60	17.10	4.30	-	-	-	-
C1-2	2.5	45.94736	-61.13331	0.00	66.56 ± 3.34	13.52	4.15	-	-	-	-
C1-3	4.5	45.94736	-61.13331	0.00	144.70 ± 5.54	28.23	3.84	-	-	-	-
C1-4	6.5	45.94736	-61.13331	0.00	146.91 ± 51.42	7.16	4.31	-	-	-	-
C1-5	8.5	45.94736	-61.13331	7.35 ± 0.00	197.75 ± 25.00	0.00	3.18	-	-	-	-
C1-6	10.5	45.94736	-61.13331	14.27 ± 0.16	200.70 ± 6.67	0.00	3.90	-	-	-	-
C1-7	12.5	45.94736	-61.13331	45.75 ± 0.24	192.23 ± 2.65	0.00	1.85	-	-	-	-
C1-8	14.5	45.94736	-61.13331	98.40 ± 0.83	208.11 ± 3.63	0.00	1.12	-	-	-	-
C1-9	22.5	45.94736	-61.13331	194.28 ± 0.67	210.11 ± 2.22	0.00	2.33	-	-	-	-
C3-1	1	45.94736	-61.13331	-	-	-	-	0.56	5.80	10.42	0.94
C3-1.1	2	45.94736	-61.13331	-	-	-	-	0.75	6.73	9.02	-
C3-2	3	45.94736	-61.13331	-	-	-	-	0.55	5.68	10.28	-
C3-3	4	45.94736	-61.13331	-	-	-	-	0.53	5.80	11.00	0.93
C3-3.1	5	45.94736	-61.13331	-	-	-	-	0.65	6.03	9.25	-
C3-4	6	45.94736	-61.13331	-	-	-	-	0.56	5.88	10.42	-
C3-5	7	45.94736	-61.13331	-	-	-	-	0.55	5.93	10.79	0.91
C3-5.1	8	45.94736	-61.13331	-	-	-	-	0.56	5.30	9.45	-
C3-7	9	45.94736	-61.13331	-	-	-	-	0.48	4.99	10.43	0.89
C3-9	10	45.94736	-61.13331	-	-	-	-	0.43	4.38	10.08	0.87
C3-11	11	45.94736	-61.13331	-	-	-	-	0.39	3.98	10.11	0.86
C3-13	13	45.94736	-61.13331	-	-	-	-	0.36	3.84	10.72	0.84
C3-15	15	45.94736	-61.13331	-	-	-	-	0.29	3.25	11.08	0.73
C3-17	17	45.94736	-61.13331	-	-	-	-	0.27	3.07	11.21	0.71
C3-19	19	45.94736	-61.13331	-	-	-	-	0.30	3.37	11.16	0.70

Table A.2: *Sediment core average concentrations (mean ± SD) collected in the Whycocomagh Basin at the reference (R1) site in 2019. Refer to Fig. 3.5 for core sites.*

Core Sample ID	Sediment Depth (cm)	Latitude	Longitude	Total Sulfide (µM)	Ammonium (µM)	Iron (µM)	Nitrate+Nitrite (µM)	TC (%)	TIN (%)	C:N Ratio	Porosity (%)
C2-1	1.5	45.9488	-61.1298	4837.96 ± 24.56	2721.70 ± 90.50	0.00	3.61	-	-	-	-
C2-2	3.5	45.9488	-61.1298	-	3931.30 ± 383.50	0.00	3.07	-	-	-	-
C2-4	7.5	45.9488	-61.1298	10862.02 ± 87.92	4209.70 ± 251.60	0.00	2.90	-	-	-	-
C2-5	9.5	45.9488	-61.1298	7452.82 ± 113.22	4499.50 ± 73.60	0.00	1.50	-	-	-	-
C2-6	11.5	45.9488	-61.1298	9558.19 ± 187.65	4381.80 ± 220.60	0.00	1.02	-	-	-	-
C2-7	13.5	45.9488	-61.1298	9291.79 ± 455.73	4055.50 ± 444.60	0.00	1.05	-	-	-	-
C2-8	15.5	45.9488	-61.1298	10685.29 ± 69.84	3740.50 ± 336.80	0.00	2.26	-	-	-	-
C2-9	21.5	45.9488	-61.1298	12154.17 ± 1377.93	3012.60 ± 86.60	0.00	2.05	-	-	-	-
C10-1	1	45.9488	-61.1298	-	-	-	-	20.08	1.85	10.86	0.92
C10-3	3	45.9488	-61.1298	-	-	-	-	19.29	1.80	10.72	0.91
C10-5	5	45.9488	-61.1298	-	-	-	-	14.27	1.50	9.55	0.90
C10-7	7	45.9488	-61.1298	-	-	-	-	9.32	0.89	10.52	0.90
C10-9	9	45.9488	-61.1298	-	-	-	-	7.87	0.79	9.91	0.90
C10-11	11	45.9488	-61.1298	-	-	-	-	6.67	0.67	9.98	0.89
C10-13	13	45.9488	-61.1298	-	-	-	-	6.04	0.62	9.74	0.82
C10-15	15	45.9488	-61.1298	-	-	-	-	5.72	0.59	9.71	0.88
C10-17	17	45.9488	-61.1298	-	-	-	-	5.58	0.59	9.45	0.87
C10-19	19	45.9488	-61.1298	-	-	-	-	5.63	0.60	9.40	0.86
C10-21	21	45.9488	-61.1298	-	-	-	-	5.57	0.57	9.85	0.85
C10-23	23	45.9488	-61.1298	-	-	-	-	5.95	0.61	9.70	0.89
C10-25	25	45.9488	-61.1298	-	-	-	-	5.75	0.60	9.65	0.89

Table A.3: *Sediment core average concentrations (mean ± SD) collected in the Whycocomagh Basin at the fish pen (F1) site in 2019. Refer to Fig. 3.5 for core sites.*

Core Sample ID	Sediment Depth (cm)	Latitude	Longitude	Total Sulfide (µM)	Ammonium (µM)	Iron (µM)	Nitrate+Nitrite (µM)	TC (%)	TIN (%)	C:N Ratio	Porosity (%)
C5-1	0.5	45.9475	-61.1306	387.17 ± 5.24	233.03 ± 22.17	0.00	1.25	-	-	-	-
C5-3	4.5	45.9475	-61.1306	756.48 ± 4.45	419.27 ± 12.10	0.00	0.57	-	-	-	-
C5-4	6.5	45.9475	-61.1306	1125.64 ± 14.02	467.14 ± 13.00	0.00	4.45	-	-	-	-
C5-5	8.5	45.9475	-61.1306	1078.96 ± 6.36	556.45 ± 38.65	0.00	1.18	-	-	-	-
C5-6	10.5	45.9475	-61.1306	1061.30 ± 5.78	606.93 ± 16.33	0.00	5.75	-	-	-	-
C5-7	12.5	45.9475	-61.1306	1696.19 ± 24.58	625.78 ± 30.10	0.00	2.70	-	-	-	-
C5-8	14.5	45.9475	-61.1306	2277.48 ± 100.56	650.73 ± 34.58	0.00	11.40	-	-	-	-
C5-9	20.5	45.9475	-61.1306	3014.17 ± 112.56	819.94 ± 13.88	0.00	1.69	-	-	-	-
C12-1	1	45.9475	-61.1306	-	-	-	-	5.16	0.60	8.67	0.96
C12-3	3	45.9475	-61.1306	-	-	-	-	6.28	0.66	9.47	0.92
C12-5	5	45.9475	-61.1306	-	-	-	-	5.50	0.58	9.46	0.89
C12-7	7	45.9475	-61.1306	-	-	-	-	5.56	0.58	9.52	0.88
C12-9	9	45.9475	-61.1306	-	-	-	-	5.54	0.57	9.76	0.86
C12-11	11	45.9475	-61.1306	-	-	-	-	5.52	0.56	9.94	0.83
C12-13	13	45.9475	-61.1306	-	-	-	-	5.55	0.53	10.45	0.81
C12-15	15	45.9475	-61.1306	-	-	-	-	5.46	0.54	10.20	0.79
C12-17	17	45.9475	-61.1306	-	-	-	-	5.19	0.51	10.24	0.78
C12-19	19	45.9475	-61.1306	-	-	-	-	5.09	0.49	10.36	0.77
C12-21	21	45.9475	-61.1306	-	-	-	-	5.02	0.49	10.16	0.76
C12-23	23	45.9475	-61.1306	-	-	-	-	4.79	0.47	10.25	0.76
C12-25	25	45.9475	-61.1306	-	-	-	-	4.65	0.46	10.10	0.63

Table A.4: *Sediment core average concentrations (mean ± SD) collected in the Whycocomagh Basin at the shallow (S2) site in 2020. Refer to Fig. 3.5 for core sites.*

Core Sample ID	Sediment Depth (cm)	Latitude	Longitude	Total Sulfide (µM)	Ammonium (µM)	Iron (µM)	Nitrate+Nitrite (µM)	TC (%)	TIN (%)	C:N Ratio
C1-1	1	45.94736	-61.13331	9.07 ± 0.80	319.58 ± 4.22	57.06 ± 0.00	2.22	5.97	0.58	9.71
C1-2	3	45.94736	-61.13331	6.86 ± 0.31	447.98 ± 10.64	8.89 ± 0.02	4.30	6.46	0.62	9.91
C1-3	5	45.94736	-61.13331	118.40 ± 1.13	535.14 ± 61.38	0.00	4.15	6.91	0.60	11.44
C1-4	7	45.94736	-61.13331	295.52 ± 3.74	583.34 ± 34.98	0.00	3.84	5.53	0.47	11.88
C1-5	9	45.94736	-61.13331	127.78 ± 14.41	550.54 ± 6.90	0.00	4.31	6.05	0.53	11.48
C1-6	11	45.94736	-61.13331	136.68 ± 7.93	723.46 ± 33.28	0.00	3.18	5.36	0.47	10.91
C1-7	13	45.94736	-61.13331	434.53 ± 34.42	909.22 ± 42.78	0.00	3.90	5.67	0.50	11.39
C1-8	15	45.94736	-61.13331	638.71 ± 38.79	1044.14 ± 45.60	0.00	1.85	5.08	0.46	10.97
C1-9	17	45.94736	-61.13331	582.03 ± 0.00	927.45 ± 74.80	0.00	1.12	4.75	0.43	11.12
C1-10	19	45.94736	-61.13331	1029.95 ± 9.18	963.50 ± 14.18	0.00	2.33	4.53	0.40	11.38
C1-11	21	45.94736	-61.13331	1000.64 ± 69.12	885.92 ± 52.56	0.00	1.80	5.06	0.43	11.89
C1-12	23	45.94736	-61.13331	1155.11 ± 5.13	1190.80 ± 31.75	0.00	1.60	4.98	0.43	11.56
C1-13	25	45.94736	-61.13331	737.54 ± 16.02	1140.20 ± 71.55	0.00	1.39	6.38	0.47	13.50
C2-1	1	45.94736	-61.13331	27.65 ± 2.51	351.30 ± 3.35	4.59 ± 0.01	1.97	5.38	0.51	10.62
C2-2	3	45.94736	-61.13331	285.81 ± 5.83	653.56 ± 63.96	0.00	1.55	7.11	0.73	9.71
C2-3	5	45.94736	-61.13331	833.89 ± 27.82	779.04 ± 9.96	0.00	1.47	7.18	0.73	9.89
C2-4	7	45.94736	-61.13331	925.50 ± 0.00	1032.20 ± 2.05	0.00	1.54	7.26	0.67	10.79
C2-5	9	45.94736	-61.13331	936.71 ± 15.48	1017.55 ± 66.55	0.00	2.03	6.74	0.65	10.38
C2-6	11	45.94736	-61.13331	918.80 ± 7.12	926.40 ± 80.50	0.00	2.33	5.70	0.55	10.40
C2-7	13	45.94736	-61.13331	903.22 ± 9.70	876.00 ± 39.55	0.00	2.39	5.08	0.48	10.63
C2-8	15	45.94736	-61.13331	995.69 ± 43.79	913.05 ± 65.65	0.00	1.93	5.57	0.51	10.97
C2-9	17	45.94736	-61.13331	975.23 ± 13.63	948.00 ± 79.30	0.00	2.01	5.90	0.50	11.92
C2-10	19	45.94736	-61.13331	953.76 ± 16.34	-	0.00	1.58	5.16	0.47	10.99
C2-11	21	45.94736	-61.13331	995.35 ± 29.65	894.40 ± 15.80	0.00	1.39	5.00	0.43	10.87
C2-12	23	45.94736	-61.13331	1045.71 ± 11.01	992.65 ± 32.55	0.00	2.03	4.99	0.46	11.76
C2-13	25	45.94736	-61.13331	1033.93 ± 11.71	1026.04 ± 19.70	0.00	1.85	4.95	0.42	11.71

Table A.5: *Sediment core average concentrations (mean ± SD) collected in the Whycocomagh Basin at the reference (R2) site in 2020. Refer to Fig. 3.5 for core sites.*

Core Sample ID	Sediment Depth (cm)	Latitude	Longitude	Total Sulfide (µM)	Ammonium (µM)	Iron (µM)	Nitrate+Nitrite (µM)	TC (%)	TIN (%)	C:N Ratio
C5-1	1	45.9466	-61.1297	776.36 ± 19.01	394.20 ± 11.35	0.00	0.82	6.08	0.66	9.23
C5-2	3	45.9466	-61.1297	1538.93 ± 71.75	448.40 ± 40.65	0.00	2.53	6.18	0.65	9.50
C5-3	5	45.9466	-61.1297	1651.00 ± 93.51	601.90 ± 32.70	0.00	3.32	5.32	0.54	9.94
C5-4	7	45.9466	-61.1297	1767.30 ± 124.1	846.75 ± 71.95	0.00	3.17	4.76	0.47	10.10
C5-5	9	45.9466	-61.1297	1988.53 ± 106.97	576.90 ± 36.90	0.00	4.20	5.46	0.54	10.07
C5-6	11	45.9466	-61.1297	1796.63 ± 34.99	691.80 ± 38.15	0.00	3.40	5.52	0.54	10.25
C5-7	13	45.9466	-61.1297	2107.08 ± 36.56	805.65 ± 10.10	0.00	4.79	5.20	0.48	10.76
C5-8	15	45.9466	-61.1297	2434.81 ± 27.72	774.10 ± 8.30	0.00	2.79	5.06	0.49	10.33
C5-9	17	45.9466	-61.1297	2636.77 ± 42.46	813.05 ± 39.40	0.00	4.19	5.22	0.51	10.31
C5-10	19	45.9466	-61.1297	1633.29 ± 80.37	740.35 ± 85.00	0.00	1.89	5.20	0.52	10.08
C10-1	1	45.9466	-61.1297	1181.82 ± 89.92	644.85 ± 7.10	0.00	1.58	6.33	0.61	10.34
C10-2	3	45.9466	-61.1297	1567.95 ± 19.36	790.80 ± 45.10	0.00	4.76	5.90	0.60	9.89
C10-3	5	45.9466	-61.1297	1947.97 ± 51.26	860.20 ± 24.10	0.00	3.34	4.93	0.49	10.11
C10-4	7	45.9466	-61.1297	2297.28 ± 322.65	1077.15 ± 65.20	0.00	3.38	4.95	0.49	10.13
C10-5	9	45.9466	-61.1297	2149.48 ± 102.97	1131.05 ± 45.85	0.00	3.58	4.83	0.48	9.98
C10-6	11	45.9466	-61.1297	2712.14 ± 89.98	1158.95 ± 8.85	0.00	3.13	5.17	0.49	10.57
C10-7	13	45.9466	-61.1297	2542.78 ± 90.35	1475.20 ± 98.95	0.00	2.61	4.92	0.46	10.62
C10-8	15	45.9466	-61.1297	2844.55 ± 64.07	1029.65 ± 19.90	0.00	2.92	5.22	0.50	10.39
C10-9	17	45.9466	-61.1297	2795.06 ± 103.04	1295.45 ± 35.00	0.00	2.16	4.92	0.49	10.09
C10-10	19	45.9466	-61.1297	2360.19 ± 58.20	1314.45 ± 71.05	0.00	2.41	5.10	0.50	10.27

Table A.6: *Sediment core average concentrations (mean ± SD) collected in the Whycocomagh Basin at the fish pen (F1) site in 2020. Refer to Fig. 3.5 for core site.*

Core Sample ID	Sediment Depth (cm)	Latitude	Longitude	Total Sulfide (µM)	Ammonium (µM)	Iron (µM)	Nitrate+Nitrite (µM)	TC (%)	TIN (%)	C:N Ratio
C11-1	1	45.9488	-61.1298	3155.71 ± 399.29	1833.00 ± 0.40	0.00	2.81	10.07	1.08	9.29
C11-2	3	45.9488	-61.1298	3970.30 ± 788.89	3799.50 ± 51.90	0.00	3.47	5.74	0.56	10.20
C11-3	5	45.9488	-61.1298	6773.02 ± 45.20	3417.00 ± 47.00	0.00	4.01	4.90	0.47	10.49
C11-4	7	45.9488	-61.1298	6734.54 ± 211.86	2271.10 ± 185.40	0.00	3.34	4.72	0.46	10.17
C11-5	9	45.9488	-61.1298	5380.89 ± 83.37	1729.50 ± 39.90	0.00	4.34	4.98	0.48	10.44
C11-6	11	45.9488	-61.1298	3839.35 ± 1348.27	1474.10 ± 47.20	0.00	3.92	5.59	0.52	10.69
C11-7	13	45.9488	-61.1298	5269.53 ± 115.39	1264.20 ± 17.50	0.00	2.28	4.73	0.44	10.72
C11-8	15	45.9488	-61.1298	4678.50 ± 218.50	1230.40 ± 94.10	0.00	2.58	5.45	0.52	10.53
C11-9	17	45.9488	-61.1298	4295.91 ± 6.42	1182.90 ± 53.90	0.00	2.46	5.19	0.49	10.63
C11-10	19	45.9488	-61.1298	2624.97 ± 64.34	1461.10 ± 13.90	0.00	2.61	5.21	0.49	10.67
C12-1	1	45.9488	-61.1298	2536.58 ± 58.45	1130.80 ± 21.00	0.00	1.72	9.14	1.02	9.00
C12-2	3	45.9488	-61.1298	5364.46 ± 391.10	2188.80 ± 22.40	0.00	2.45	6.47	0.68	9.35
C12-3	5	45.9488	-61.1298	6848.43 ± 40.32	2396.60 ± 52.80	0.00	5.16	5.54	0.56	9.98
C12-4	7	45.9488	-61.1298	5438.01 ± 169.39	2677.50 ± 5.40	0.00	4.11	5.13	0.53	9.66
C12-5	9	45.9488	-61.1298	6360.92 ± 828.67	1982.80 ± 11.00	0.00	3.49	5.13	0.49	10.41
C12-6	11	45.9488	-61.1298	5512.38 ± 286.43	1762.60 ± 175.40	0.00	4.32	5.32	0.50	10.58
C12-7	13	45.9488	-61.1298	4123.75 ± 117.15	1381.20 ± 51.40	0.00	4.55	5.72	0.53	10.78
C12-8	15	45.9488	-61.1298	4902.07 ± 298.69	1609.80 ± 6.00	0.00	2.96	5.04	0.46	10.91
C12-9	17	45.9488	-61.1298	4673.53 ± 128.52	1428.30 ± 141.50	0.00	3.00	5.07	0.48	10.52
C12-10	19	45.9488	-61.1298	3354.21 ± 542.51	1321.80 ± 66.50	0.00	3.33	5.90	0.56	10.57
C12-11	21	45.9488	-61.1298	2772.37 ± 64.20	1228.50 ± 48.90	0.00	3.13	5.66	0.54	11.13

APPENDIX B

B.1 Equations Used in Analysis

Formulas used in the methods and reactive-transport model analysis.

Table B.1: *Equations and subsequent numbering and pages.*

Equation Formula	Number	Page
$\Delta\rho_w = \rho(T, S, db)$	Eq. 1	28
$N^2 = \left(\left(-\frac{g}{\rho_{w(0)}}\right)\left(\frac{\delta\rho_w(z)}{\delta z}\right)\right)$	Eq. 2	29
$Porosity\ (P_t) = Pore\ Volume\ (Vp)\ /Total\ Volume(Vt)$	Eq. 3	35
$\int_0^{20cm} \varphi\ [C]_i\ dz$	Eq. 4	93
$\int_0^{20cm} (1-\varphi)\rho_s\ [C]_i\ dz$	Eq. 5	93
$Rate = \frac{\left(\int_0^{20} C_{(t_1)}\, dz - \int_0^{20} C_{(t_0)}\, dz\right)}{(t_1 - t_0)}$	Eq. 6	95
$(CH_2O)(NH_3)_{(0.08)} + 0.5(SO_4^{2-}) \rightarrow (CO_2) + 0.5(TS^{2-}) + 0.08(NH_4^+)$	Eq. 7	96
$CH_4 + SO_4^{2-} \rightarrow HCO_3^- + HS^- + H_2O$	Eq. 8	97
$(CH_2O)(NH_3)_{(0.08)} + 0.5(H_2O) \rightarrow (CO_2) + 0.5(CH_4) + 0.08(NH_3)$	Eq. 9	97

Equation Formula	Number	Page
$\left(\frac{\Delta totS^{2-}}{\Delta NH_4^+}\right) = \frac{(0.5 \times R_{SO4})}{(NC \times R_{SO4}) + (NC \times R_{CH4})}$	Eq. 10	97
$C_{rem} = R_{SO4} + R_{CH4}$	Eq. 11	98
$R_{SO4} = \frac{\left(\frac{\Delta TS^{2-}}{\Delta NH_3} \times CN \times C_{rem}\right)}{0.5}$	Eq. 12	98
$\frac{\Delta[TS^{2-}]}{\Delta t} = \frac{(Flux_{in} - Flux_{out})}{(\Delta V)} + \Sigma Reactions$	Eq. 13	107
$\frac{d[TS^{2-}]_i}{dt} = \frac{\Delta_i(E \cdot \Delta[TS^{2-}]_i)}{\Delta V_i} + \frac{1}{\Delta V_i} \int F_{TS^{2-}}^{swi} \delta S - k_{sox}(z)[TS^{2-}]_i$	Eq. 14	107
$F_{TS^{2-}}^{swi} = \frac{D_{TS^{2-}}}{DBL}([TS^{2-}]_{sed} - [TS^{2-}]_i)$	Eq. 15	108
$k_{sox}(z) = y_0 \times \frac{e^{-\frac{(z-z_L)}{aL}}}{1 + e^{-\frac{(z-z_L)}{aL}}}$	Eq. 16	110